Statistical Representations of Extreme Precipitation in East Africa under Climate Change using a Convection-Permitting Model

Claire West

Supervisors: John Marsham, Mark Trigg

November 2019

Abstract

Climate change is projected to affect the global pattern of rainfall and increase extreme precipitation over the coming century. This is a particular concern for the African continent, where both population and infrastructure development are anticipated to grow to unprecedented levels, making local communities vulnerable to extremes. It is well established that the parametrisation of convection in climate simulations can reduce the climate change increase in extreme rainfall. This has recently been shown for one in one-year storms over Africa using the ten year time-slice simulations of the first pan-African convection-permitting model (CP4-A) climate simulation (Kendon et al., 2019). This project aims first to quantify how extreme precipitation events in eastern Africa are affected by an explicit versus parametrised representation of convection and how this depends on the spatial and temporal scales of these extremes. The second aim is to understand the physical mechanisms for increased rainfall extremes on timescales of hours to days and how this is captured as a function of the representation of convection. The results show that that reasonable estimates of climate change in one in ten-year events can be generally be made, despite the 10-year duration of the runs. In many locations explicit convection predicts larger fractional increases in precipitation extremes under a warming climate but that some present-day long-term return period precipitation rates exceed future climate estimates, contrary to predictions from the parametrised model. From the parametrised model, it has been shown that the precipitation rate for the ten-year return period may more than double for 25% of east Africa under climate change.

Contents

1 Project Aims

Analysis of the first convection-permitting climate runs for Africa have shown, consistent with studies from other regions, that an explicit rather than parametrised representation of convection on average gives a larger increase in 25 km scale extreme rainfall, where extreme is defined as the 99.9th percentile of three-hourly precipitation (Kendon et al., 2019), which is well sampled by the ten-year CP4-A runs. Africa is vulnerable to extreme rain changes, with different space and time scales feeling different impacts (hourly local rainfall may be most relevant to flash pluvial flooding whereas basin wide multi-day accumulation may be most relevant to river flooding). Often, it is events much rarer than the one in one-year that have the largest impacts. There is therefore a need to determine how explicit convection affects projected changes in rainfall extremes for rarer events, even though the rare tail is not well sampled by 10-year runs.

This first chapter of this work therefore aims to:

- develop a robust methodology for analysing climate change in rare extreme rainfall events from the CP4-A and P25 models.
- establish how an explicit rather than parametrised representation of convection affects model changes in return periods of rare rainfall events for time-scales of one hour to several days and space scales of 4km to 150km.
- determine the uncertainty in these, especially for the rarer events and hence ascertain how rare a return period we can usefully determine such changes for from the 10-year simulations.

The second part of the project aims to analyse and understand the underlying reasons why these precipitation extremes change under a warming climate, in particular looking at the physical mechanisms behind the storms that cause the rainfall. The changing properties of these storms will be investigated, including the behaviour of updraft speeds, CAPE (convective available potential energy) and storm velocity to determine what changes contribute to the rare rainfall events analysed in the previous chapter.

1.1 Introduction

It is widely acknowledged that globally, the Earth's climate has changed substantially over the preceding century and will continue to do so, significantly impacting vulnerable populations across the globe (Pachauri et al., 2014). Crucially, under a warming climate, precipitation variation is one of the factors that has the most impact on susceptible areas, where there is evidence that differences will be amplified in already wetter and drier regions (Chou et al., 2004; Held et al., 2006; Polson et al., 2017). This implies that climate change is likely to enhance problematic issues in parts of the world that already suffer from extremes such as droughts or flooding.

A particularly exposed region is Africa, where extreme droughts and heavy rainfall events are already common and have significant societal impact on the fast-growing populations across the continent. The most recent assessment report from the Intergovernmental Panel on Climate Change (IPCC) identified Africa as having already observed significant impact from increasing temperatures, specifically in relation to water-related features such as rivers, lakes, floods and droughts (Pachauri et al., 2014). Under the wet-gets-wetter, dry-gets-drier paradigm (see Sec. A.2 for more detail), it suggests that these problems will only be exacerbated in coming years with a warming climate, with the effects of climate change felt most directly through meteorological extremes. Another difficulty for Africa is the precipitation variation between regions. It is expected that parts of the Sahara and southern Africa will on average become drier, whereas the eastern Sahel is predicted to have an average precipitation increase of as much as 50% by the end of the century under high emissions scenarios (Pachauri et al., 2014). This makes the study of Africa as a continent enormously challenging, with many regional variations which depend on local and global atmospheric instabilities, orography, coastlines and proximity to the tropics. Generally though, total precipitation is not expected to rise significantly on a global scale, around 1-3% K^{-1} (Pachauri et al., 2014), however many areas, particularly in the tropics, will likely experience more in terms of precipitation extremes. Both the intensity and frequency of these events are projected to increase with warming. It is expected that the intensity of a storm with a

return period of 20 years will increase by 2.5-12.5% K^{-1} (Pachauri et al., 2014), so quantifying the future risk for local populations is vital.

To improve our understanding of the consequences of a warmer future climate, simulated data from global and regional climate models can be used to predict various atmospheric changes under different scenarios. These scenarios often correspond with various radiative forcings, determining the potential future temperatures as a way of dictating the changing climate. The accuracy of the results from these models depend on many factors. The model physics, grid size, boundary conditions and various parametrisations all influence the sensitivity to aspects such as topographic features, diurnal cycles and land cover. Assessing the effects of grid-size and parametrisations on model output is an essential task in order to effectively predict long-term extreme events in a reliable way.

Using model data, it is possible to represent extreme precipitation in a way that is suitable for use by civil engineers and hydrologists. This is particularly important in regions where historical rain gauge data are sparse and substantial increase in rates of urbanisation and infrastructure development is expected to occur. This can help make predicting the local and practical impact of climate change possible. By improving extreme rainfall models and future climate predictions, it will aid the development of strategies to target at risk communities and structures on a very local scale. Specific statistical methods are commonly used to extrapolate information far beyond the length of the simulated data to provide return periods of extremely rare precipitation events. The choice of method depends on the duration of the data set, the number of intense rainfall periods and the type of information required.

This report is organised as follows: a review of the relevant topics and literature - climate modelling and the African climate; climate model shortfalls; and current statistical procedures for estimating long-term extreme events. Methods, ongoing work and results are then detailed, followed by a research plan and summary. Some background information relating the physics of extreme precipitation events is included in the appendix.

2 Literature Review

Reviewed here are a selection of observational and climate modelling results with respect to precipitation extremes. A review of the thermodynamic and dynamical mechanisms behind changes in precipitation patterns due to temperature increase included in the appendix. Relevant model uncertainties are discussed, specifically for simulations of Africa. Finally, an overview of statistical and probabilistic methods of predicting long-term return periods of events is presented.

2.1 Observations and Modelling of Global Precipitation Extremes

It is generally accepted that globally, the frequency and intensity of extreme precipitation events will exceed mean precipitation under climate change (Emori et al., 2005; Kharin et al., 2013; Norris et al., 2019). As a result, a vast amount of investigation has been conducted using global and regional climate models to interpret this. Although computerised weather forecasting began in the 1950s (Phillips, 1956), only in the past 20-30 years has the emphasis been put on longer-term climate modelling due to the limitations computational power imposed on obtaining feasible and reliable results within a reasonable timescale. A broad field of research emerged in the early 1990s onwards, with publication of the first IPCC report. These considered atmospheric variations under warming, often by simulating increased radiative forcing from added CO_2, resulting in an increase in temperature and moisture (e.g. Delworth et al., 2000; Meehl et al., 2000; Mitchell et al., 2000; Lucarini et al., 2002).

An earlier study by Hennessy et al. (1997) considered results from two global climate models (GCMs) and found that generally, if global average precipitation increased by 10%, then high, middle and low latitudes all have an increase in intense convective events but a decrease in wet-days (apart from high-latitudes). Specifically, extreme events were considered in relation to return periods T_i (average interval i (years) between similar events). It was found that for return periods exceeding one year, precipitation intensity increased by 10-25% globally and the return period decreased by a factor of a half to a fifth. When considering the climatic response to doubling CO_2 using two GCMs, Zwiers et al. (1998) found that the T_{20} daily precipitation increased by around 11%, where the mean only increased by 4%. A more recent, comprehensive study by Kharin et al. (2013) looked at changes in temperature and precipitation extremes using different emission scenarios (Fig. 1). The magnitude of precipitation extremes over land areas increases under the RCP2.6, RCP4.5 and RCP8.5 (Representative Concentration Pathways; (Moss et al., 2010)) scenarios by about 6%, 12% and 30% respectively by 2100. This corresponds to current day T_{20} reducing to 14, 11 and 6 years. Although there is considerable numerical scatter among model results relating to extreme values, the trend in changes is robust. It has been noted that differences in model behaviour is at least in part due to vertical motion simulation (Trenberth et al., 2009).

Historically, it has been observed that intense precipitation events in the United States increased by 3% decade^{-1} during the period 1931-1996 for 1-7 day events with a return period >1 year (Kunkel et al., 1999). Alexander et al. (2006) did a comprehensive analysis of observed global changes in extreme temperatures and precipitation, showing an increase in wetter conditions, particularly towards the end of the 20th century. Westra et al. (2013) used 30 years of observational records and more than 8000 land-based observational stations of which two-thirds showed an annual maximum daily precipitation increase over that period.

2.2 Africa under Climate Change

The climate in Africa is complex and diverse, ranging from humid equatorial, seasonal tropical-arid, arid and Mediterranean-type, also exhibiting sometimes significant temporal variability (Hulme et al., 2001). The changing climate in Africa has been acknowledged as far back as the 1930s where the expansion of the Sahara and regional drying of West Africa were noted (Stebbing, 1935; Aubréville et al., 1949). Despite these early observations, the African continent has received relatively little attention with respect to long-term climate scenario studies compared with other continents such as Europe and North America (Pachauri et al., 2014). Early climatic studies looking at regional areas of Africa include Charney (1975), Cunnington et al. (1986) and Zheng et al. (1997), however all only focussed on the northern African region. This lack of focus, the

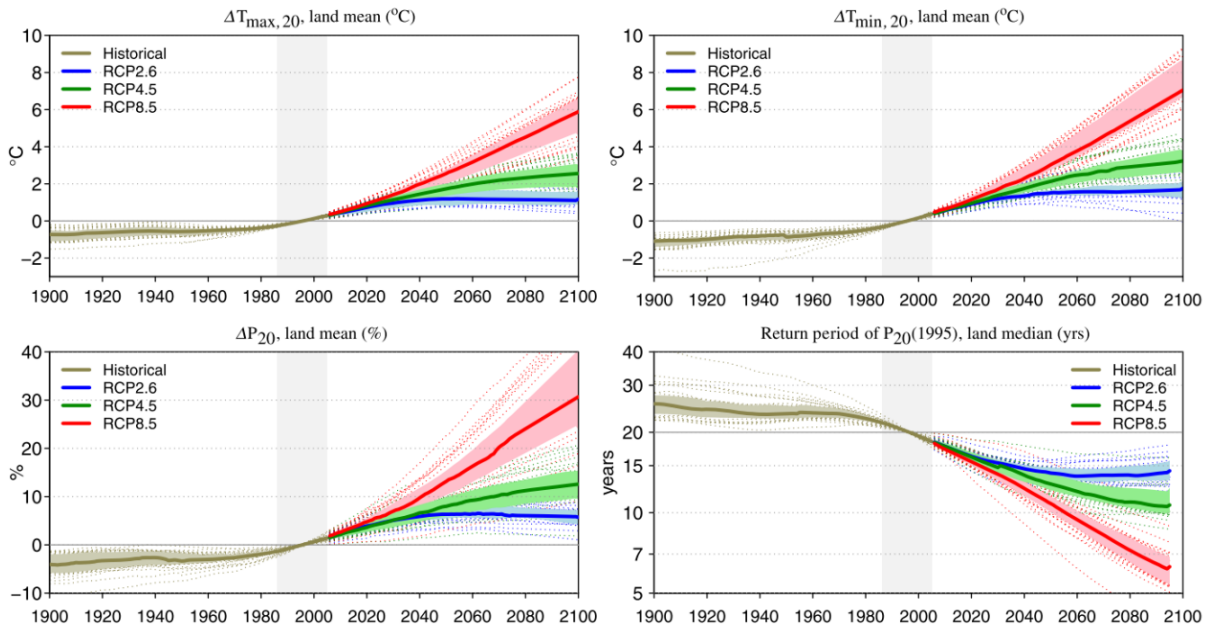

Figure 1: Change in multimodel 20-year return periods for three emissions scenarios and historical data between 1900-2100. Top left is change in annual maximum temperature. Top right is change in annual minimum temperature. Bottom left is percentage change to annual extremes of daily rainfall and bottom right is the change in the return periods of the 20-year return period from 1995. Shading indicates interquartile range. Dotted lines are individual models, solid lines are ensemble medians. From Kharin et al. (2013).

minimal observational records and the highly variable climates across the continent have made Africa a challenging region for study.

2.2.1 Climate Change Studies for the African Continent

Despite the well-known consequences and risks of a warming climate in the tropics, there is little consensus between global climate models (GCMs) on the spatial or temporal changes in precipitation throughout many areas of the African continent (Donat et al., 2016; Rowell et al., 2018). This uncertainty in precipitation modelling is most significant in the deep tropics, especially for Africa (Rowell, 2012). Until the late 20th century, studies of the African climate were mostly performed as part of larger global projects. Mitchell et al. (1990) looked at precipitation changes in the Sahel region, along with four other areas on different continents; Kittel et al. (1997) who again considered the Sahel region as part of a larger study and Giorgi et al. (2000) who analysed 23 regions across five continents, including much of Africa. One of the earliest studies to focus specifically on longer-term climate changes in Africa was performed by Tyson (1991) who looked at precipitation variations between 1990-2050 in southern Africa using GCMs. Other earlier climate studies of Africa-specific regions include several studies by Joubert et al. who considered impacts of warming on various regions of Africa and the effectiveness and uncertainties in GCM simulations (Joubert et al., 1996; Joubert et al., 1997). They found that precipitation is expected to increase considerably by 2050, although this result should be interpreted with caution since the GCMs did not accurately simulate the past 100 years.

A large proportion of Africa is in the tropics and sub-tropics, where features such as the seasonal migration of the tropical rain belt and the WAM (west African monsoon) pose significant challenges to climate models. Related factors such as organised convection (Jackson et al., 2009; Marsham et al., 2013; Birch et al., 2014) as discussed in Sec. A.6 and aerosol emissions from extremely arid regions such as the Sahara (Engelstaedter et al., 2006; C. J. Allen et al., 2013) add complications and complexity to the validity of model outputs. Another challenge with Pan-African models is the difficulty in reproducing the spatial variables such as orographic features due to the generally low resolutions used over such a large and diverse region

(James et al., 2018).

More recently, interest in the African climate has increased. Using GCMs, studies have begun to apply empirical dynamical downscaling to GCMs to smaller scales for better resolution, allowing in-depth study of specific regions. A particular surge in this method occurred when the World Climate Research Program (WCRP) launched its COordinated Regional Climate Downscaling EXperiment (CORDEX; Giorgi et al., 2009) who chose the initial region of focus to be Africa. A comprehensive climate study following CORDEX methodology by Laprise et al. (2013) looked at the effectiveness of RCMs and the generated future climate projections at moderate emissions scenario RCP4.5 between 1950-2100 for the entire of Africa. Misrepresentations of the seasonal cycles of precipitation and the WAM in future and current projections are argued to be due to errors in boundary conditions from the GCMs drivers. It was noticed too that the RCMs have significantly different results to the GCMs. The diurnal cycle from the models lagged several hours behind the satellite observations for all regions and the peak values were too low, apart from the Ethiopian Highlands region. Generally though, precipitation rates in Africa are expected to grow throughout the 21st century, even with only moderate emission increases. Daily intensities in rainfall predicted by the models are lower than observations for current simulations. Precipitation changes for future climate are minimal in JFM between models. The tropical rainbelt is observed to narrow in JAS with increase in the intensity with drying around the Guinea coast. Despite these changes, no noticeable difference was seen in the current and future annual cycles. The lack of changes in annual cycles is disputed by Dunning et al. (2018) who used 29 GCMs to show that rainfall intensity increases under climate change across west and central Africa, with the wet season shifted by 5-10 days forward for west Africa and the Sahel region.

2.2.2 CP4-A

A very recent 10-year pan-African simulation has been run using a regional version of the latest configuration of the Met-Office Unified Model (UM) (Walters et al., 2017) called CP4-A (Stratton et al., 2018) as part of the Future Climate for Africa (FCFA) IMPALA (Improving Model Processes for African cLimAte) project. It is the first convection-permitting (CP) model to be run across the entirety of Africa, performed for both current and future climate simulations (1997-2007 and end of the 21st century respectively) using high emissions scenario RCP8.5. The surface level data is recorded at hourly intervals, the pressure level data at 3-hourly intervals, with 4.5 km grid-spacing at the equator. The model has 83 vertical levels, up to 38 km, with denser layers in the boundary layer to upper troposphere to aid the modelling of tropical convective processes. The model is nested within the Met Office global UM (with convection parametrisation), driven by the lateral boundaries and applied over Africa with boundary conditions using sea-surface temperature analyses for 1997-2006.

An independent complimentary simulation called P25 was run alongside this using the Met Office UM with a nearly identical set-up to CP4-A. P25 has the same domain and temporal scales as CP4-A but with parametrised convection, a different cloud scheme and a 26 x 39 km grid scale. Several studies have been published analysing the results of CP4-A compared with P25. These results are discussed in Sec. 2.3.2 where issues surrounding convective parametrisations are detailed.

2.3 Model Uncertainty

Currently, most climate model simulations struggle to accurately model the daily character of precipitation, often as too frequent and too early with insufficient intensity. Therefore model uncertainty is of significant concern and is particularly troublesome with tropical precipitation predictions due to strong diurnal cycles and convection driven precipitation. There is significant variability in the model results (O'Gorman et al., 2009), which are often attributed to the challenges of simulating moist convection, a major cause of extreme precipitation in equatorial regions.

2.3.1 Parametrisation in Climate Models

Climate models, even with high resolutions, are still too coarse for numerical grids to represent many processes. Boundary layer and micro-turbulence, circulations interacting with small scale orography, cumulus

convection and the small-scale physics that occur within clouds are all too challenging to simulate explicitly. It is impossible to represent all physical processes on all scales, so to simplify this, they can be parameterised. Parametrisation is used to describe these unresolvable scales in terms of resolvable scales and approximates the 'bulk' or average effects of processes that are too small or complex to be explicitly represented. Processes that are commonly parameterised include radiation, cloud dynamics and convection. The latter is of interest in this report relating to precipitation in the tropics. Unlike horizontal processes that transport quantities such as momentum or heat, any process that is redistributed vertically tends to have a major part that is sub-grid scale. Hence deep convection is commonly parameterised in larger regional or global models with coarser grids (Prein et al., 2015).

Parametrisation of convection, as an approximation, will naturally introduce error into model results. The interaction between convection and other factors like cloud microphysics, radiation and boundary layer schemes leads to a knock-on effect of the inaccuracies into other components of the model code. The complexity of simulating precipitation processes such as cloud microphysics is also acknowledged to be an issue. It can lead to misrepresentation of extremes, the diurnal cycle and temporal characteristics of precipitation. Generally, parameterised models tend to simulate too much light precipitation (Dai, 2006; Y. Sun et al., 2006; Stephens et al., 2010; Dirmeyer et al., 2012). They do not model MCSs well (e.g. Davis et al., 2003). Many models have shown an underestimation in extreme rainfall (Allan et al., 2008; Dai, 2006; Y. Sun et al., 2006; Stratton et al., 2012). The temporal organisation of precipitation is also not accurately portrayed, generally displaying a 'negative lag' in the diurnal cycle with precipitation compared to observations (Dai, 1999; Betts et al., 2002).

In terms of extremes, an assessment of the 99.9th percentile of daily precipitation from 11 different models was performed considering the tropics and extra-tropics (O'Gorman et al., 2009). It showed that the models were significantly over or under-predicting extremes in the tropics and to improve the simulation of vertical velocities (and so the convective parametrisations) is necessary to increase the result accuracy. The result from the extra-tropics simulations however were more accurate due to them being less dependent on convective parametrisations. Many other studies mentioned previously in this section also discuss the need for improved resolution of the vertical processes associated with extreme precipitation and convection (e.g. Dai, 2006) and is a well-known source of error in models with parameterised convection (e.g. Kendon et al., 2014; Willetts et al., 2017).

2.3.2 Explicitly Calculated Convection

In order for processes such as convection to be calculated explicitly, a finer model grid size is necessary in order to simulate what would normally be sub-grid processes such as larger storms and MCSs. Due to continually increasing processing power more models are now able to explicitly represent these terms.

Although CP models have been used extensively for short-range weather forcasting (Lean et al., 2008), they have only more recently been used to look at longer-term climate related problems. Earlier studies were often over small areas or individual seasons. An early study considering convection over land using CP models found that as long as the model has a small enough grid-size, $\mathcal{O}(1$ km), the diurnal cycle can be accurately simulated (Guichard et al., 2004). This finding was echoed by Dirmeyer et al. (2012) who suggested that large eddy simulations or very high resolution limited area models from around several 100 m to several km was the most likely way of simulating accurate water cycles. The study found that although the diurnal cycle accuracy in CP models was vastly improved, as was seasonal mean precipitation and peak rainfall hour forecasts when compared to satellite data, both CP and parameterised models still had major shortfalls in modelling the diurnal cycle completely due to resolution. Another study by Kendon et al. (2014) also suggest grid scales of $\mathcal{O}(1$ km) for more accurate results. The prospect of simply increasing the resolution of parameterised models has been addressed and has not been found to reduce the inaccuracies of extreme event intensity and diurnal timings (Dirmeyer et al., 2012; Ploshay et al., 2010).

CP simulations have been shown to improve various aspects of climate projections from parameterised models. In particular, the diurnal cycle of precipitation can be better represented using a CP model. Simulations of west Africa using CP models have shown that for the west African monsoon (WAM), explicit

convection provides improved modelling. Latent heat release, more realistic precipitation intensities and temporal patterns including diurnal cycles all show increased precision (Marsham et al., 2013). Enhanced performance in areas of orographic significance and increased accuracy of afternoon rainfall have also been observed, although continuing issues are noted with nocturnal rainfall peaks (G. Zhang et al., 2016). A very high resolution grid (1.5 km spacing) was used to perform future climate simulations over the United Kingdom using an hourly CP model and found that although some rainfall events were too intense, the model was superior in representing hourly precipitation and extremes, especially in summer (Kendon et al., 2014). This is logical since more precipitation is due to convection during that season. The simulations also showed an increase in intensity and frequency in short duration extremes for future climate. Another recent study considers the Indian summer monsoon which presented improvements in the diurnal rainfall peak and greater accuracy of extreme precipitation using 2.2, 4, 8 and 12 km grid-spacing model and explicit convection, with the 2.2 km model in best agreement with observations (Willetts et al., 2017).

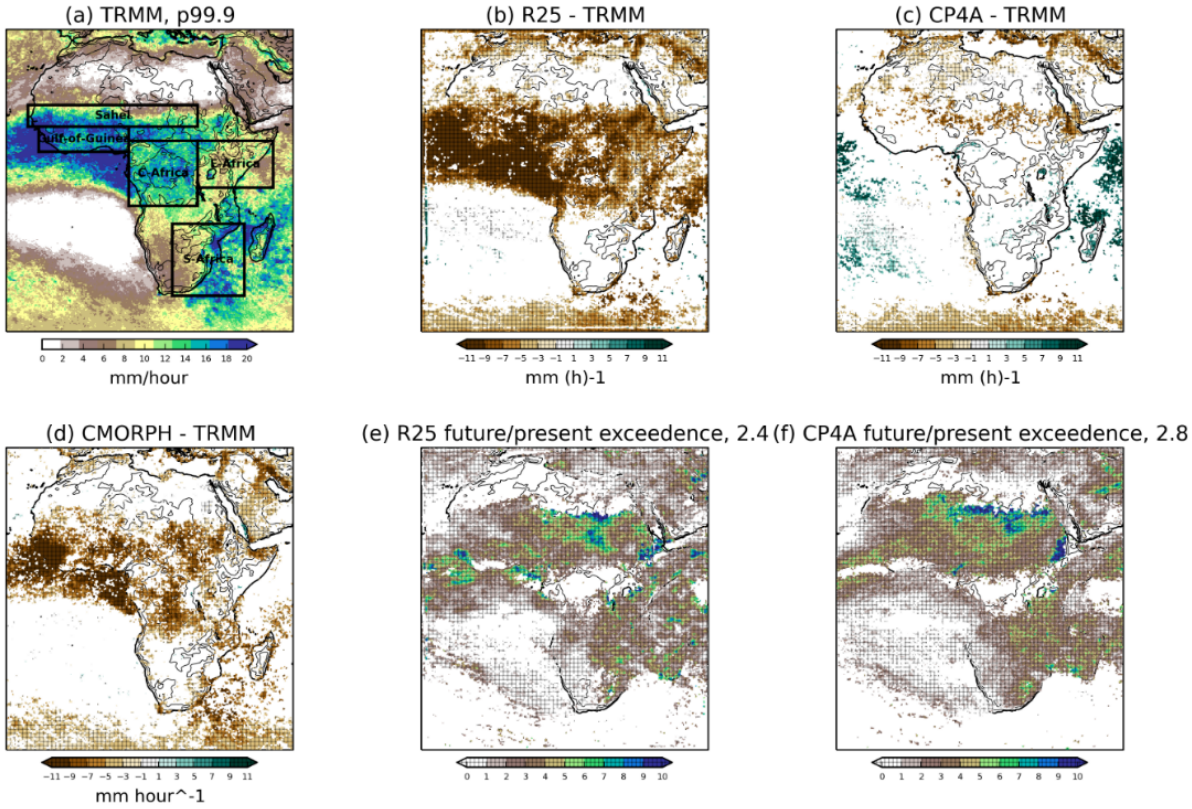

Figure 2: Current extreme precipitation (99.9th percentile of 3 hourly) in the wet season for (a) TRMM satellite observations, (b) P25 - TRMM and (c) CP4-A - TRMM. Differences between CMORPH and TRMM in (d). Ratio of the future frequency of exceedence against frequency of exceedence of current precipitation for (e) P25 and (f) CP4-A. from Kendon et al. (2019).

In the last few years, increased domain and temporally longer CP models have been employed to investigate current and future climate scenarios on a continental scale. A continent-wide CP model was recently run across the United States with 4 km grid-spacing and hourly frequency, for a current and future climate scenario (RCP8.5) (Prein et al., 2017). It showed that almost the entire of the land regions within the United States will experience a median increase of 31.9% for DJF and 26.8% for JJA in extreme (99.95th percentile) hourly precipitation events under warming (Fig. 3).

Another recent large-scale model, CP4-A, is a 10-year pan-African 4.5 km grid simulation for current and future climate (see Sec. 2.2.2). Several studies using this data have been released, analysing the effective-

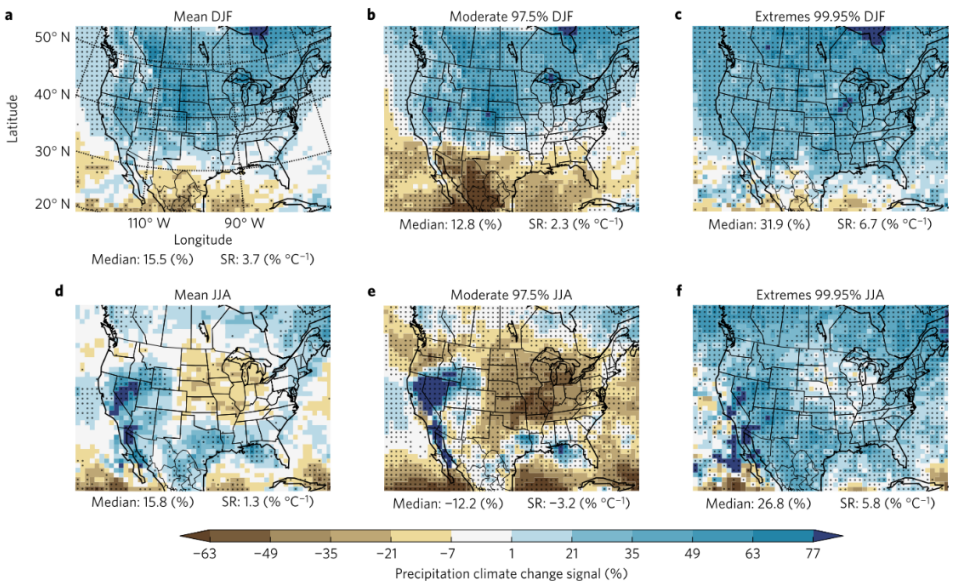

Figure 3: Hourly precipitation relative change between present day and future climate for a convection permitting model run across the continental United States; showing (a) mean increase from DJF; (d) mean increase from JJA; (b) moderate (97.5th percentile) for DJF; (e) moderate (97.5th percentile) for JJA; (c) extreme (99.95th percentile) for DJF; and (f) extreme (99.95th percentile) for JJA. Dotted areas denote regions of significant change. The respective SR (scaling rate; precipitation change divided by mean temperature change) shown below each image. From Prein et al. (2017).

ness of the model compared with an equivalent coarser 25 km parameterised version (P25) with the same specifications and domain. A study analysing the first five years of simulations for JJA noted considerable improvement in average rainfall, plus a notable decrease in the dry bias in west Africa when compared to the parameterised model (Stratton et al., 2018). A more comprehensive study has been released comparing both models against satellite products Tropical Rainfall Measuring Mission (TRMM; Huffman et al., 2001) and CMORPH (CPC MORPHing technique data) (Kendon et al., 2019) (Fig. 2). Extreme precipitation intensity (99.9th percentile) relating to the C-C scaling was investigated, where three hourly extremes were shown to be higher (around 7.8% K^{-1}) than P25 (5.1% K^{-1}) (Fig. 4). In fact, 11% of the grid points in CP4-A showed greater than double the scaling, compared with only 4% for P25. This suggests that the explicit model is capturing more of the dynamical behaviour that enhance the events beyond the thermodynamic scaling as discussed in Sec. A.3. Generally, CP4-A shows enhanced representation of precipitation patterns including extremes compared with P25 which is too light and frequent. Both models demonstrated issues with overestimates around lakes and mountains, which were more pronounced by CP4-A.

The accuracy of CP4-A has been tested over west Africa, where the climate is particularly complex. The model was again compared with P25 and found to provide far better representation of precipitation in terms of frequency and intensity (Berthou et al., 2019). It also displayed better performance with respect to the diurnal cycle, particularly the spatial behaviour around coasts and orography. Simulation of the Sahelian zone precipitation was particularly improved compared with P25. Areas for improvement were noted; the WAM progression (which lasts too long) was seen in both P25 and CP4-A with some wet biases in CP4-A that were more apparent than in P25. Both models predicted the African easterly jet to be too wide, possibly causing wet areas to be wetter and dry areas to be drier. CP4-A showed rainfall as too intense over regions of orography. At grid scale, CP4-A over and under predicts precipitation intensities. Crook et al. (2019) also used models including CP4-A and P25 to analyse the accuracy of MCS simulations in West Africa using a storm-tracking algorithm. The CP models generally simulated numbers of MCSs and rainfall more realistically than parameterised ones. The precipitation rate from simulated storms, however, was not improved in CP4-A, showing too high intensity, with parametrised models having better agreement with satellite data. In agreement with Berthou et al. (2019), large over and under estimates were observed, especially in the Guinea Highlands. It is suggested that the satellite radar data likely under estimates the

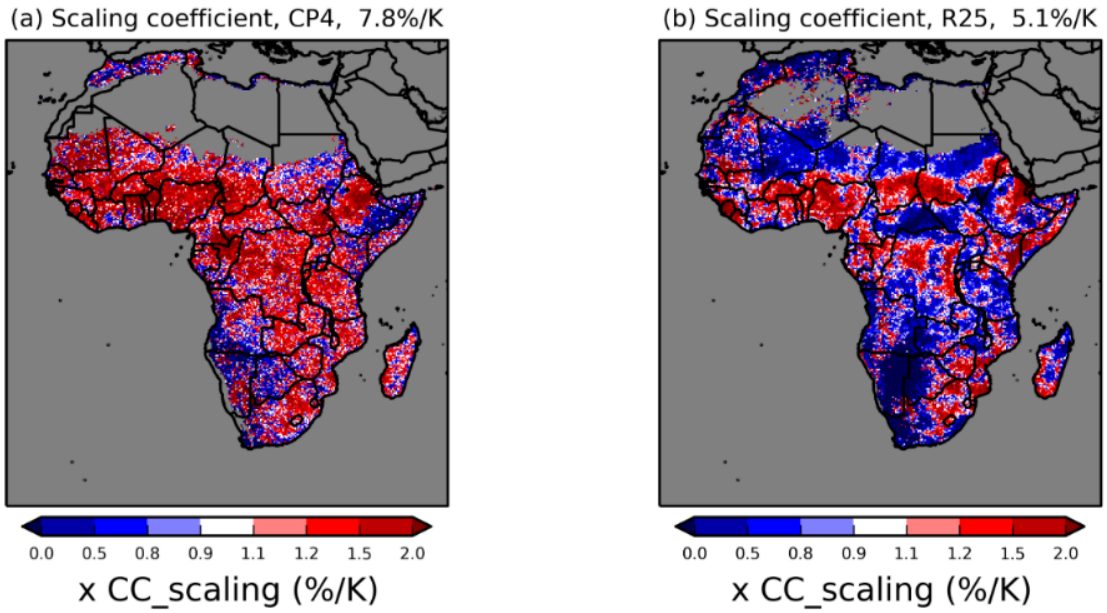

Figure 4: Changes in the Clausius-Clapeyron scaling for 3-hourly extreme precipitation (95th percentile of wet values (>0.1 mm h^{-1})) CP4-A and P25 from current to 2100. Scaling coefficient is divided by C-C relation of 6.5%, so 1 on the scale corresponds to C-C. Areas where less than 5% of data is wet are grey. From Kendon et al. (2019).

largest rain rates, potentially reducing the bias shown for the convection-permitting model.

2.4 Quantifying Extreme Events

Quantifying and predicting long-term extreme precipitation events under climate change is essential for the longevity and well-being of at-risk communities, especially in the global south. Identifying not only individual events but accelerating hydrological trends is a vital process with the anticipated intensification of precipitation under climate change. Here, methods of extrapolating information from existing data sets are described and discussed, with the emphasis on practicality for civil engineering, climatology and hydrology projects. To aid this, well-known statistical methods are outlined however they are heavily documented elsewhere so proofs are omitted, see associated references for details. Commonly used approaches for extremal modelling in hydrology, specifically annual (or block) maxima and peaks over threshold (or partial duration series) methods are considered. The statistical processes mentioned can be used with the hydrology modelling approaches to construct intensity-duration-frequency (IDF) or depth-duration-frequency (DDF) curves. These are often used to graphically display long-term return periods of rare precipitation events and are described in the final sub-section.

From the numerous studies performed using regional and global models, it is almost unanimous that the rate of change of frequency and intensity of extreme precipitation events will exceed mean precipitation under climate change (Kharin et al., 2013). It is therefore important to first consider what the definition of an 'extreme event' is. There is no definitive answer to this, however the way an event is defined has a direct impact on the way it would vary under a warming climate (Pendergrass, 2018). Schär et al. (2016) examined how results gained using three different common percentile indices used to describe extreme precipitation provide very different interpretations of the same scenario. It was concluded that all-day percentiles, wet-day percentiles and frequency of events above a threshold all show significant differences. So although the growth in extremes is not being questioned, the quantitative increase is uncertain. The difference between the type of extreme - whether it be an increase in frequency or an increase in intensity can also change the appearance

of the results from the same study (Fig. 5).

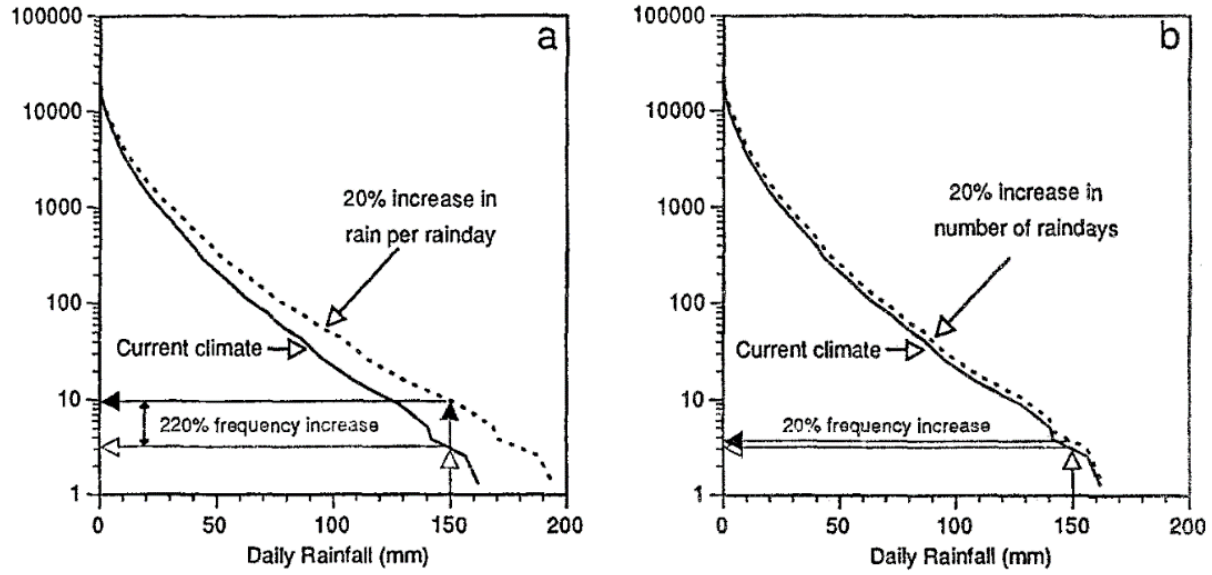

Figure 5: Frequency distributions before and after a 20% increase in precipitation for measurements in Auckland, New Zealand, showing (a) the daily rain intensity increase per wet-day; and (b) an increase in the number of wet-days. Dotted lines are the values with a 20% increase. Solid lines are current (1909-1986) data. Vertical axis is the number of days per 100 years precipitation value will occur. A distinctly different impression can be observed from the results depending on the type of measurement used. From A. Fowler et al. (1995).

There is no consensus on the 'best' definition for an extreme event. The size and type of the individual data sets plus the type of result required should be considered. 'Soft' extremes, typically 90th and 95th percentiles are useful for shorter length data sets with few extremes or for studies not considering long-term or extremely rare events. For less frequent events, larger data sets and for longer return periods, specific selection criteria (discussed in Sec. 2.4.4) with statistical distributions is generally accepted to be more effective. Previous computational and observational studies considering precipitation extremes have used a wide variety of methods to define extreme events. These range from using simple yearly or daily maximum rainfall values or intensity classes (e.g. Räisänen et al., 2001, A. Fowler et al., 1995) to more complex statistical sampling approaches required by the use of asymptotic distributions (e.g. Zwiers et al., 1998; H. Fowler et al., 2007; Zolina et al., 2009).

2.4.1 Statistical Methods of Representing Extremes

The probabilistic theory of extreme values is well understood (for detailed information, see Leadbetter et al. (2012)). In terms of flood and rainfall frequency analysis, extremal studies can be traced back to 1852 (Stewart et al., 1999). Very early work on statistical extremes include Gumbel (1941), who considered the return period of flood events and later wrote one of the first books on the statistics of extremes (Gumbel, 1958). Since then, practical modelling of extreme events using asymptotically justified models has been an active topic in research, especially in hydrological studies, economics and socio-economics. This methodology can be employed with existing data sets that have long enough records (for discussion on appropriate lengths, see Sec. 2.4.4), allowing extrapolation beyond the range of existing data to analyse rare events not well sampled by the data set (e.g. in extremely rare precipitation events). For precipitation peaks, a continuous distribution is required. The two main classes of extreme value distribution of interest for this project are the asymptotic distributions for a sequence of maximum or minimum values - the generalised extreme value distribution; and the distribution for all peaks over a chosen threshold - the generalised Pareto distribution.

2.4.2 The Generalised Extreme Value and Pareto Distributions

The generalised extreme value (GEV) distributions (Jenkinson, 1955) are continuous 3-parameter probability distributions, encompassing the three asymptotic models: Gumbel, Frechet and Weibull types from the extremal types theorem (see Gnedenko (1943) for derivation). They can be used to infer the probability of extreme values beyond the length of the data set or function by gaining inference on the tails of these distributions. It is well suited to a data set with a large number of peaks in a block/year where the parent distribution is normal, dictated by the central limit theorem (Coles et al., 2001). The cumulative distribution function (CDF) is:

$$G(x;\mu,\sigma,\xi) = \exp\Big(-\Big[1+\xi\Big(\frac{x-\mu}{\sigma}\Big)\Big]^{-1/\xi}\Big) \tag{1}$$

for parameter space $\{(\mu,\sigma,\xi) : \mu \in \mathbb{R}, \sigma > 0, \xi \in \mathbb{R}\}$ where μ, ξ and σ are the location, shape and scale parameters respectively and x the data values. The parameter set for various distributions is often referred to as the vector θ. The shape parameter determines which of the three types above are used: $\xi = 0$ is Gumbel, $\xi < 0$ is Frechet and $\xi > 0$ is Weibull type. When ξ is zero (for the Gumbel type), G is undefined, so the distribution is taken as $\xi \to 0$:

$$G(x;\mu,\sigma) = \exp\Big[-\exp\Big[-\Big(\frac{x-\mu}{\sigma}\Big)\Big]\Big] \tag{2}$$

with parameter space $\{(\mu,\sigma) : \mu \in \mathbb{R}, \sigma > 0\}$. These distributions are used to fit curves to data sets of functions which have independent and identically distributed (IID) variables. For minimum values of a data set, Weibull is useful and Gumbel is often used for the block maxima method which uses one value per block of data (often a maximum annual value) which are then evenly distributed and very likely independent (see Sec. 2.4.4). The location parameter (μ) is broadly equivalent to the mean (determines the centre position of the distribution), scale (σ) is similar to the variance, and shape (ξ) relates to the skewness, so how the tail decays. Many studies have considered the effectiveness of this method; Haktanir et al. (1993) considered the performance of nine distributions with the annual maxima method in relation to flood extremes, determining that GEV predicted the $>T_{100}$ year return period better than other distributions. GEV and Gumbel were both deemed most effective at modelling the annual maximum rainfall in Athens with a 136 year data set, although Gumbel was more suitable for shorter length series (Koutsoyiannis et al., 2000).

Another important distribution that is effective at describing the peaks above a threshold approach (see Sec. 2.4.4) is the Generalised Pareto (GP) distribution (Pickands III et al., 1975). This two-parameter distribution, derived from (1) (see Leadbetter, 1983) and applied to a data set $\{x_1, x_2, ..., x_i\}$ exceeding a known threshold u where $x_i : x_i > u$, with parameter space $\{y : y > 0, (1+\frac{\xi y}{\tilde{\sigma}}) > 0\}$ (where $\tilde{\sigma} = \sigma + \xi(u-\mu)$) is defined by:

$$G(x;\xi,\sigma) = 1 - \Big(1+\frac{\xi y}{\tilde{\sigma}}\Big)^{-1/\xi}, \ \xi \neq 0 \tag{3}$$

$$G(x;\sigma) = 1 - e^{-y/\tilde{\sigma}}, \qquad \xi = 0 \tag{4}$$

This distribution has used to predict long-term return periods of precipitation. Knote et al. (2010) investigated changes in extremes under climate change for various climatic features including precipitation for an area of Germany using a CP simulation and chose the POT method due to a short data set length; the GP distribution was applied to daily rainfall in Western Australia to investigate a decreasing trend in extremes and was used to identify changes in rainfall behaviour between 1930 and 2001 (Li et al., 2005);

and Shongwe et al. (2011) considered extreme rainfall in east Africa under climate change using the GP distribution, projecting an increase in intensity for one in ten-year events and less severe dry extremes.

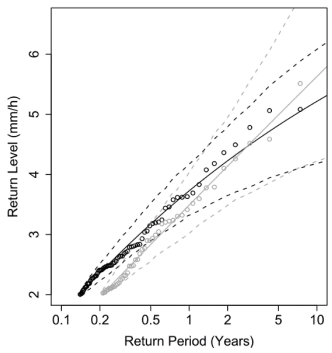

Figure 6: Precipitation return periods for a region of Germany determined from the GP distribution. Dotted lines are 95% confidence intervals. Solid black is 1960-69 and grey is present day climate (2015-24). From Knote et al., 2010.

Extreme value theory is a standard methodology for predicting rare events and is widely used, however it should be noted that there are several reasons why systematic under-estimation often occurs when employing this method. Firstly, acknowledging uncertainty is essential but regularly overlooked. Secondly, it is common to reduce the dimensions of the probability distributions for the simple reason of complexity. This can lead to unjustified levels of confidence when predicting the likelihood of an extreme event.

2.4.3 Parameter Estimation

In order to estimate appropriate location, scale and shape parameters for the distributions, several methods are available. This includes probability weighted moments or linear combinations of L-moments (probability weighted moments (PWMs); Landwehr et al., 1979; Greenwood et al., 1979); method of moments (MM); and method of maximum likelihood (MML; Dupuis et al., 1998). PWMs are a popular method for predicting hydrological extremes as they are computationally simple, work well with smaller sample sizes and are less sensitive to outliers (Hosking et al., 1985; Hosking, 1990). A downside is that it is more difficult to incorporate covariates (Katz et al., 2002). Method of maximum likelihood is another popular choice (Davison et al., 1990):

$$L(\theta; M_1, M_2....M_i) = \prod_{a=1}^{i} f(m_i; \theta) \tag{5}$$

where L is the probability of observing the data provided, M_i are the series values, θ is the unknown parameter vector and f the asymptotic distribution. This can be simplified by taking the *log* as this is a strictly increasing function and will not effect the outcome for θ, providing the log-likelihood function:

$$l(\theta) = \log L(\theta) = \sum_{i=1}^{n} \log f(m_i; \theta) \tag{6}$$

This provides a simple method of maximising or minimising the parameter vector θ.

2.4.4 Determining Sampling Methods for Extreme Rainfall Estimation

Identifying the most appropriate extreme values from a potentially large series to use with the asymptotic distributions noted in Sec. 2.4.1 can be troublesome. Obtaining estimates for the return period, T_i, a statistical definition that defines the average interval i between each event of a particular probability occurring

(sometimes called a re-occurrence interval), has two commonly used approaches.

The most common method of predicting re-occurrence intervals of extreme precipitation in engineering and hydrology is sampling using the block or annual maxima (AM) method (here it will be referred to as the annual maxima method since yearly maximums are of interest) (Kharin et al., 2007; H. Fowler et al., 2007; Min et al., 2011). This takes a sequence of independent and identically distributed (IID) variables X_i such that $M_n = \max\{X_1, X_2, ..., X_n\}$ for i blocks, leaving a set of maximum values $\{M_{n,1}, M_{n,2}....M_{n,i}\}$ (the annual maxima series). This method is relatively easy to obtain the data series for as it is extremely unlikely that two peaks in consecutive years are from one single event. The challenge is to determine what happens as $M_{n,i} \to \infty$. As discussed in Sec. 2.4.1, the GEV and Gumbel distributions are a commonly used and appropriate choice for modelling the AM method as they approximate the sampling behaviour of maximas chosen from regularly sized blocks (Stewart et al., 1999; Kharin et al., 2007).

Rather than considering maximas in fixed time periods, it is possible to use exceedances over a threshold instead. The peak-over-threshold (POT) analysis takes all distinct values $\{x_i\}$ above a designated threshold u for the data series. This can be more beneficial that the annual maxima method since it excludes any unusually small maximums in selected years/blocks and potentially provides a larger data set. This may provide a more comprehensive as it includes all extremes no matter how many fall in one year. However, it is necessary to determine an appropriate threshold - this is a subjective judgement that makes it difficult to compare one study to the next, whereas the annual maxima method has a predetermined series size which is excellent for reproducible studies. Depending on the choice of probability distribution, it is also essential not to include too many values, i.e. ensure the threshold is not chosen too low or too high. It is a balance between precision (lower threshold will provide more points, potentially increasing the certainty of the results) and bias (EVT is only valid for modelling the tail end of most normal distributions). Another complication in the POT method is defining the criteria for independent events, as several adjacent peaks could be considered the same event, so it is another arbitrary choice (depending on the physical basis of your sample) as to how to determine the temporal dependence of these events.

The sensitivity of extreme-value modelling to the choice of threshold is a well-documented issue (Wadsworth et al., 2012; Carreau et al., 2009). With long-term meteorological records, for simplicity, a typical choice for the POT threshold is one that provides between two and five peaks a year (Stewart et al., 1999). The FEH Volume 3 quotes an average of four or more peaks a year (Robson et al., 1999). More complex methods exist for determining the most effective choice of threshold such as mean residual life plots (Davison et al., 1990). By plotting the mean exceedence above the threshold as a function of threshold (calculated by taking the mean of the exceedences above u, minus u), it is possible to determine the best choice based on where the plot is approximately linear. (Fig. 7) shows a mean residual life plot from Coles et al. (2003) where the study chose $u = 10$ for the threshold where the line becomes more linear.

Threshold choice is important since it is assumed that the occurrence of threshold exceedances are consistent with a Poisson distribution. This assumption of a Poisson rate of extreme events is made more complex since most extreme data for climate variables will have a tendency to cluster due to periodic behaviour (e.g. diurnal or seasonal cycles). A threshold choice too low will compromise the assumption of asymptotic extreme values and introduce bias, whereas a choice too high will limit the number of values available for analysis. Relatively little attention has been received in relation to the trends in climatic phenomena for the POT method and often the AM method is used as an alternative to avoid this issue (Katz et al., 2002).

Both AM and POT have been compared to determine the most effective approach for estimating return periods. Madsen et al. (1997) considered POT with a GP distribution and AM with a GEV distribution to determine the accuracy of estimated T-year events. It was argued that POT is generally preferred. The UK Flood Estimation Handbook (FEH, Robson et al., 1999) recommends POT where appropriate data is available, especially the case with less than 14 years of data as it is claimed to ahow improved accuracy in the results. A study by Coles et al. (2003) considered rainfall data at one location in Venezuela with 30-50 years of daily rainfall data. The calculated return period curves for Gumbel, GEV, GP and a Bayesian method were compared and can be seen in Fig. 8. The Gumbel model underestimates the return period, the GEV

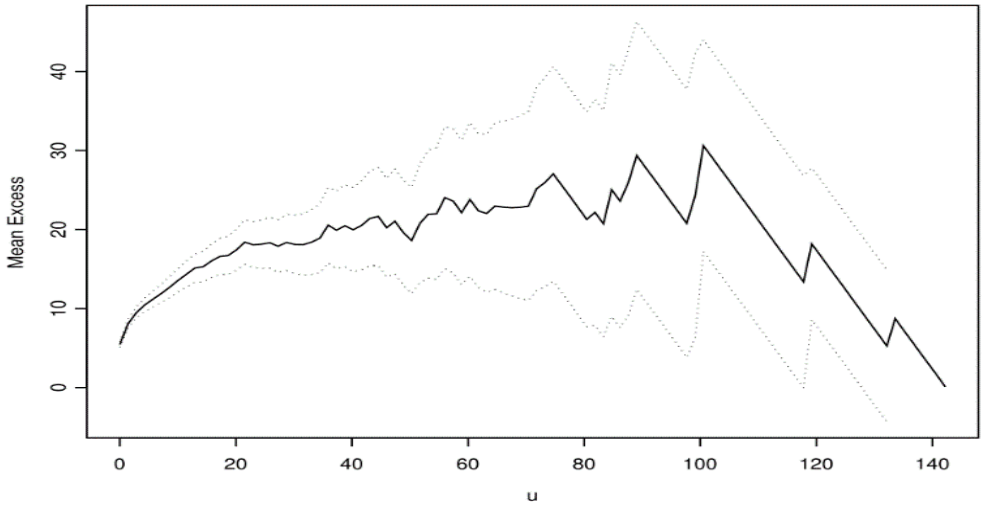

Figure 7: Mean residual life plot for daily rainfall in Venezuela. Dotted lines are 95% confidence intervals. From Coles et al. (2003).

overestimates and the GP is reasonably close with a slight overestimate. Without investigating the Bayesian method further which is closest to predicting the most extreme event, the GP method is determined to be an excellent choice for rare event predictions in this region.

2.4.5 Identifying Independent Events

An issue with using either AM and POT is the question of independence. As mentioned in Sec. 2.4.1, the data points must be IID - independent and evenly spaced. With AM, it is unlikely that the values extracted from adjacent years will be part of the same cluster or event. However, with POT, this is far more challenging to determine. The definition of an independent event is addressed by Cunnane (1979) who determined that a peak is independent if the value between peaks drops below a particular value and the time between events exceeds a critical length. However, this is subjective and fully depends on the required result and data set. Several studies other have described procedures by which a point-precipitation series can be split into statistically independent events, however the methods are data dependent and are only applicable under certain circumstances (Restrepo-Posada et al., 1982; Brown et al., 1985).

De-clustering is a technique whereby only the highest peak in a multi-peak event is used to avoid the effect of temporal dependence (Ferro et al., 2003). For an univariate sequence, such as a time-series in climatology, two well-known schemes can be used; blocks or runs. Blocks method splits the series into equal length sections and determines everything belonging to individual blocks as independent of values in all others. The other option is runs which stipulates that any value over the threshold separated by fewer than r non-extreme values is dependent. The second is far more appropriate when considering climatological events such as storms, as a storm could easily fall over the boundary of a segment in the blocks method.

2.4.6 Graphically Representing Extremes

Intensity-Duration-Frequency (IDF) or Depth-Duration-Frequency (DDF) curves are useful graphical methods of quantifying extreme rainfall. They provide intensity and duration precipitation predictions for often very long return periods. These are commonly used in civil engineering and urban planning to aid in infrastructure design of drainage systems, bridges and roads to mitigate risk of flooding and damage.

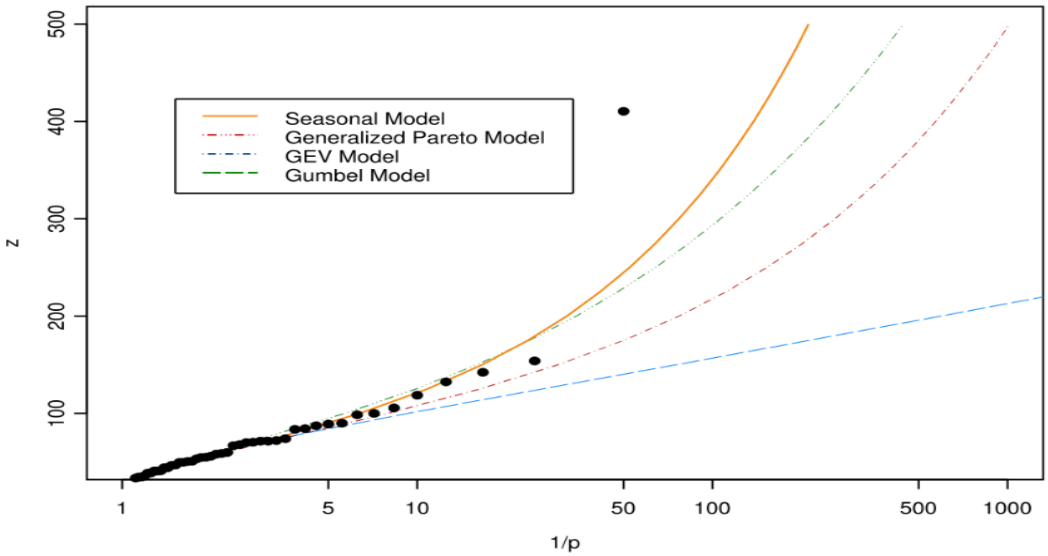

Figure 8: Comparison of different asymptotic models, with daily rainfall rate on the vertical axis. From Coles et al. (2003).

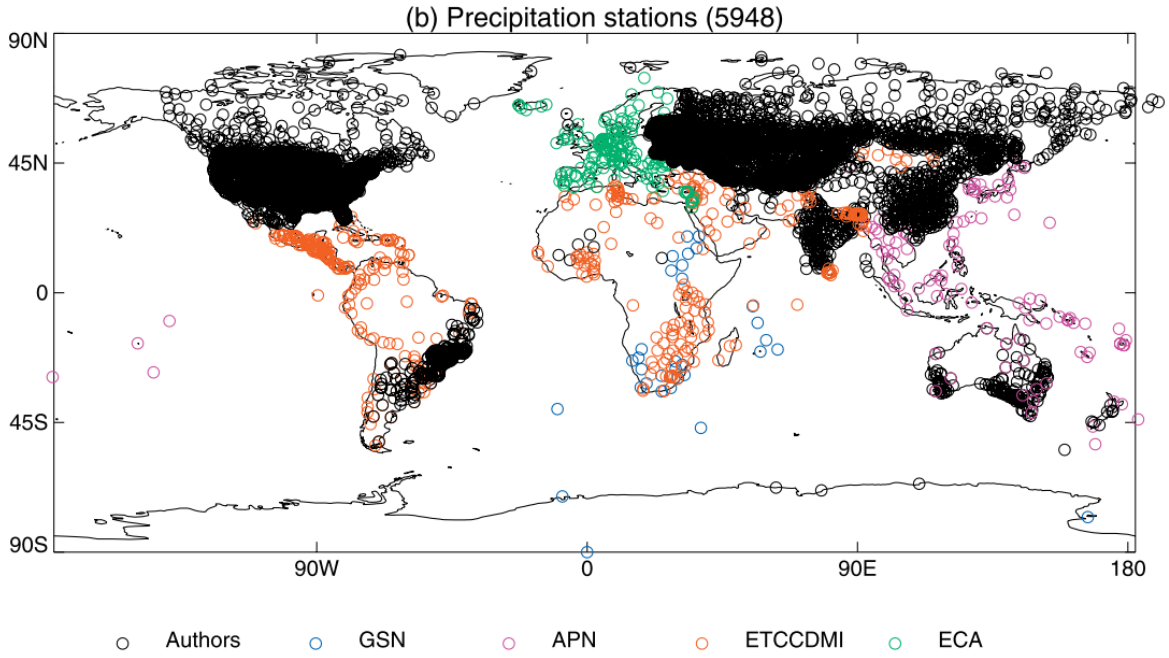

Figure 9: 5984 global precipitation stations from various different climate monitoring organisations. From Alexander et al. (2006).

A challenge with creating IDF curves is the lack of long-term reliable rain gauge records (Fig. 9). This is a particular problem in many areas of the global south, where regional records are often fragmented, discontinuous or simply have an absence of systematic data management (Lumbroso et al., 2011). Large sections of the African continent are particularly affected by this (Giesen et al., 2014). Observation stations are, apart from South Africa and at airports, very sparse (Basic Systems (CBS), 2009, see Fig. 10). This means that often, to produce IDF curves for a particular region involves using data from a climatologically

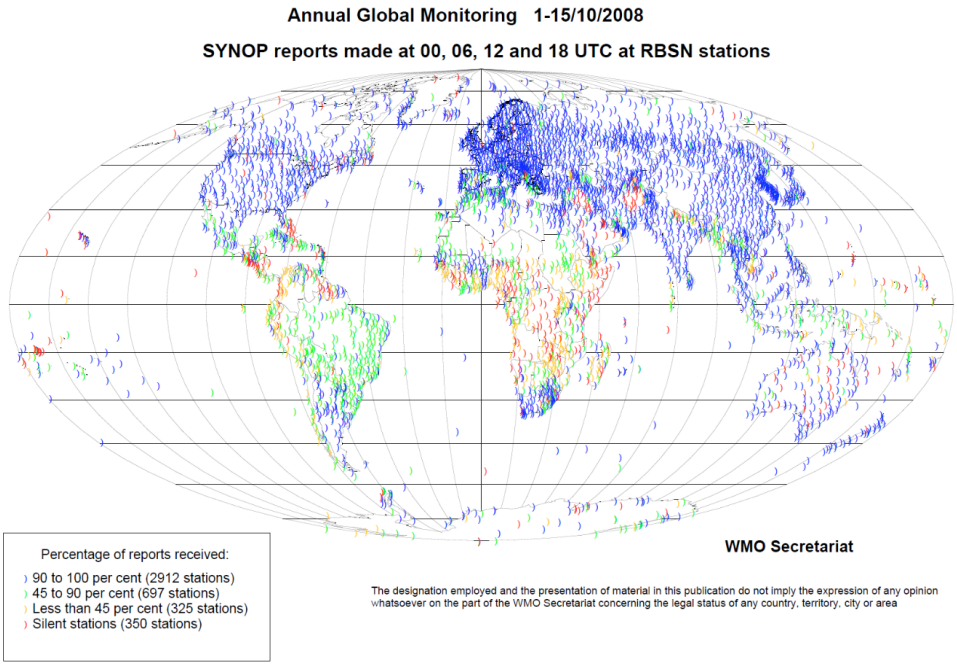

Figure 10: Global precipitation stations showing percentage of reports received and silent stations. From Basic Systems (CBS) (2009).

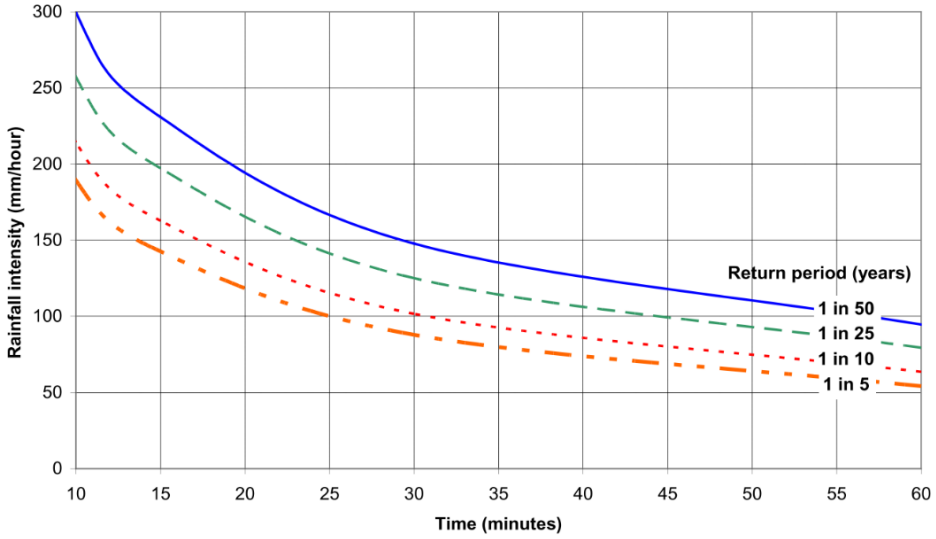

Figure 11: A short duration intensity-duration-frequency curve for an airport in the Bahamas. From Lumbroso et al. (2011).

similar region, or take parts of different regions where data was available and 'stick' them together. Another way of dealing with the scarcity is to interpolate between observations which does not work well when measurements are spatially far apart (Kumari et al., 2017). The temporal resolution can also be an issue. Only rarely do historical rain records have sub-daily data, making infrastructure design for flood water drainage challenging. It is also recommended that to construct reliable IDF curves, a minimum of ten years of data is available (Lumbroso et al., 2011).

2.5 Summary

Using the impacts of climate change as a motivation, precipitation extremes were discussed, followed by a review of the African climate, highlighting weaknesses in climate modelling such as the parametrisation of convection. By focussing on the parametrisation of convective terms, substantial issues, especially in tropical regions were highlighted. Generally, CP models behave better, especially in tropical regions where deep convection is a significant cause of precipitation. A new pan-African climate model was introduced and the benefits and drawbacks highlighted. Finally, statistical methods of predicting long-term return periods for precipitation events was presented, considering the best options for differing types of data, highlighting the EVT as an appropriate choice for AM series and GP for POT methods. There are other families of probability distributions that may be appropriate, however the literature puts emphasis on the above methods. Alternative distributions and Bayesian methods could be reviewed in future work (Coles et al., 2003).

3 Methods

The aim of the first part of this project is to analyse the simulation data from two climate models and examine how return periods are modified under climate change for both simulations over large areas of east Africa. The secondary aim is to determine differences between the results from the parameterised and CP model when subject to temporal and spatial smoothing, as extremes on varying space and time scales have different consequences (as mentioned in Sec. **??**). This section includes a brief introduction to the data currently being used for this project, as well as methods and ongoing work. Some (in process) results are presented in Sec. 4.

3.1 P25 and CP4-A Simulation Data

The data used for this project is the hourly precipitation from both CP4-A and P25 simulations, created within the Met Office led IMPALA project of the DFID/NERC FCFA programme using the IPCC RCP8.5 scenario (introduction in Sec. 2.2.2). The rainfall values are hourly, with 2100 x 2000 and 366 x 236 (latitude x longitude) spatial grid points respectively over a ten year time-span. For a time-series at any location there are 86400 values for each model, for current (1997-2007) and future (end of the century) data sets. Current work has been focussing on the P25 simulation and much of the data used in the first part of this section is from a particular location in Kenya for analysis and method development. As both P25 and CP4-A have the same temporal scales, the methods used below will be valid for both data sets. Spatially re-gridding the CP4-A native finer grid to the coarser P25 grid will be necessary to make reasonable comparison between models.

Much of the following section uses data for a particular location - Kampala in Uganda - a city near the edge of Lake Victoria, a large inland lake in eastern Africa. However the methods used have been applied to multiple individual locations across east Africa, including coastal and inland locations (such as Nairobi, Kenya; Mogadishu, Somalia; and Kisumu, Kenya; plots included below where appropriate) to check for consistency before applying to a larger region of Africa (for locations and domain map see Fig. 12). These processes are then applied to larger areas across central/east Africa, providing maps of T-year return periods. This area was chosen due to the geographical variety provided to test the effectiveness of the extreme value modelling. The ratios of the change in precipitation under climate change are also mapped, demonstrating the predicted changes in T-year return periods between current and future simulations.

3.2 Processes

The initial aim of this part of the project is to identify independent extreme precipitation events and predict rainfall rates for associated return periods, potentially beyond the time-series length using extreme value distributions. The changes in these return periods under climate change will then be addressed. Both block/annual maxima (AM) and peak over threshold (POT) methods with associated asymptotic distributions are analysed for effectiveness and applied at locations in Africa. In order to do this, there are various aspects that need addressing when considering methods for long-term extreme precipitation predictions; sampling methods (including appropriate threshold determination); the best way to identify an independent event; and most fundamentally, which model is the most effective at predicting long return periods for the data sets available.

3.2.1 Sampling Method

For annual maxima, the sampling is trivial. The largest precipitation rate in each yearly block is chosen, providing a set of 10 data points for each simulation. For POT, the sampling is more complex. A threshold must be chosen and a method of identifying individual precipitation events is needed.

There are several different suggested guidelines for how a threshold should be chosen for the POT method, as discussed in Sec. 2.4.4. Some studies simply advise to choose a threshold that provides a certain average number of values per year or all independent values above a chosen percentile. Another method in the

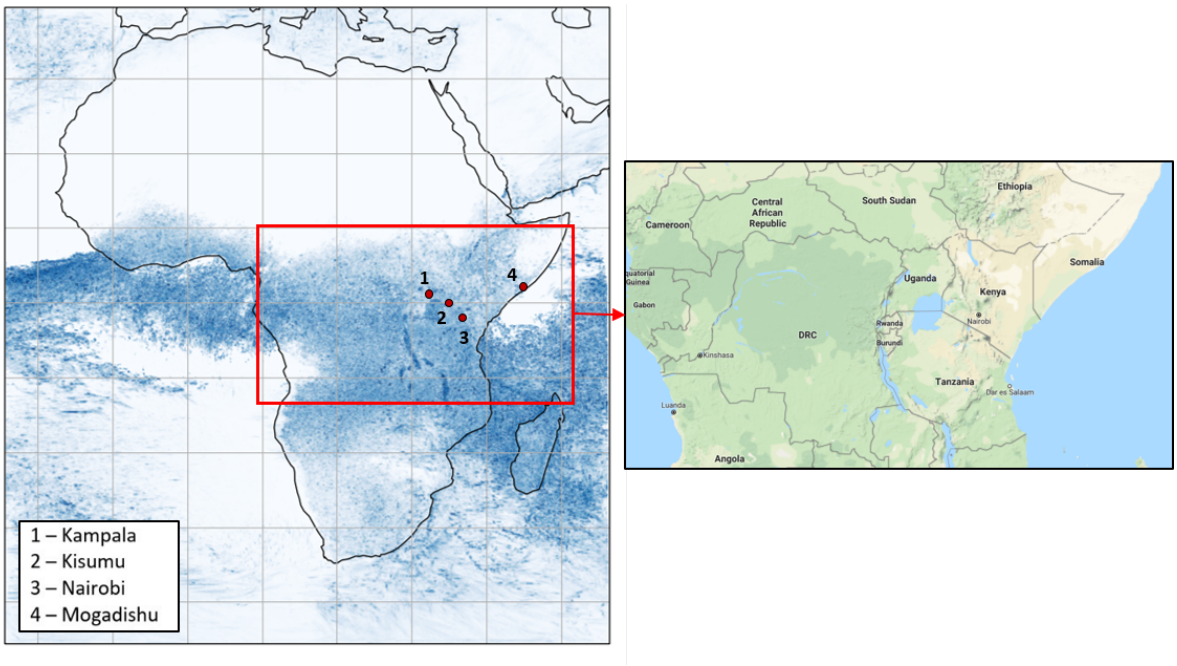

Figure 12: Domain map of P25 and CP4-A including the individual locations considered here and region of interest. The example map used here is showing a contour plot for maximum rainfall values in MAM in 1997. Map provided by Google Maps.

literature suggests mean residual life plots (Sec. 2.4.4). This is a procedure to estimate the most appropriate choice of threshold and an example is shown for this data in Fig. 14. The region where the graph is approximately linear is suggested to be an appropriate choice, in this case, between 10-20 mm hr^{-1}. It is generally sensible to choose the lowest reasonable threshold value to include as many data points as possible for analysis (Coles et al., 2003).

The mean residual life plot shown in Fig. 14 is an effective way of identifying a threshold for an individual location, however it is not always a simple task to interpret the results and most certainly would not be a straightforward option for applying to a large selection of data points across Africa. The option of taking all independent points above a particular percentile or an average number per year would most likely be just as effective assuming it was chosen within an appropriate range. Determining this appropriate range is the aim of the following sections.

The other consideration when choosing a threshold is that when a time series is temporally aggregated, the magnitude of the threshold will change. The percentile will also need to vary, as the smoothing will reduce the number of 'sharp' peaks.

3.2.2 Determining Independent Events

The problem of independence with the POT method is still an active question. Very few places in the reviewed literature explicitly state what should be classed as an independent event in a rainfall time-series and many do not mention how it is determined at all. To identify what the storms looked like over a threshold and to determine the approximate length of them, the raw data was plotted with a threshold of 56 mm hr^{-1} (the 99.96th% percentile) as shown in Fig. 13. This shows a total of 28 independent values exceeding the threshold. To ensure the peaks are from independent events, a chosen hourly distance either side of a peak was calculated, within which all data was determined to belong to the same event. This time-period was estimated by looking at the duration of storm peaks at different thresholds (Fig. 15). This plot highlights an interesting feature, that at any of the thresholds above an almost zero value of 0.04mm hr^{-1}, the storm durations are approximately the same. So for thresholds up to around 7mm hr^{-1}, the largest storm duration

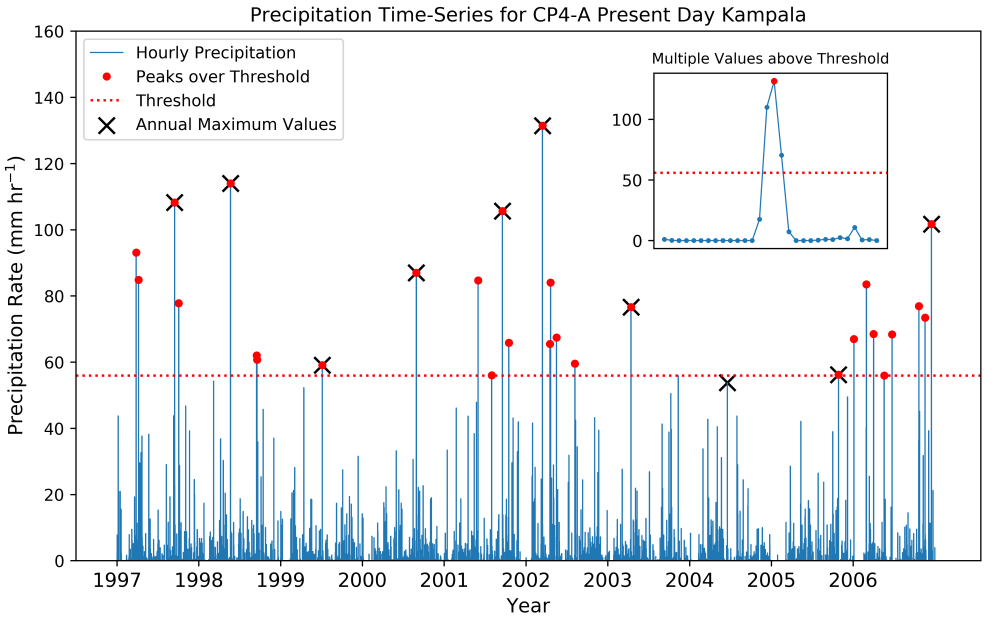

Figure 13: Precipitation time-series from Kampala using CP4-A present day data, with the peaks over an example precipitation threshold (red points) of 56 mm hr^{-1} (99.96th percentile), shown by red dotted line. AM values marked in black. Inset: close-up of the largest peak, near the beginning of 2002. A second and third peak over the threshold can be observed in the 6-hour interval either side of the first event, therefore not independent values and discounted.

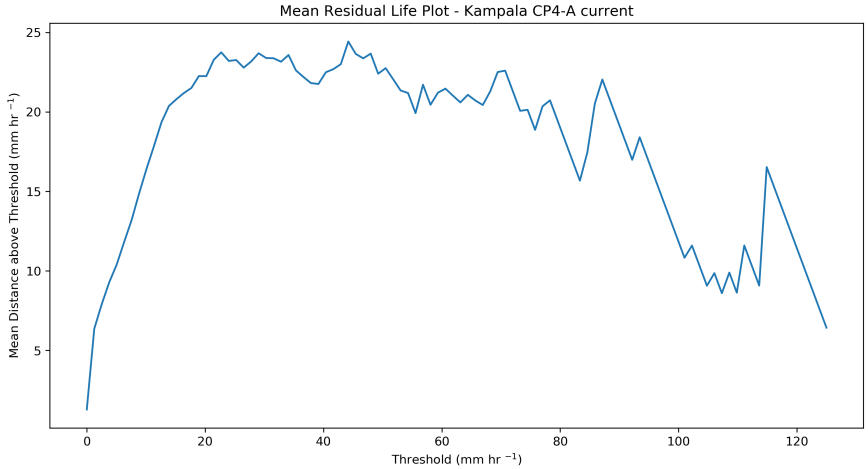

Figure 14: Mean residual life plot - Kampala CP4-A present day data, showing an appropriate threshold choice of around 10-20 mm hr^{-1} where the plot is approximately linear.

appeared to be a maximum of approximately six hours. This value is consistent with other locations in east and west Africa.

The peaks highlighted in Fig. 13 can be considered individually. Fig. 16 shows the 28 event peaks with 6 hours either side for Kampala using CP4-A present day simulation. The dotted lines show a six hour window with the peak at the centre and the average rainfall over that period is denoted by the solid horizontal light blue line. The six hour window appears to capture the storm events for this location.

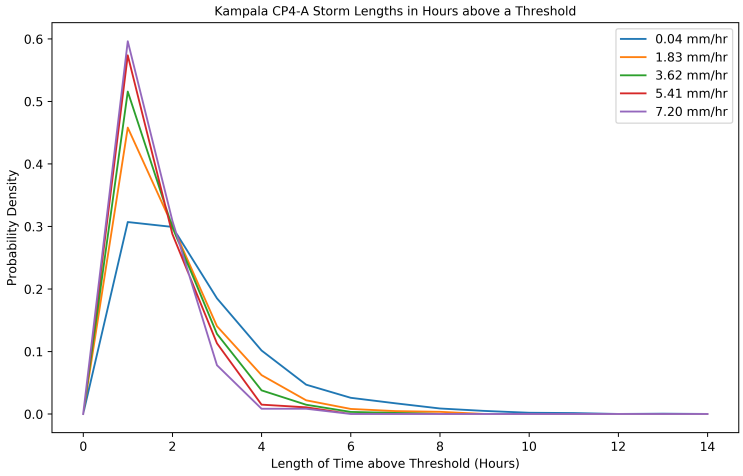

Figure 15: Probability density for storm widths (in hours) using five different thresholds

3.2.3 Spatial and Temporal Smoothing

So far, the data has only been analysed on an hourly basis. IDF curves display a set of relevant durations which would necessitate different temporal averaging periods. Options for averaging include consecutive blocks, for example, an average over each daily block using a specified start time (ideally avoiding interrupting the peak diurnal rainfall). This is a simple process but would involve different start times depending on which location in Africa was chosen. Convolutions (or sliding box averages) are another option which would retain the same number of points (nearly) as the time-series and not necessitate a starting value. There is a strong argument against this method however as it potentially decreases the independence of the points. It is worth considering if this is helpful for predicting very short rare events as it 'spreads' the data. There is also a limit to the duration of the averaging before the data becomes too spread out, fundamentally 'hiding' individual events. However, it is very effective for considering every possible combination of hours, meaning it will not inadvertently miss a rare event due to the consecutive block cut-off and can be applied pan-Africa without the concern of varying diurnal cycles for different regions.

The effect of the averaging changes the fundamental characteristics of the storm events. Fig. 17 shows storm durations (like Fig. 15) for various sliding average durations. Averages for 7, 13 and 25 hour periods (odd numbers are most appropriate for convolutions) were calculated for the ten-year time-series for five different precipitation thresholds. The average storm duration widens and the peak decreases in intensity with each increased smoothing applied, as expected. This does however give an unrealistic view of the storm duration and will affect how rare events appear. As the intensity decreases with smoothing, the threshold will also need to be lowered to accommodate this. The distance between each peak to identify independent events will also have to be larger. The plots show that the most common storm duration relates to the averaging length. The duration of the storm for a smoothing of 7 hours is up to around 20-25 hours. For 13 and 25 it is far less clear and there is more noise, but event duration do not settle down until 50 or 60 hours. This would suggest that the minimum duration across the centre of a peak for these values may have to be as long as 60 or more hours.

Something to consider is that different spatial locations will have varying rainfall patterns. The seasonal and diurnal intensity and patterns will vary vastly between the diverse regions of the continent. The primary location used here has noticeable diurnal and seasonal precipitation characteristics as expected in the tropics, whereas other regions may not. Some locations, such as Burkina Faso in the Sahel region, show very strong relations between seasons (and on a smaller scale, time of day). This means that the data may be considered more or less independent in certain regions, suggesting that there may be different distributions/statistical methods that would suit different areas. It is important to note that for a data set such as hourly precipitation values over several years, there may be temptation to consider using a normal distribution (central limit theorem states that the sum and the mean of an arbitrary finite distribution are normally distributed

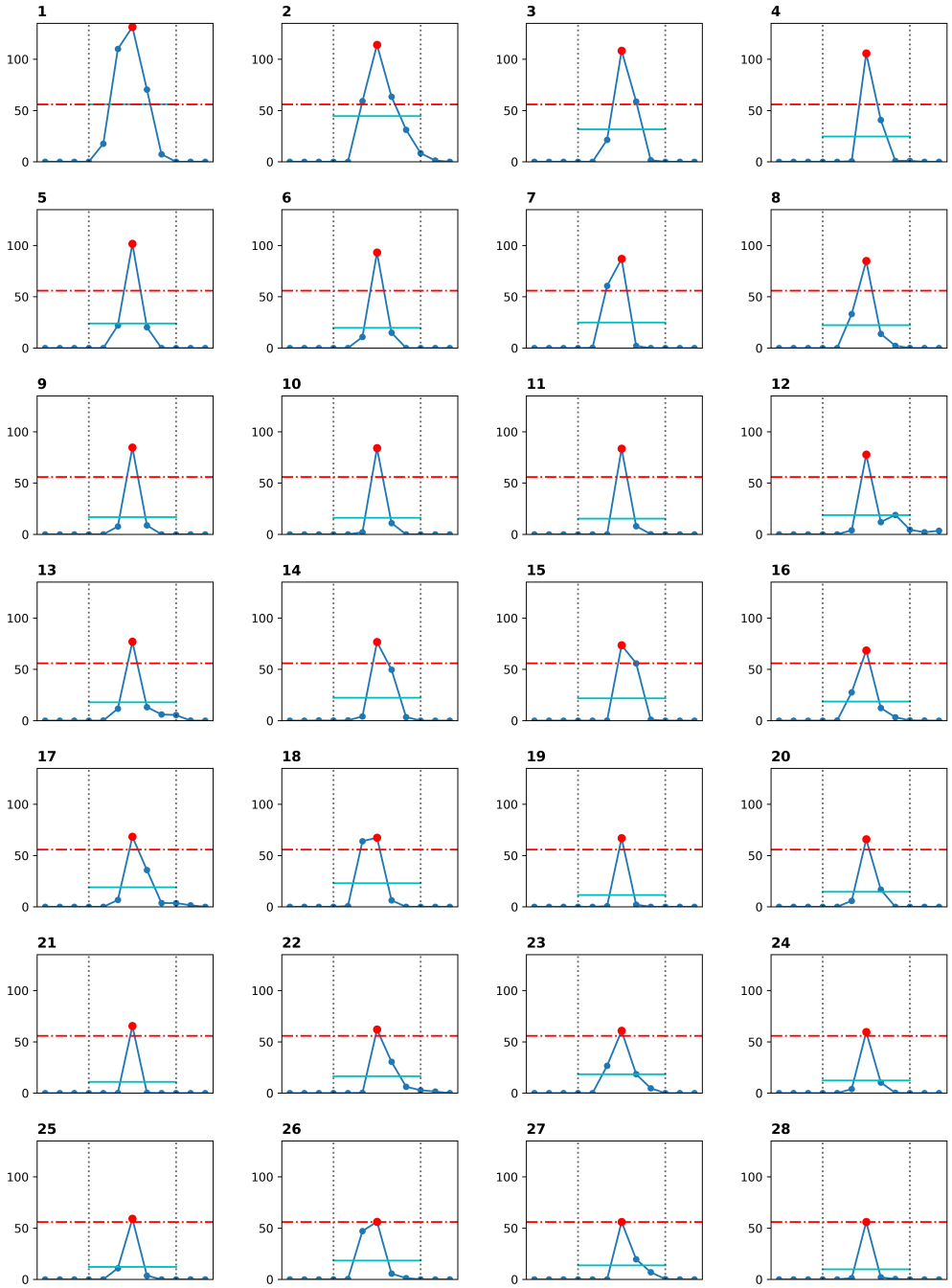

Figure 16: Individual plots of all 28 storm events for Kampala over a threshold of 99.96% as seen in Fig. 13. Red dotted lines show the threshold. Location in the 10 year time-series (x-axis) is not currently relevant here so time axis is missed off for ease of viewing. Each data point along the x-direction is an hour. The y-axis is precipitation rate in mm hr^{-1}. The light blue line shows a three hour interval either side of the red point (peak event) with the height of the blue line as the average rainfall during the interval. Storm events are in order of descending peak intensity.

under the condition that the sample size is sufficiently large) as it would likely model this data adequately. Here, the data that is being utilised is only the extreme values and therefore a normal distribution would not be appropriate. For the distributions to be valid, the peak or maximum values should follow a Poisson distribution. However from preliminary tests with this particular time-series, the data does not appear to follow this distribution from plots produced of Poisson distributions against data bins. Precipitation data

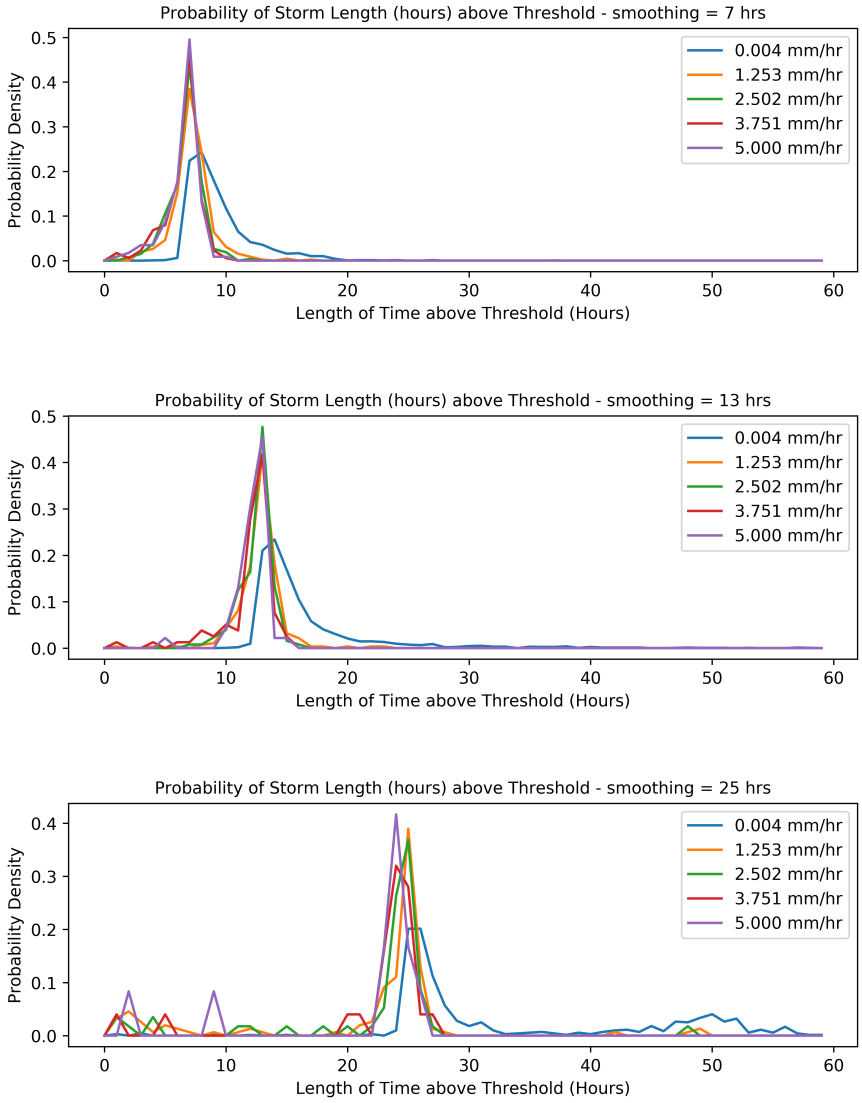

Figure 17: Probability density plots for top: 7 hours; middle: 13 hours; and bottom: 25 hours smoothing for the present day CP4-A time series showing storm/peak time widths in hours. Five low thresholds were used to determine if the storm lengths shortened considerably.

from Venezuela in Coles et al. (2003) can be seen in Fig. 18. The data is far more regular with less clustering of peaks compared to the time-series from Kampala (Fig. 13).

Spatially and temporally aggregating the data will need to be addressed. Appropriate temporal intervals will be decided and the effect of these will be analysed. Larger spatial areas will be considered, but the higher resolution (CP4-A) model will need to be regridded to be comparable to the coarser P25. Both models can then be compared for differences. Going forward, using the number of events as a threshold choice suits time aggregated data as the threshold value would not need to change - although it is possible that a different number of events would be needed with different averages.

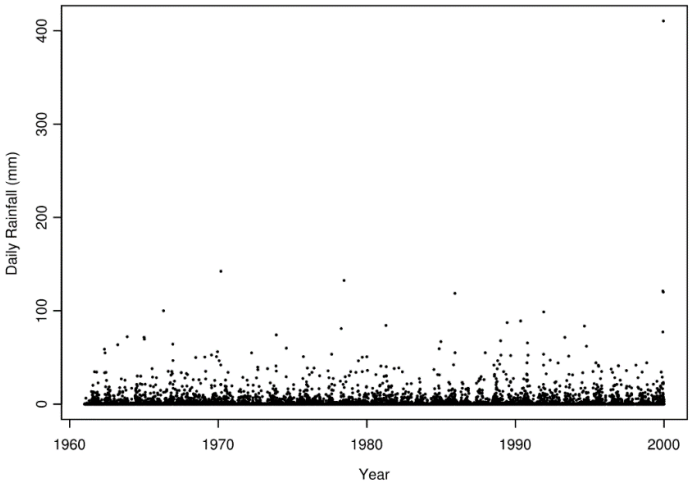

Figure 18: 40 years maximum daily precipitation for a location in Venezuela from Coles et al., 2003.

3.2.4 Choosing a Distribution

From the annual maximum values identified from the data in Fig. 13, the GEV and Gumbel distributions have been applied to the data from various locations and can be seen in Fig. 19. Having only ten-years of data limits the number of values for use with the distributions which is likely to reduce the precision of the results. Weekly and monthly maximum values were also plotted with the GEV and Gumbel distributions and both distributions perform similarly, in that they model the lower parts of the data reasonably but struggle at the tail end (higher return periods). These results suggests that the sample size of ten (annual data) is too small and the larger samples (weekly or monthly) are not necessarily independent. As EVT distributions model independent variables as they $\rightarrow \infty$ then the more values, the better the precision. However higher bias is introduced when using larger data sets, as the data needs to be independent (so should not follow a trend), it is a potential concern when using weekly or monthly peak data in certain regions. The GP distribution can also be seen alongside the GEV and Gumbel distributions in Fig. 19 for various locations and simulations. The inaccuracy of the latter two distributions can be seen against the empirical values which show them struggling to model the precipitation in the tail end of the data for the CP4-A simulation. In Fig. 19(c), the GEV model is unable to fit the data at all. The Gumbel distribution appears to have slightly closer agreement, with a better estimate of the longer-term return periods.

The ten-year data sets used in this project are on the lower end of what is deemed an acceptable length for the AM method as they only contains ten points, limiting the amount of information that can be utilised to predict future rare events. This follows much of the literature that suggests that for smaller data sets, using the GP distribution is more appropriate. It allows for more data to be included in the analysis and minimises waste of potentially valuable information. The plots in Fig. 19 also highlight how many peak values are lost when only using the AM values.

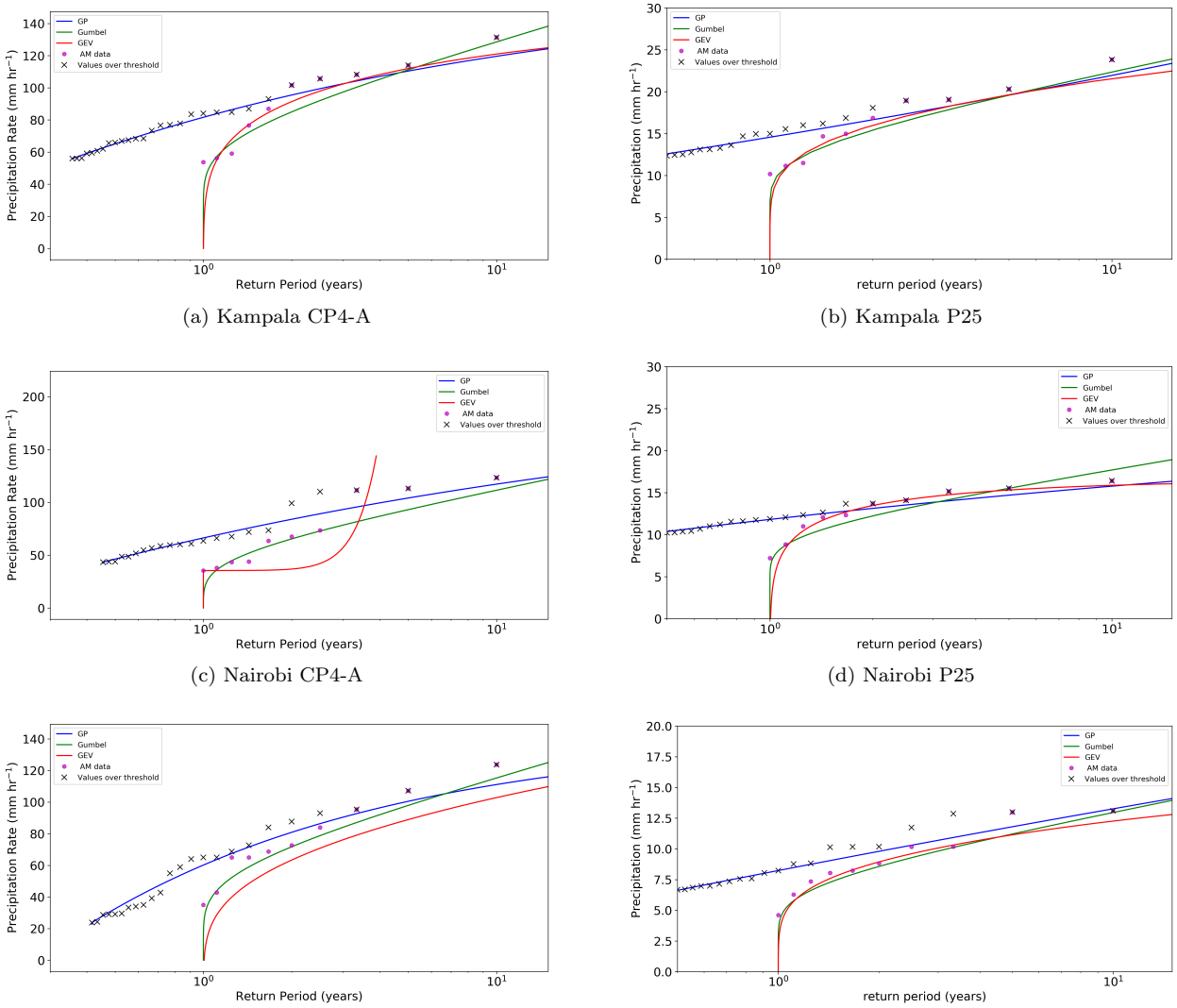

(a) Kampala CP4-A

(b) Kampala P25

(c) Nairobi CP4-A

(d) Nairobi P25

(e) Mogadishu CP4-A

(f) Mogadishu P25

Figure 19: Examples of the three distributions GEV, Gumbel and GP fitted to present day CP4-A and P25 data for three locations: (a) Kampala CP4-A; (b) Kampala P25; (c) Nairobi CP4-A; (d) Nairobi P25; (e) Mogadishu CP4-A; and (f) Mogadishu P25, using a threshold of the 99.96th percentile independent extreme events for GP and largest 10 peaks for GEV and Gumbel.

4 Results

Presented here are some in-progress results. There is still further processing and investigation to be done to complete this chapter of the project, details discussed in the project plan in Sec. 5. From this section onwards, for ease, P25 will refer to the present day P25 simulation data, P25-fc will refer to the future climate P25 data. CP4-A will refer to the present day CP4-A data and CP4A-fc will refer to the future climate simulation unless otherwise specified. T10 and T5 refer to the 10-year and 5-year return period precipitation as predicted by the GP distribution. The i-year return period will be referred to as Ti. All precipitation measurements discussed in this section are hourly and occur at grid-point scale. Spatial and temporal aggregation is left for future work.

4.1 Specific Locations

The GP distribution was chosen as the most appropriate distribution as per discussion in Sec. 3.2.4. Fig. 20 shows the GP distribution applied for P25 and CP4-A present day and future climate simulations at four individual locations - Kampala, Nairobi, Mogadishu and Kisumu, chosen for their importance to the region of east Africa and their geographic diversity.

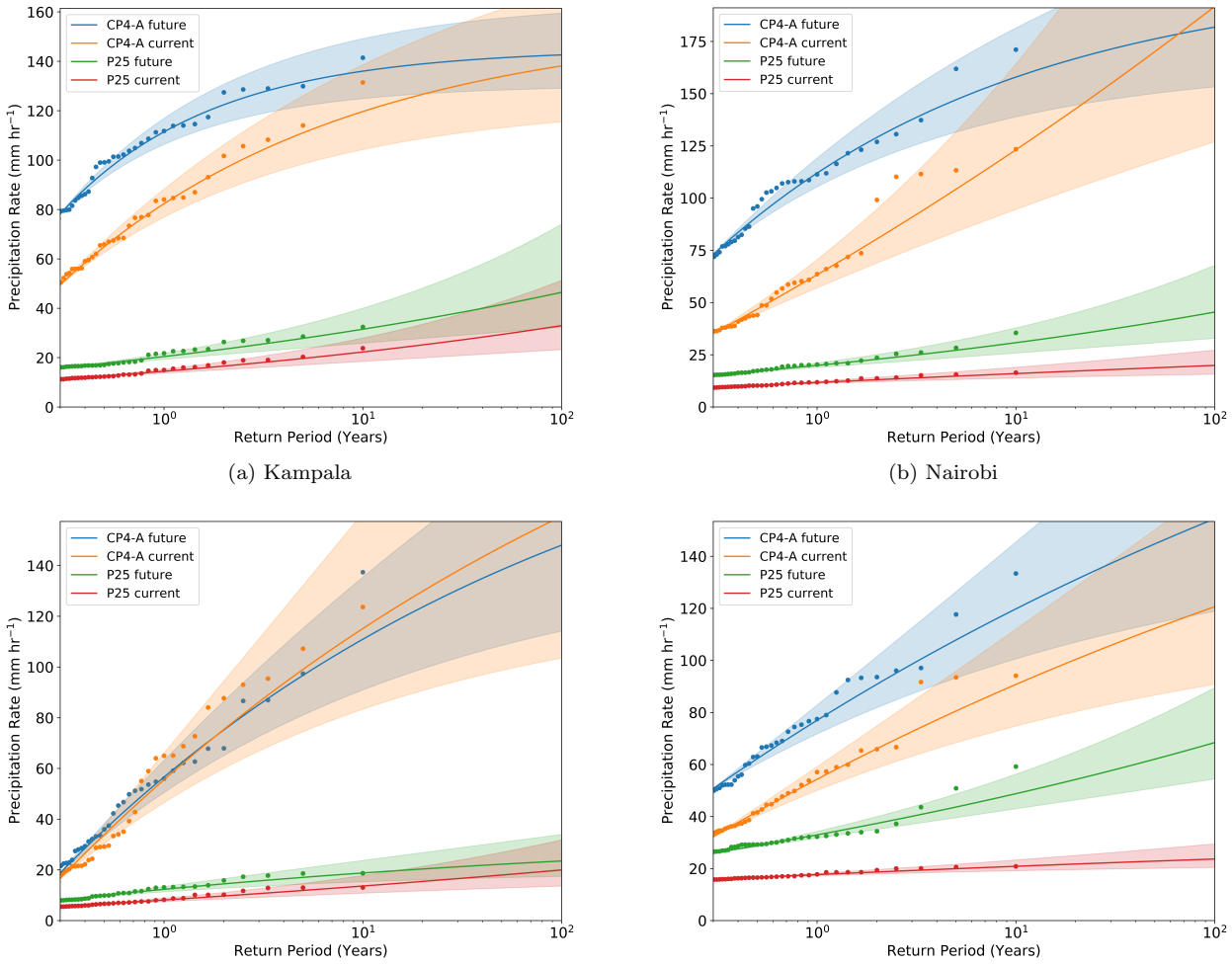

(a) Kampala

(b) Nairobi

(c) Mogadishu

(d) Kisumu

Figure 20: CP4-A, CP4A-fc, P25 and P25-fc with the GP distribution return period precipitation predictions up to the 100 year return period for (a) Kampala; (b) Nairobi; (c) Mogadishu; and (d) Kisumu, using a threshold of the top 40 independent extreme events from the ten-year period with 95% confidence intervals.

For these plots, the threshold was chosen to be the 40 largest independent precipitation events for simplicity, so going forward, the threshold limit will be in units of number of events. A range of thresholds were trialled with these locations and 40 events appeared, at least visually, to be a reasonable fit for all four. The threshold value is investigated further in the following sub-sections.

Generally, the GP distribution appears to fit reasonably well to the four sets of data. Most of the data is within the 95% confidence intervals and although the ten-year return period is sometimes a little below the simulation value in some of the locations, the GP distribution is what is we would expect to get after many realisations so is not expected to always match the simulation data exactly.

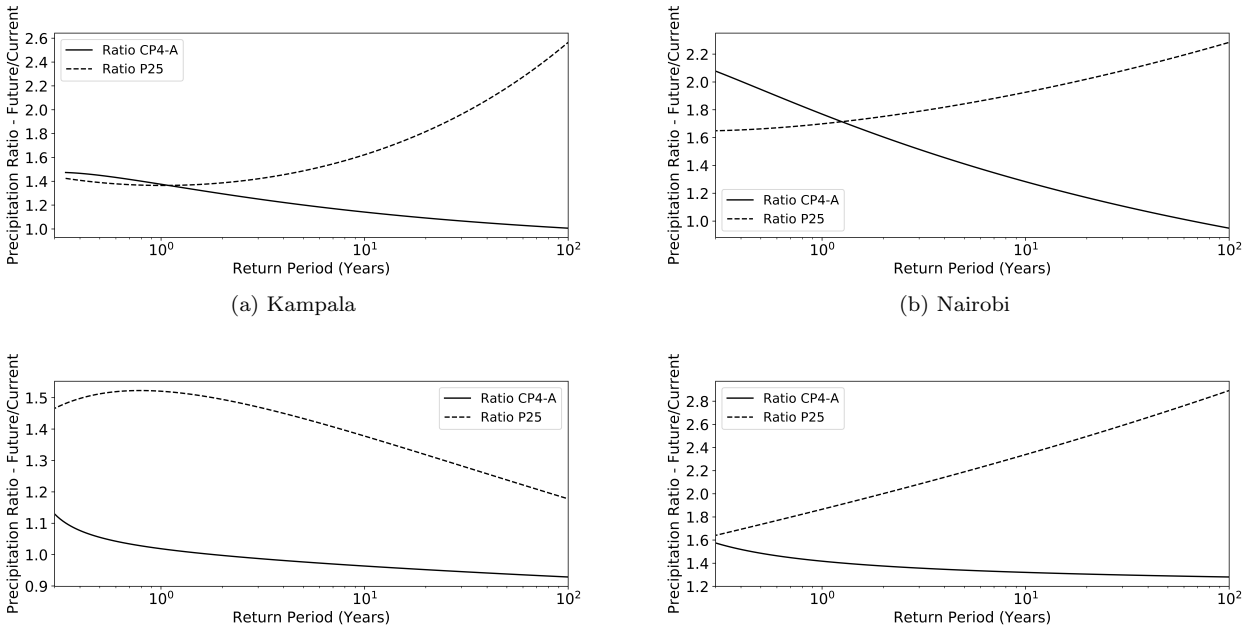

(a) Kampala

(b) Nairobi

(c) Mogadishu

(d) Kisumu

Figure 21: Return period precipitation ratio between CP4A-fc and CP4-A; and P25-fc and P25; for: (a) Kampala; (b) Nairobi; (c) Mogadishu; and (d) Kisumu, up to 100 year return period.

There are noticable differences in the return period behaviours between models and locations. Fig. 20(a) shows that although CP4A-fc has around 1.5 times the expected precipitation of CP4-A at return periods below one year, this difference decreases significantly as the return period increases (Fig. 21(a)). When the return period is above ten years, the ratio has reduced to below 1.2 and continues to decrease, reducing by more than 33% by T100. If the data was extrapolated further beyond T100, the CP4-A return period would be expected to exceed CP4A-fc. This is in contrast to the P25-fc and P25 GP distributions, which show an increasing ratio between the P25-fc and P25 models, with a more gradual increase in return period precipitation values but a far more rapid increase in ratio, nearly doubling. This same pattern can be seen in Nairobi (Fig. 20(b); 21(b)), where the future and current CP4-A return period ratio reduces to below one around T75, meaning the present-day model T75 exceeds the future model T75. The P25-fc and P25 return period ratio contrasts this result with a gradual increase of around 30% from around 1.7 to 2.2 between T1 and T100. Kisumu (Fig. 20(d); 21(d)) again displays similar behaviour but with a much slower reduction in the CP4A-fc/CP4A ratio - the current day prediction does not exceed future within the T100 plot. The P25-fc/P25 ratio increases nearly linearly by more than 50% between T1 and T100.

Mogadishu is a city on the east coast of Africa and therefore has a different geography and meteorological environment to the other cities considered here. In Fig. 20(c), the CP4-A distribution very quickly exceeds the CP4A-fc predictions as the return period increases, around T1, varying from the other locations in this regard. This may be explained by local sea breezes, which have been investigated by Finney et al.

(2019) who using CP4-A simulation data determined that under climate change, the increase in sea breezes in that region may actually reduce the total precipitation under a warming climate. Again, unlike other locations, the behaviour of the P25-fc/P25 ratio for Mogadishu was different, with a decreasing ratio, from around 1.5 to 1.2 between T1 and T100 (Fig. 21(c)).

It is worth noting that although the ratios between the P25 distributions are sometimes large, these do not relate to large changes in precipitation values, as the magnitude of the initial rainfalls are relatively small compared with CP4A-fc and CP4-A. For future work, this will be repeated with the CP4-A simulations regridded to the coarser P25 grid. To do this, the CP4-A values will be spatially averaged, potentially bringing down the magnitude of the extreme precipitation events and changing the behaviour of the return period curves.

4.2 Wider Regions

This section currently contains only data for P25 and P25-fc simulations, however future work will include the regridded CP4-A and CP4A-fc data here using the same methods. Contour plots of P25 and P25-fc simulation data for the one in ten-year precipitation event and the one in five-year precipitation event across central/east Africa can be seen in Fig. 22. These plots are used as a reference for the predicted return periods from the GP distribution. The following sub-sections consider both the T10 and T5 values. The same analysis is performed for both to determine how the GP distribution fit compares between the two.

4.2.1 Ten-Year and Five-Year Return Predictions for P25

All of the analysis below was performed for the five and ten-year return periods and respective extreme events for both P25 and P25-fc, however only certain plots are included where necessary to avoid repetition.

Contour plots of T10 for the P25 simulation over central/east Africa can be seen in the left column of Figs. 28 and 29 for six threshold choices between 20 and 250 events. This was done to demonstrate any significant differences in the return period predictions between these threshold choices. For threshold choice, specific numbers of events per location were chosen due to the effectiveness of this for applying to larger regions (as in Sec. 4.1). Particular percentile thresholds (such as 99.9th, 99.99th etc.) were also trialled, but showed that often locations had too few or too many points for GP to fit adequately across the domain. Using mean residual life plots for each location is not simple to automate for large numbers of data sets (the central/east Africa region used here has 12000 locations) so was discounted. Instead, the largest magnitude 20, 40, 60, 100, 150 and 250 independent events were used with the GP distribution (similar to the red peaks in Fig. 13 but determined by a number of events). Scales on the colour bars were clipped to allow for clearer reading as several points were hugely overestimated by the GP model, making the contours unreadable (see Fig. 24).

The higher threshold choices (20, 40 and 60 events) all show very similar results for the return periods. From these, the 20 point threshold shows a small number of unrealistic values, mostly clustered over central Africa. These regions are where the GP model has significantly 'overshot' and predicted unrealistic rainfall values for the ten-year return period (see example in Fig. 23). These unrealistic values can also be seen in the 40 and 60 point threshold plots. The lower (100, 150 and 250 events) threshold plots seem to predict less extreme over-estimates for the central region compared with the higher thresholds, however predict higher rainfall than would be expected over the Atlantic ocean to the west and over Somalia in the north east of the plot region. This suggests that the GP distribution is having difficulty modelling certain patterns of precipitation combined with particular threshold choices.

The right column of Figs. 28 and 29 shows difference maps of the P25 T10 precipitation minus the one in ten-year event rainfall from P25 simulation data for different thresholds (Fig. 22(a)). Red and blue regions denote locations where the GP distribution is over-predicting and under-predicting the rainfall from the simulation data respectively. Again, as seen in the left column plots, it is clear that the distribution works reasonably well, with minimal extreme or unrealistic values in most areas and most values likely contained

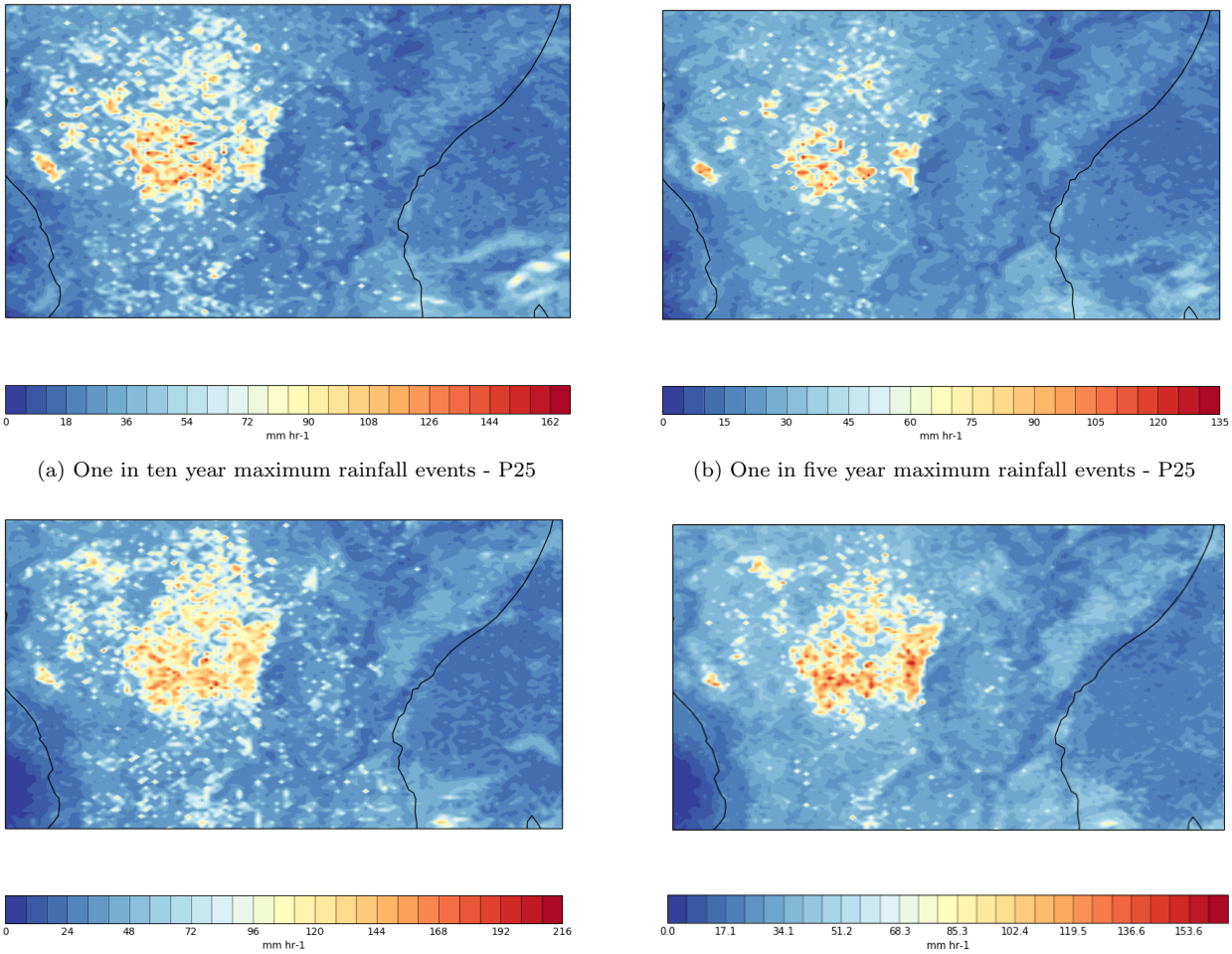

(a) One in ten year maximum rainfall events - P25

(b) One in five year maximum rainfall events - P25

(c) One in ten year maximum rainfall events - P25-fc

(d) One in five year maximum rainfall events - P25-fc

Figure 22: Contour plot of the one in ten-year and one in five-year rainfall event in mm hr^{-1} over the ten-year time period for (a) P25, one in ten year event; (b) P25, one in five year event; (c) P25-fc, one in ten year event; and (d) P25-fc, one in five year event over central/east Africa.

within a reasonable margin of error. However, it struggles with regions of large rainfall (e.g. central Africa). This is particularly the case for the higher thresholds. The lower thresholds (100, 150, 250) predict far higher T10 over the oceans and Somalia compared with the simulation data. An interesting feature emerges from the lower threshold plots along the northern coast of east Africa (the Somali coastline) where the difference in precipitation goes from heavily positive inland to slightly negative on the coast. This pattern can be seen even more intensely for the P24-fc model for the same thresholds (not shown here due to similarity). The extreme values in the simulation data along the coast of Somalia are likely of a different 'pattern' than inland and would be interesting to investigate further.

4.2.2 Unrealistic Estimates

To investigate these unrealistic predicted values further, scatter plots for different thresholds can be see in Figs. 30 and 31. The left column showing the one in ten-year simulation values for P25 plotted against the T10 values; the right column showing the one in five-year simulation values plotted against T5. Extreme, unrealistic outliers have been removed for ease of reading. For an example of these outliers, see Fig. 24. These plots shows how close the values from the GP distribution are to the simulation data in general, with the red line as a best fit line for the data. If all the return periods matched the simulations exactly, the

best fit would be the line $y = x$ and all points would lie along this. However, it is expected that the values would not lie precisely along this line. The GP distribution is used to predict the T-year return period based on each time-series of values provided, which are just used as a guide and are not representative of every ten/five-year storm possible at each location. The scatter plots are just used as a tool to determine if the GP distribution is predicting values within a realistic rainfall interval.

It is apparent that the lower thresholds (100, 150 and 250 events), particularly for T10, demonstrate a much larger deviance from the $y = x$ line. The unrealistic over-estimates noted in Fig. 29 can be seen along the lower side of the plots, parallel with the x-axis. The 250 event threshold is the only plot to have a best-fit line with a gradient of less than one due to the number of these. The higher threshold return periods show far better agreement with the simulation data, with less scatter and what appears to be more realistic predictions. The higher thresholds generally have far fewer extreme over-estimates where the model fails to fit adequately.

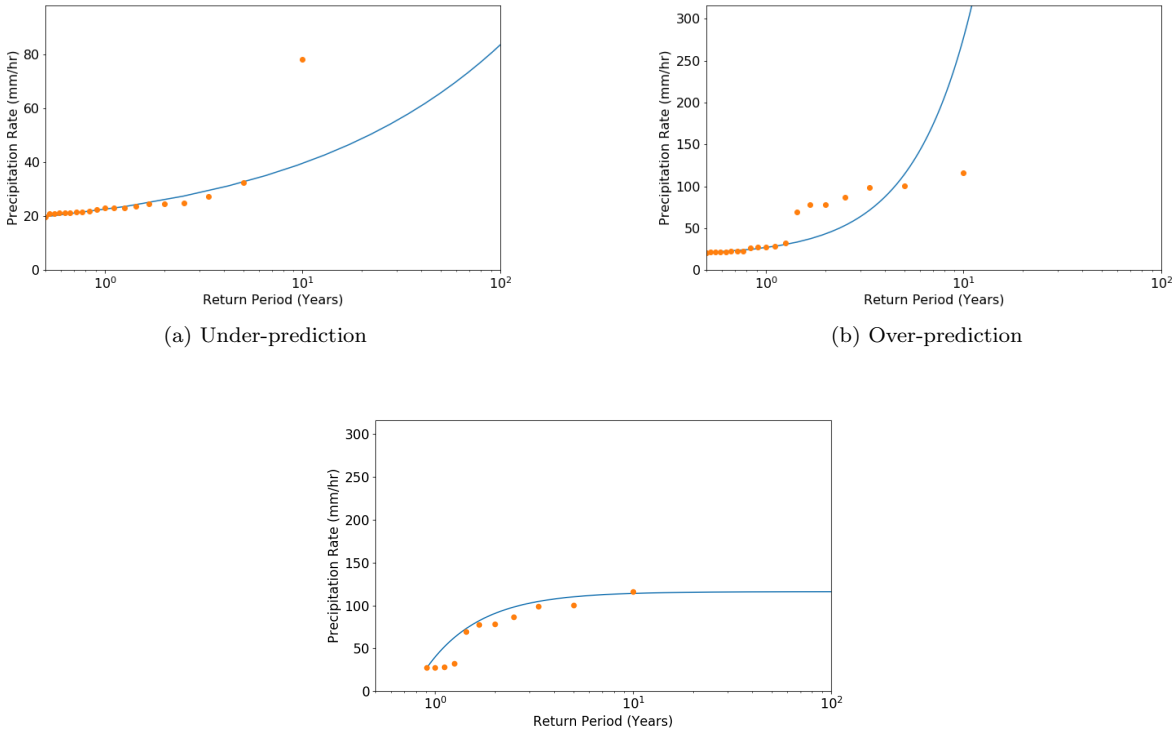

(a) Under-prediction

(b) Over-prediction

(c) Reduced threshold

Figure 23: Return period plots for locations in central Africa with at least one relatively high maximum rainfall value from the simulation data. The first two plots show the GP distribution producing unrealistic predictions for the precipitation using a threshold of 40 events for present day P25 data: (a) GP under-prediction and (b) GP over-prediction. (c) shows the same data from (a), but with a reduced threshold of 10 events.

Throughout all plots, the points skew upwards away from the middle (where the $y = x$ line would be), showing that the model generally under-predicts rather than over-predicts the simulation values when the precipitation event is above about 40mm hr^{-1}. It is worth noting that around 1-2% of the points are above 40-50mm hr^{-1}. The unrealistic GP over-predictions almost exclusively happen below this value of 40mm hr^{-1}. This suggests that there may be a change in the pattern of the extreme rainfall events from the simulation around this value. Although this has not been investigated in detail, two simple example distributions from P25 (from the central Africa region with higher rainfall) are shown in Fig. 23. These show unrealistic GP predictions using a threshold of 40 events. The left plot shows a T10 value of around half of the value

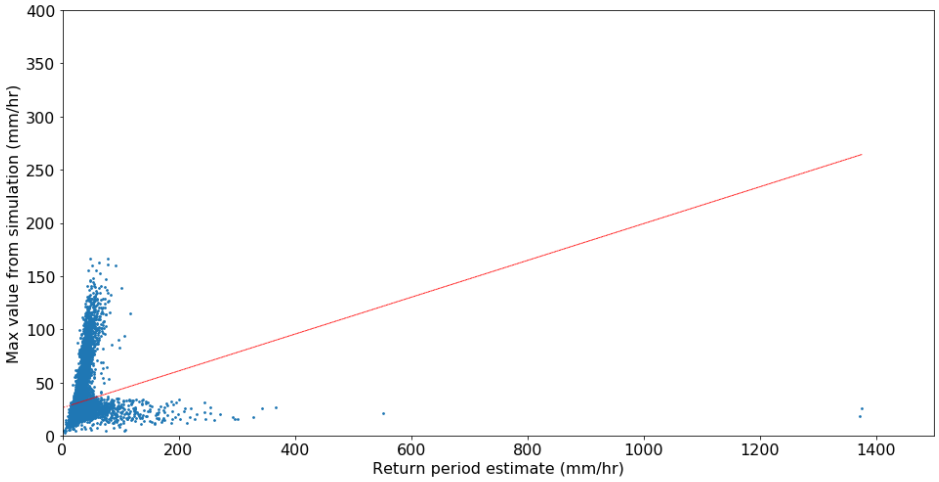

Figure 24: Scatter plot of P25 across central/east Africa showing all values of the ten-year return period predicted by the GP distribution using a threshold of 250 events. An example of unrealistic extreme over-estimates can be seen around 1400mm hr^{-1}.

from the simulation; the right shows a T10 of around 2.5 larger than the simulation value. The threshold choice certainly affects the fit and in both these cases, the lower the threshold, the better the fit. However, fit is highly influenced by the shape parameter ξ in the GP distribution, which determines the bounds of the fit line. For $\xi < 0$, the GP has an upper bound, and a curve that looks like the CP4-A data in Fig. 20(a). This curve shape is not likely to cause extreme unrealistic over-predictions. For $\xi > 0$, the GP has no upper bound and has the potential to look more like Fig. 23(b). It is likely that steep unbounded GP distributions are causing the extreme overshoots. The GP parameters are estimated from data provided, so the threshold has a big influence on the value of ξ. For Fig 23(a), if the threshold is reduced to 10 events, the tail end fits better because the GP distribution is bounded from above (Fig. 23(c)). However, this does not necessarily mean that the predictions are more precise and will require more investigation. It may be that a different distribution would be more suitable for particular data sets.

When comparing the one in five columns to the one in ten-year event columns for the different thresholds in Figs. 30 and 31, there are far fewer outliers on the five year return period plots. This is not unexpected, since the GP distribution is more likely to fit the lower return periods as the points are often more linear and follow a more predictable pattern. As the precipitation is less for a one in five-year storm, more of the values fall below the 40-50mm hr^{-1} where the model appears to behave best. The affect of the changing threshold is the same as with T10 and the upward skewed points above around 40mm hr^{-1} are still apparent.

These plots are in-progress work. In future plots, whether the simulation values fall within the 95% confidence interval of the return period estimate will be shown and percentage boundaries to highlight where the GP distribution over or under-shoots the simulation values by an unrealistic amount will be included.

4.2.3 Removing Extreme Over-Estimates

Tables 1 and 2 show the number of extreme over-estimates removed from the scatter plots in Figs. 30 and 31. The method for determining extreme over-estimates was, for simplicity, defined an outlier as any GP prediction that was 15% above the realistic maximum value of the rainfall from the simulation data. In future it would be more useful to consider predicted T10 or T5 outliers as a percentage difference from each simulated value. So any point that was e.g. 15% more or less would be included in the outliers. Another option would be to define an outlier as any value that does not fall into a chosen confidence interval.

Table 1 shows a lower number removed for the higher thresholds (20, 40, 60) than for the lower thresholds. For both simulations, 40 and 60 perform the best, although at least one value for the 60 event threshold for P25-fc was hugely over-estimated at 1954mm hr^{-1}. P25-fc appears to have more removed, possibly because some of the simulation data have sharper increases around the tail-end than P25, which can be seen in some of the individual locations in Fig. 20. In reality, the lower thresholds (100, 150 and 250) have significant numbers of underestimates as can been seen in the scatter plots (Figs. 30, 31) and difference plots (Figs. 28, 29) which would show up as outliers if say the 95% confidence interval was used as a limit.

It is worth noting that under-estimates by the GP distribution are far more common than over-estimates, but the magnitude of the difference is less, as can be seen in the scatter plots. The values in general lie within the 95% confidence interval which is reasonable and so have not been discounted or removed.

P25				
Threshold (no. of events)	T10	Largest T10 outlier	T5	Largest T5 outlier
20	15	360	0	-
40	6	496	1	283
60	8	383	0	-
100	18	430	0	-
150	17	492	0	-
250	27	1377	3	555

Table 1: Number of outliers removed from the P25 scatter plots in Fig. 30 and 31 for the six thresholds.

P25-fc				
Threshold (no. of events)	T10	Largest T10 outlier	T5	Largest T5 outlier
20	28	782	3	240
40	12	773	6	279
60	17	1954	9	584
100	20	601	6	325
150	27	828	1	350
250	35	1369	4	572

Table 2: Number of outliers removed from the scatter plots for P25-fc for the six thresholds, not shown.

4.2.4 East Africa

Based on the analysis in the previous sub-sections, any of the three higher thresholds could be chosen for use with the smaller region of east Africa. A 40-event threshold is chosen as it performed well for this particular region in the previous sections and had the least extreme outliers over central/east Africa. The area chosen here encompasses 2000 location points including the four locations chosen in Sec. 4.1.

Fig. 25 shows T10 contour plots for P25 and P25-fc for the region of interest. Scatter plots showing the one in ten-year storm plotted against the T10 value can be seen in Fig. 26. Here, the blue points denote the simulation values that lie within the T10 95% confidence interval and red points are outside. No outliers have been removed from either plot. The red dotted line shows the $y = x$ line. These plots shows the T10 predictions in excellent agreement with the respective simulation values, with around 2% outside the 95% confidence interval for both plots. Although it is not expected that the values lie along the $y = x$ line, it is encouraging to see that most values are reasonably near.

In Fig. 27, the ratio between the P25-fc and P25 ten-year return periods can be seen for east Africa.

This plot shows how climate change is expected to affect the ten-year return periods of one-hour extreme precipitation events between present day and end of the century using a simulation with parametrised convection. The ratio very rarely dips below one - suggesting that at almost no locations will the present-day precipitation exceed the future climate precipitation value for one in ten-year storms. Over half of the locations in east Africa have an increase of more than 1.4 in T10 rainfall and 25% have an increase of more than 1.6. The top 5% have more than double the increase in rainfall. Only 3% of locations have a decreased intensity for ten-year precipitation events.

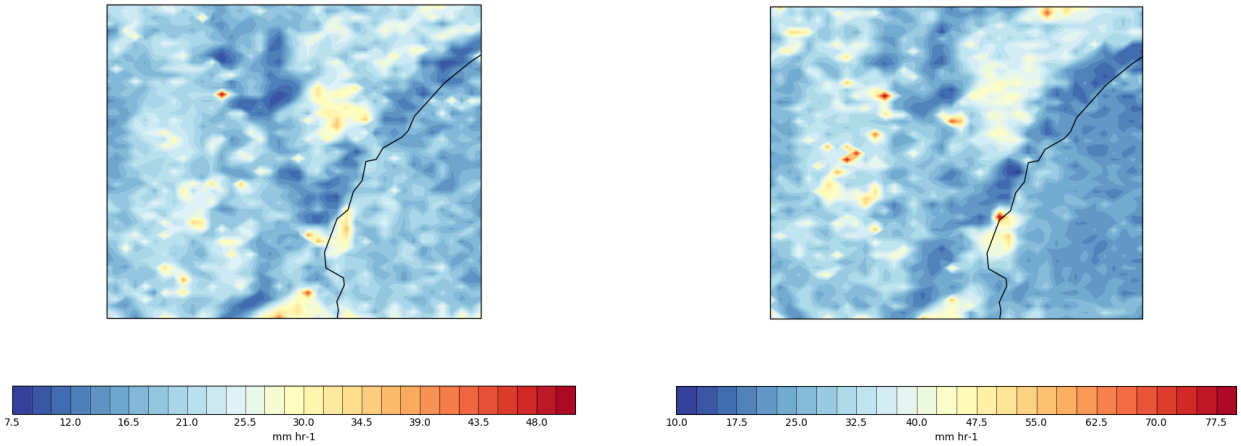

(a) P25 (b) P25-fc

Figure 25: Contour plots for east Africa showing the 10-year return period precipitation (mm hr^{-1}) predicted by the GP distribution using a threshold of 40 events for (a) P25 and (b) P25-fc.

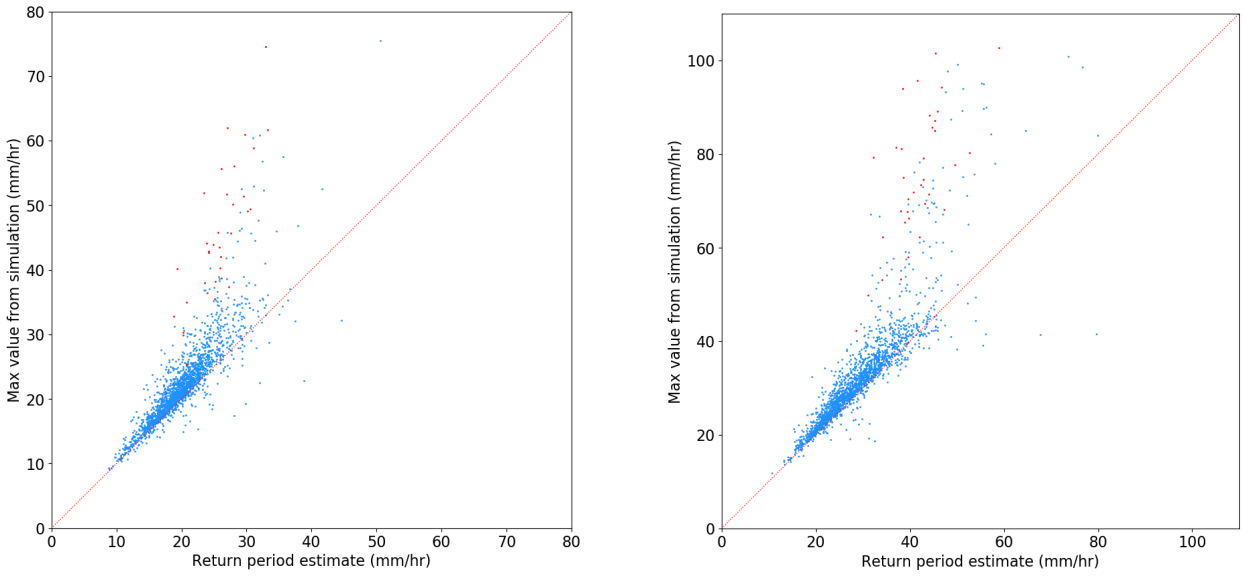

(a) P25 (b) P25-fc

Figure 26: Scatter plots of the one in ten-year event against T10 for east Africa using a threshold of 40 events for: (a) P25; and (b) P25-fc; where blue points are simulation values within the T10 95% confidence interval and red points lie outside. The red dotted line is $y = x$.

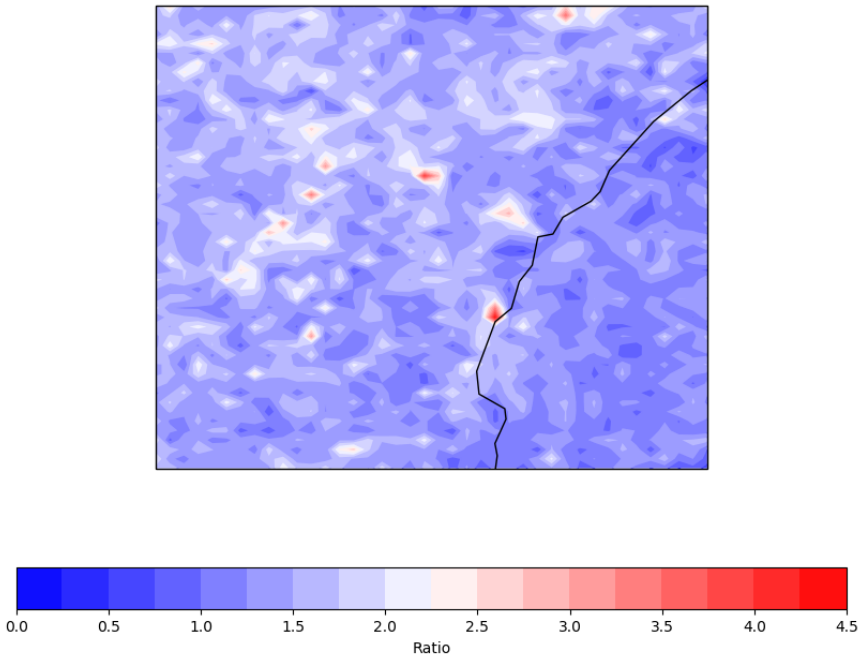

Figure 27: Ratio of the P25-fc/P25 T10 precipitation rate values from Fig. 25 across east Africa.

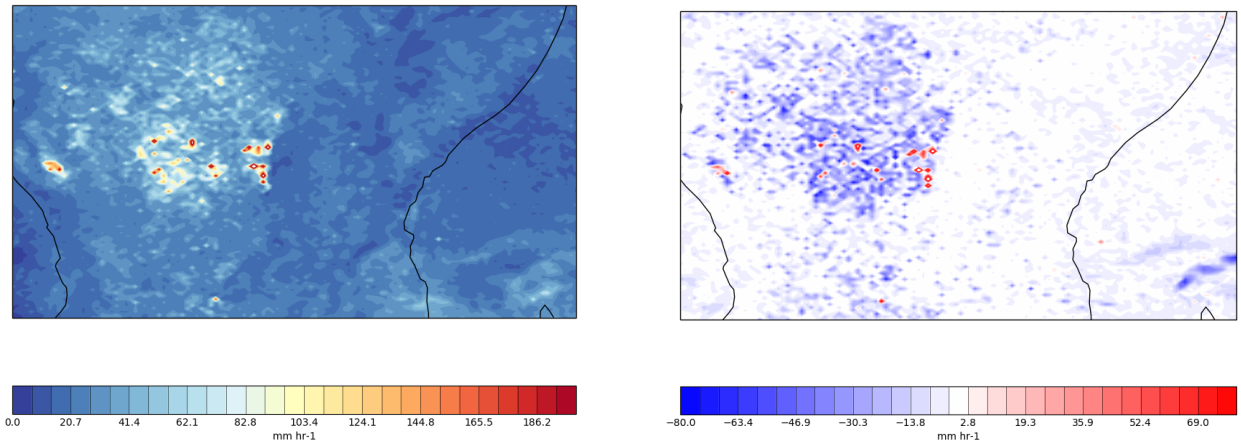

(a) 20 event threshold

(b) 20 event threshold, GP predictions - P25 data

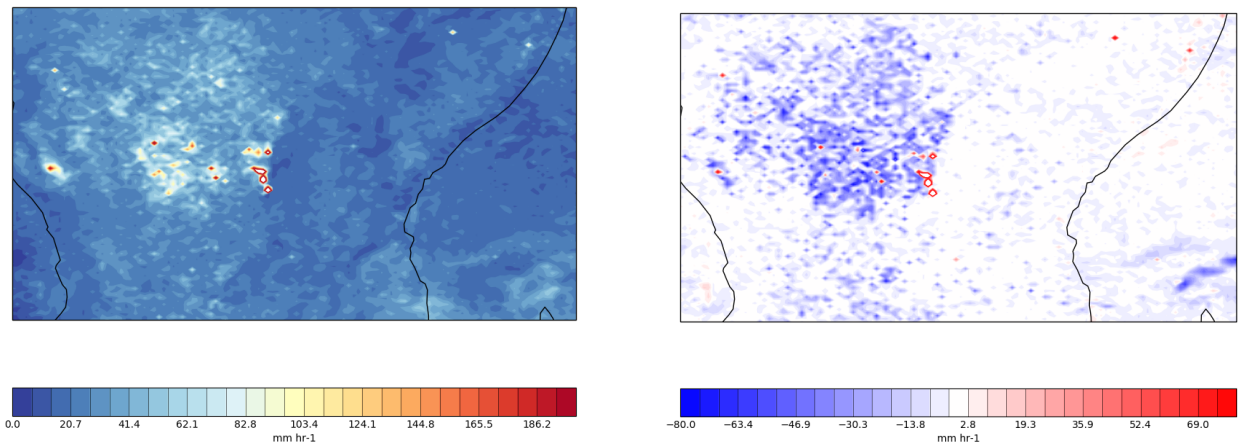

(c) 40 event threshold

(d) 40 event threshold, GP predictions - P25 data

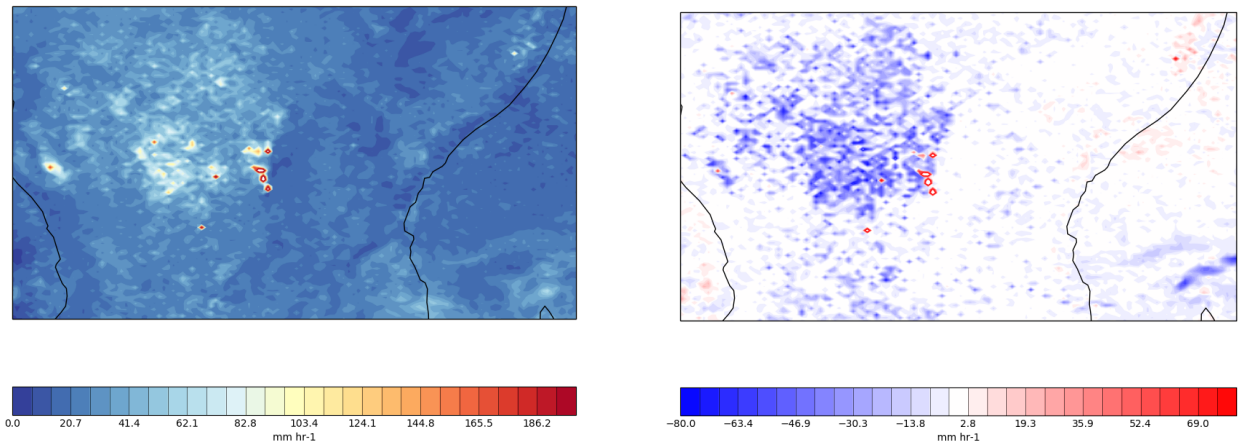

(e) 60 event threshold

(f) 60 event threshold, GP predictions - P25 data

Figure 28: Left column - contour plots for east/central Africa showing the 10-year return period precipitation (mm hr^{-1}) predicted by the GP distribution for present day P25 data. The colour bar is clipped at the top end to avoid extreme results. Each sub-plot is using a different number of events as a threshold for the GP distribution: (a) 20 events; (c) 40 events; (e) 60 events. Right column - difference between the GP distribution and the 10-year precipitation data from P25 shown in Fig. 22 for three thresholds: (b) 20 events, GP predictions - P25 data; (d) 40 events, GP predictions - P25 data; and (f) 60 events, GP predictions - P25 data. The colour bar is clipped at either end to remove extreme outliers.

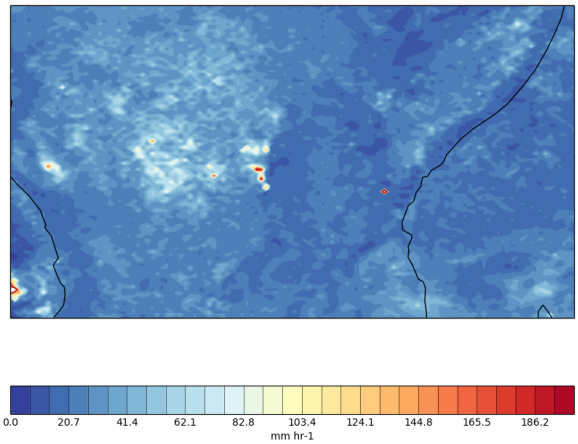

(a) 100 event threshold

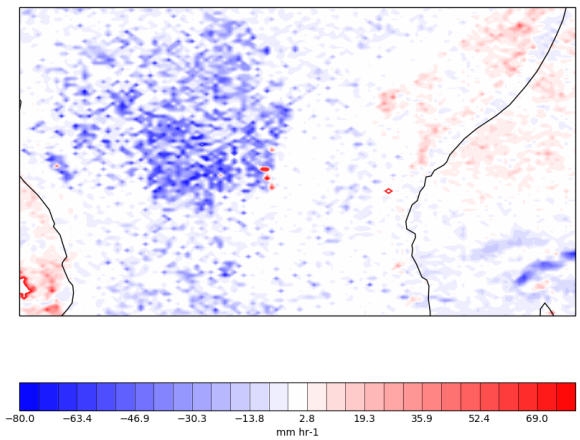

(b) 100 event threshold, GP predictions - P25 data

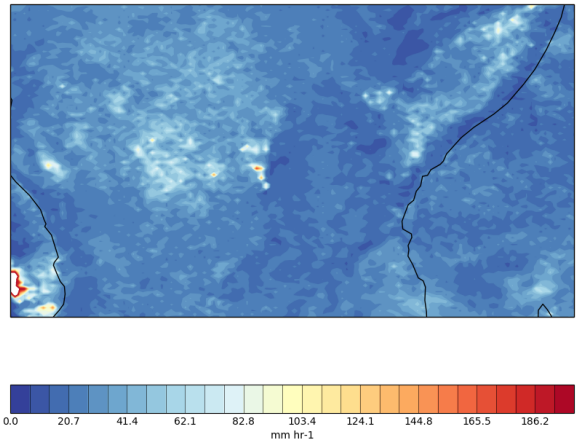

(c) 150 event threshold

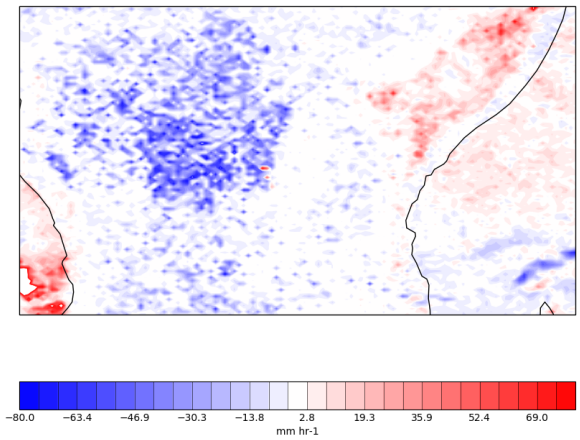

(d) 150 event threshold, GP predictions - P25 data

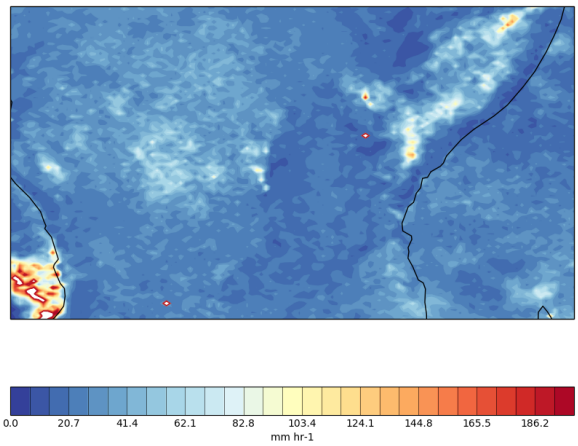

(e) 250 event threshold

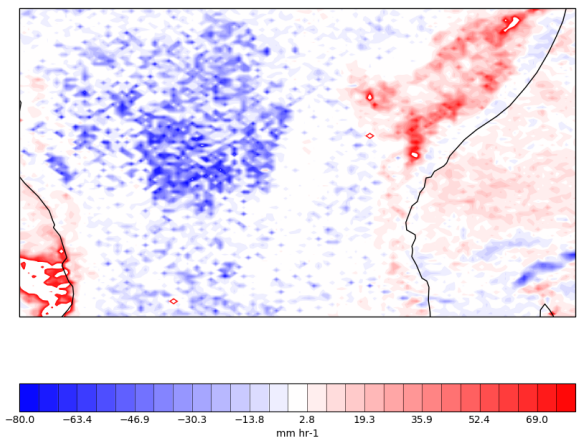

(f) 250 event threshold, GP predictions - P25 data

Figure 29: Left column - contour plots for east/central Africa showing the 10-year return period precipitation (mm hr^{-1}) predicted by the GP distribution for present day P25 data. The colour bar is clipped at the top end to avoid extreme results. Each sub-plot is using a different number of events as a threshold for the GP distribution: (a) 100 events; (c) 150 events; (e) 250 events. Right column - difference between the GP distribution and the 10-year precipitation data from P25 shown in Fig. 22 for three thresholds: (b) 100 events, GP predictions - P25 data; (d) 150 events, GP predictions - P25 data; and (f) 250 events, GP predictions - P25 data. The colour bar is clipped at either end to remove extreme outliers.

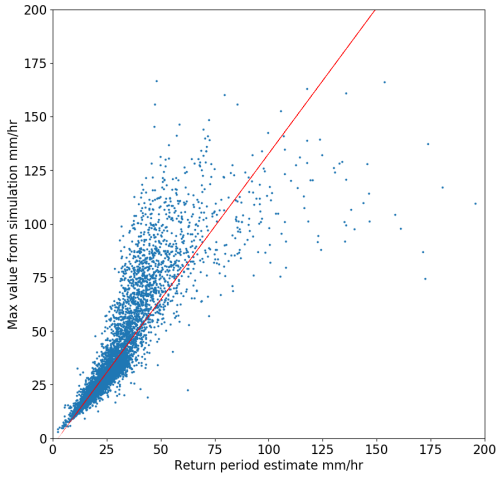

(a) 20 events - T10

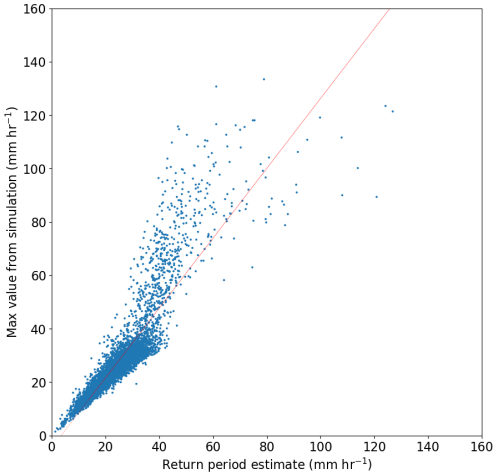

(b) 20 events - T5

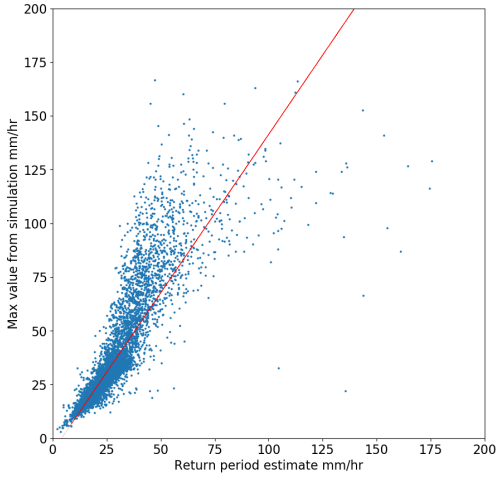

(c) 40 events - T10

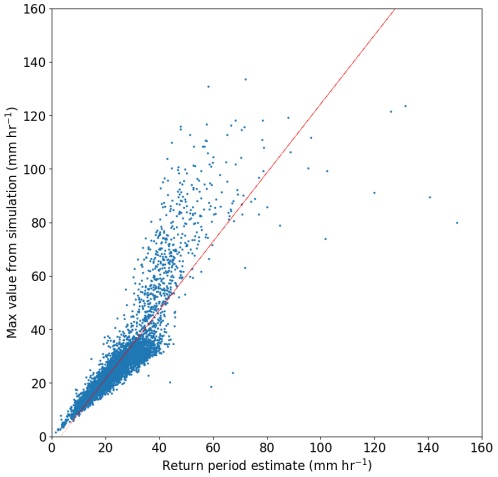

(d) 40 events - T5

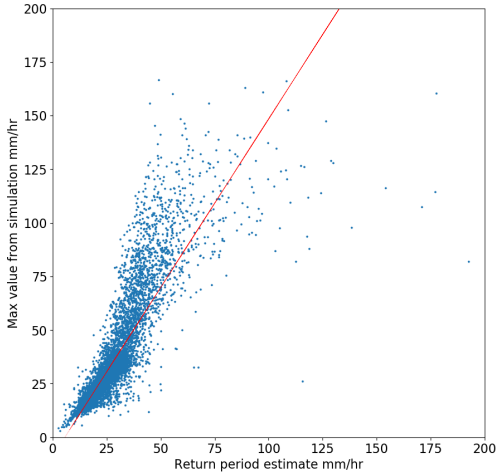

(e) 60 events - T10

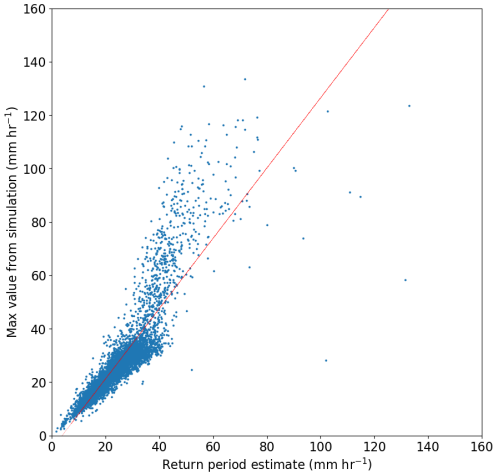

(f) 60 events - T5

Figure 30: Scatter plots of the P25 one in ten and one in five year events against the GP T10 and T5 return period predictions respectively. Left column - the one in ten year plots for three high thresholds (20, 40 and 60 events): (a) 20 events T10; (c) 40 events T10; (e) 60 events T10. Right column - one in five year plots with the same three high thresholds: (b) 20 events T5; (d) 40 events T5; and (f) 60 events T5. All with extreme outliers removed. Red line is the best fit for the data.

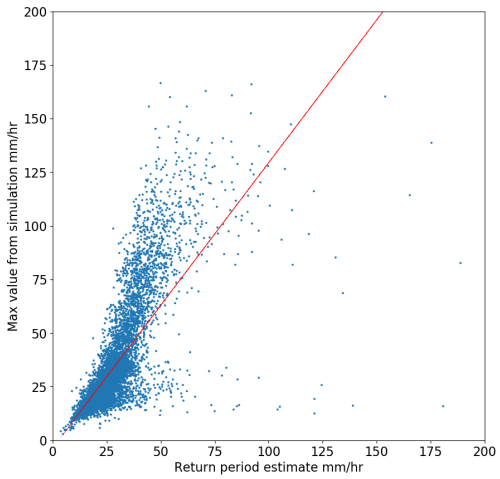

(a) 100 events - T10

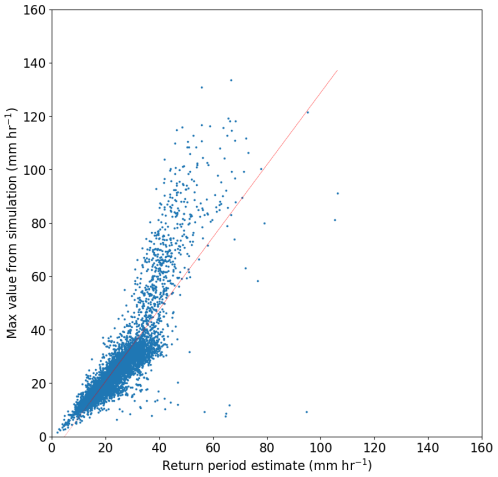

(b) 100 events - T5

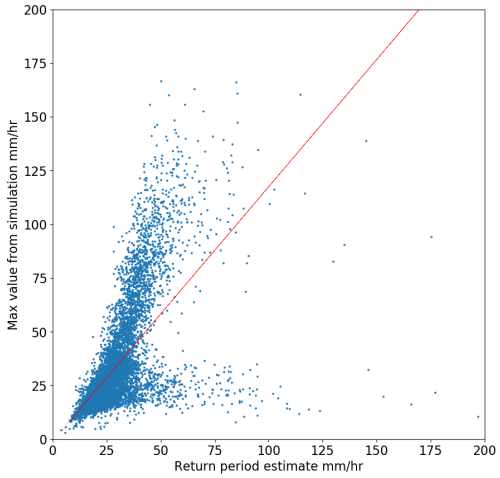

(c) 150 events - T10

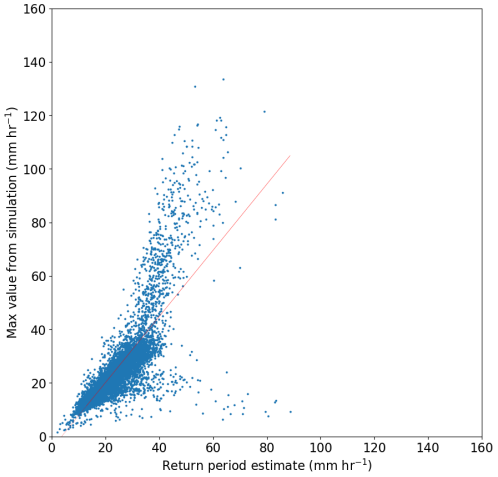

(d) 150 events - T5

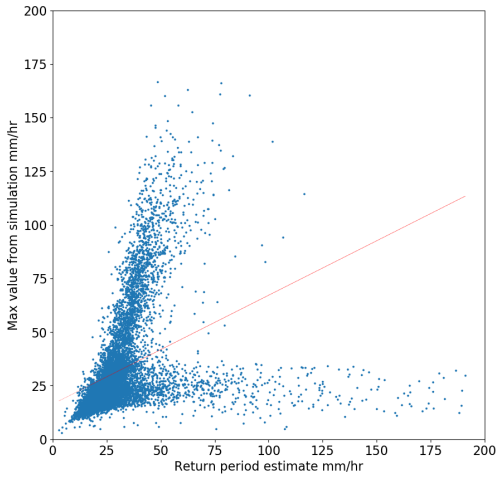

(e) 250 events - T10

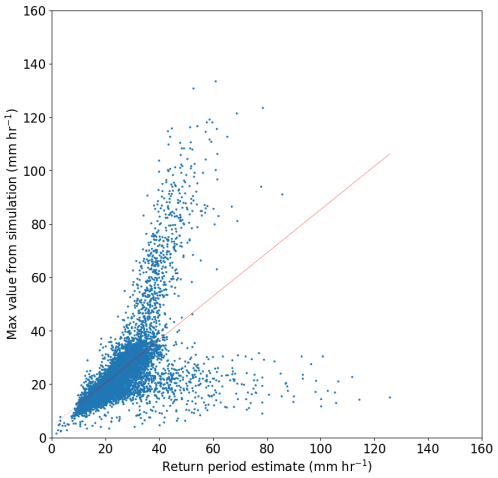

(f) 250 events - T5

Figure 31: Scatter plots of the P25 one in ten and one in five year events against the GP T10 and T5 return period predictions respectively. Left column - the one in ten year plots for three high thresholds (100, 150 and 250 events): (a) 100 events T10; (c) 150 events T10; (e) 250 events T10. Right column - one in five year plots with the same three thresholds: (b) 100 events T5; (d) 150 events T5; and (f) 250 events T5. All with extreme outliers removed.

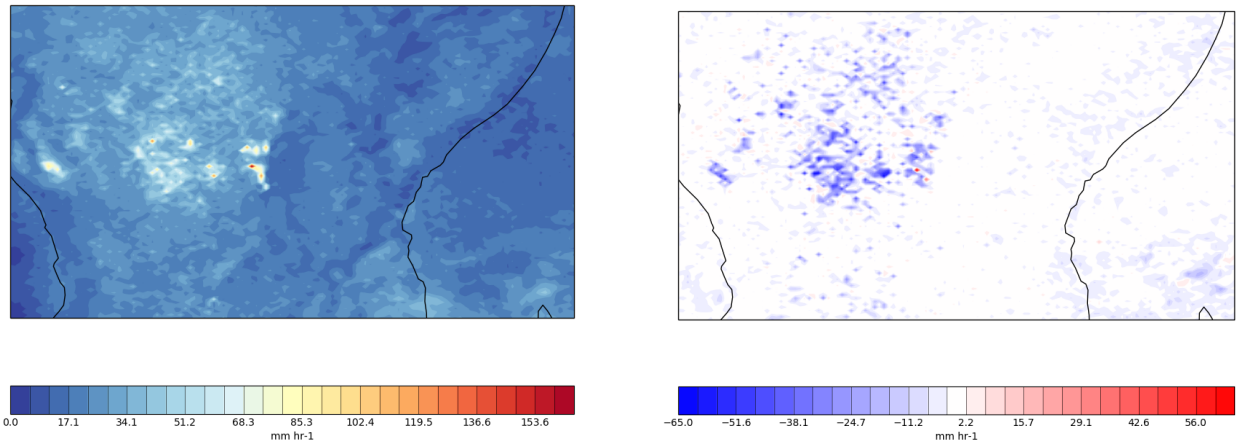

(a) 20 event threshold

(b) 20 event threshold, GP T5 predictions - P25 data

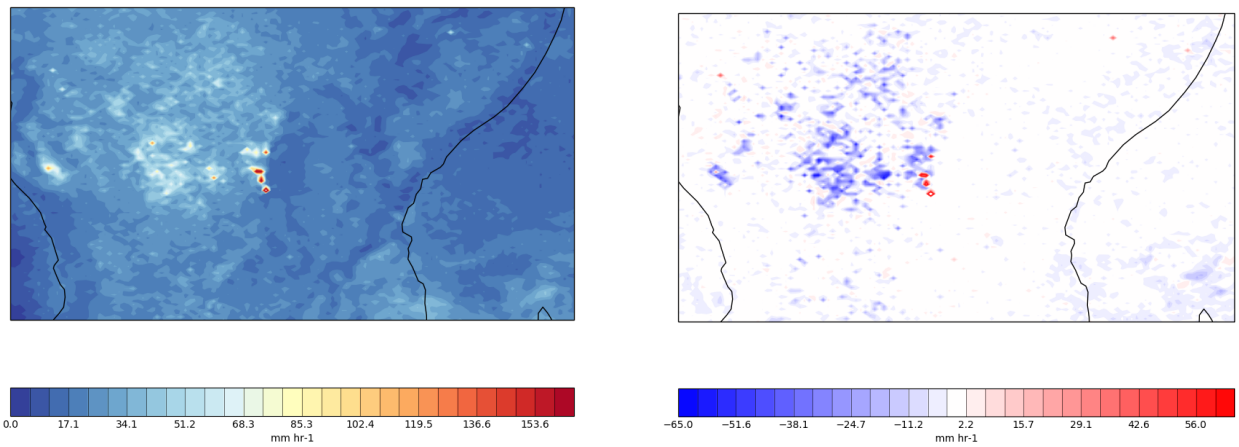

(c) 40 event threshold

(d) 40 event threshold, GP T5 predictions - P25 data

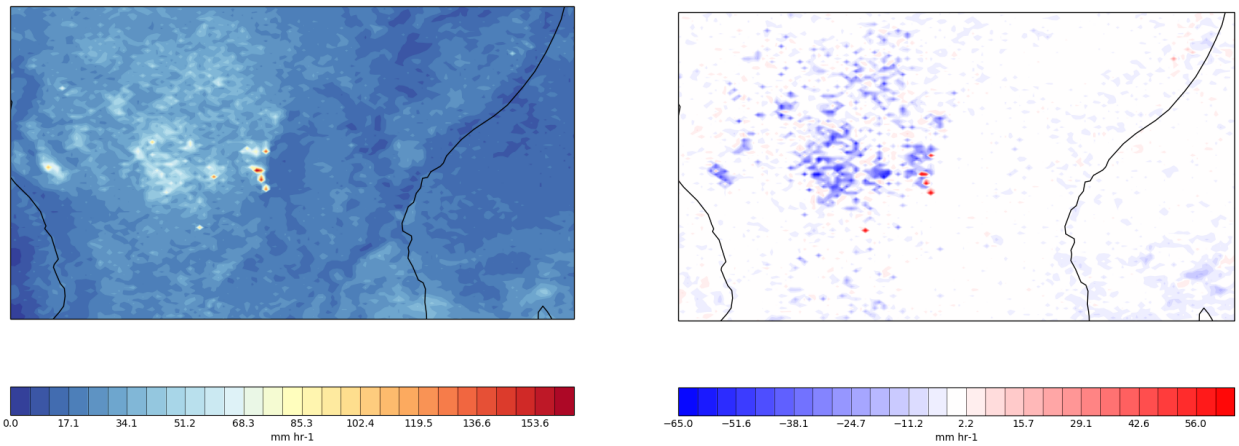

(e) 60 event threshold

(f) 60 event threshold, GP T5 predictions - P25 data

Figure 32: Left column - contour plots for east/central Africa showing the 5-year return period precipitation (mm hr^{-1}) predicted by the GP distribution for present day P25 data. The colour bar is clipped to avoid extreme results. Each sub-plot is using a different number of events as a threshold for the GP distribution: (a) 20 events; (c) 40 events; (e) 60 events. Right column - difference between the GP distribution and the 5-year precipitation data from P25 shown in Fig. 22 for three thresholds: (b) 20 events, GP T5 predictions - P25 data; (d) 40 events, GP T5 predictions - P25 data; and (f) 60 events, GP T5 predictions - P25 data. The colour bar is clipped at either end to remove extreme outliers.

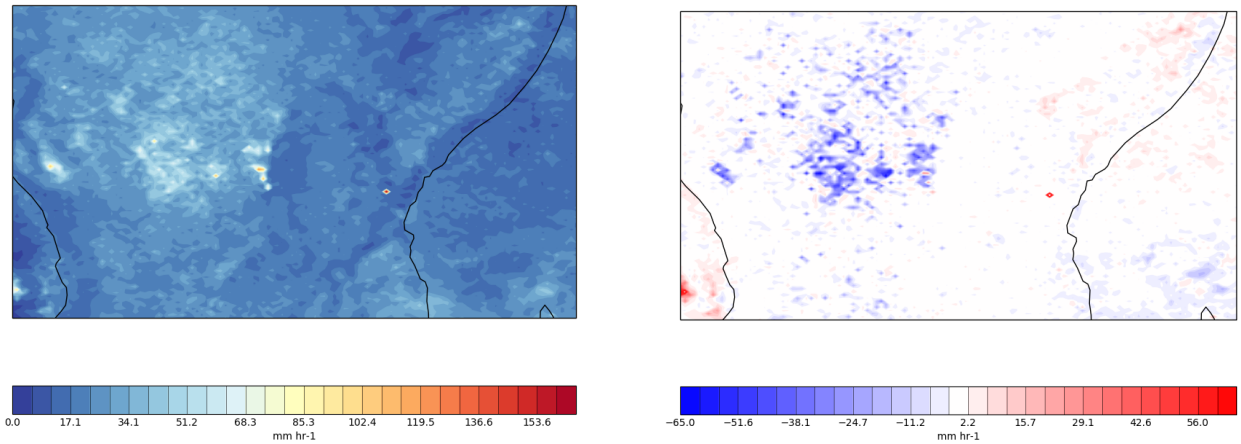

(a) 100 event threshold

(b) 100 event threshold, GP T5 predictions - P25 data

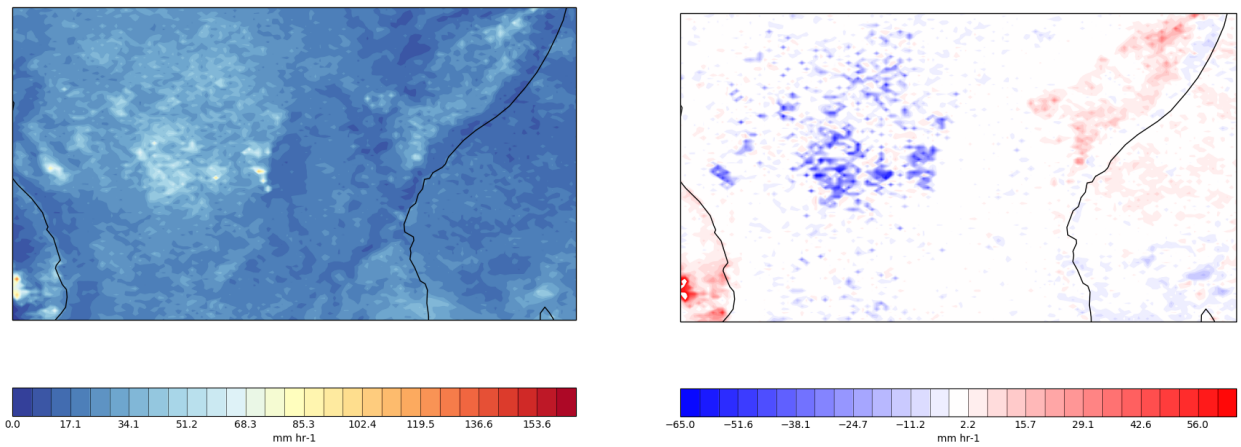

(c) 150 event threshold

(d) 150 event threshold, GP T5 predictions - P25 data

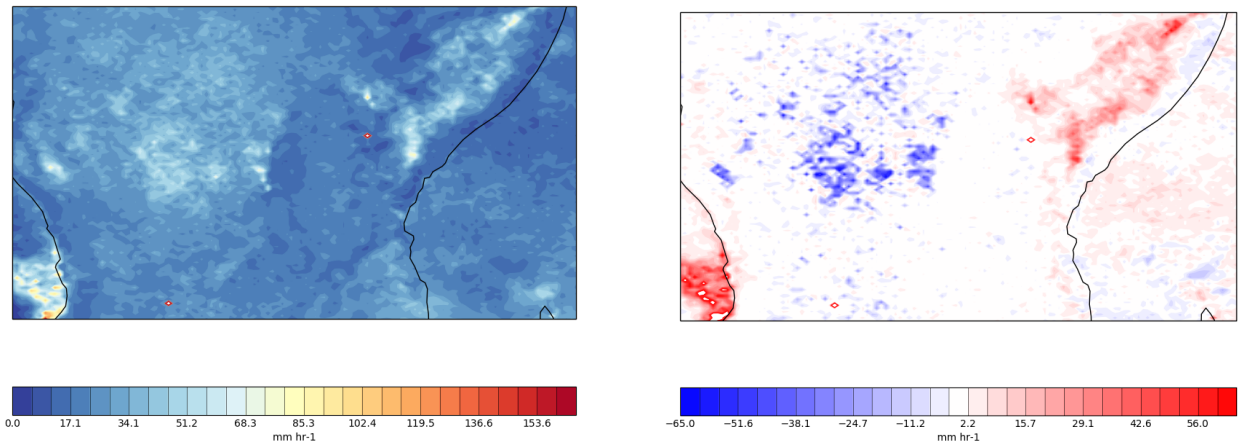

(e) 250 event threshold

(f) 250 event threshold, GP T5 predictions - P25 data

Figure 33: Left column - contour plots for east/central Africa showing the 5-year return period precipitation (mm hr^{-1}) predicted by the GP distribution for present day P25 data. The colour bar is clipped at either end to avoid extreme results. Each sub-plot is using a different number of events as a threshold for the GP distribution: (a) 100 events; (c) 150 events; (e) 250 events. Right column - difference between the GP distribution and the 5-year precipitation data from P25 shown in Fig. 22 for three thresholds: (b) 100 events, GP 5T predictions - P25 data; (d) 150 events, GP 5T predictions - P25 data; and (f) 250 events, GP 5T predictions - P25 data. The colour bar is clipped at either end to remove extreme outliers.

4.3 Conclusions

Presented here is the beginning of a study aimed at identifying the changes in long-term return periods under a warming climate in east Africa using convection-permitting and parametrised climate simulations. Several aspects have been explored for this initial work including modelling methods, specifically threshold choice for the generalised Pareto distribution; and changes in the parametrised model return periods under climate change. In addition, some analysis has been done using the convection-permitting model for individual locations but will need further work to conclude this section.

4.3.1 Return Periods

For specific locations in east Africa, GP distributions were fit to data from both simulations. Preliminary results show:

- CP4-A and CP4A-fc have larger fractional increases in rainfall between T1 and T10 than P25 for all chosen locations.
- trends in the change in precipitation rate between current and future climate was significantly different between CP4-A and P25.
- at low return periods (below T1), precipitation rate is lower for present day than future for both CP4-A and P25 at all locations.
- the ratio between the CP4A-fc and CP4-A return period precipitation decreases for all locations as the return period increases, meaning CP4-A eventually exceeds CP4A-fc. This is in contrast to the parametrised model, which shows that, with the exception of Mogadishu, the return period ratio P25-fc/P25 increases as the return period increases. Mogadishu is the only location where the P25-fc/P25 ratio decreases as the return period increases.
- Kampala and Nairobi show CP4-A return period precipitation rate exceed CP4A-fc around the one in 100-year and one in 75-year event respectively. Mogadishu showed this same behaviour, around the one in one-year event.
- the return period ratio between CP4A-fc and CP4-A changes very little in Kisumu, decreasing by around 0.1 between T1-T100. This is in contrast to the P25-fc precipitation which increases comparatively rapidly with respect to other P25-fc data sets.
- these differing trends between models suggest that using an explicit representation of convection may have a major effect on the portrayal of changing rare precipitation events under climate change.

Across east Africa, ratios between P25-fc and P25 T10 precipitation values were calculated, showing that:

- the parametrised model predicts climate change to cause an increase in one in ten-year extreme precipitation intensity across 96% of locations under the high emissions scenario.
- more than half of the region will see a 40% increase in the T10 precipitation rate under climate change.
- 5% of locations will see a doubling in precipitation intensity in the T10 event.
- maximum increase in the T10 precipitation rate at several locations in the region could be as high as 400%.
- inland regions of east Africa have, on average, a larger increase in T10 precipitation intensity than over oceans under climate change.

4.3.2 Threshold Choice

Various methods of threshold choice for the GP model were investigated, determining the most appropriate way to apply this model to large numbers of data sets with minimal manual interference needed. This study concluded that:

- the most effective threshold 'unit' is the number of events when compared with alternative options - specific high percentiles or mean residual life plots.
- for P25-fc and P25, the higher thresholds (20, 40 and 60 events) produce very few differences in the predicted return periods for both T10 and T5, especially for locations with lower extremes, below around 50 mm hr^{-1}.
- the lower thresholds (100, 150, and 250 events) perform reasonably well in certain regions of east Africa but over-predict parts of the coasts, oceans and Somali region considerably, in some cases by more than 80 mm hr^{-1}.
- the statistical distribution struggles to model very low precipitation values such the Atlantic off the west coast, plus regions of extremely high rainfall in central Africa. All thresholds produce extreme over and under-estimates in this region of more than 80 mm hr^{-1}.
- the 40 event threshold was most appropriate for east Africa. The GP distribution behaves very well over this region with only 2% of simulation values outside the T10 95% confidence interval.
- P25-fc and P25 show very similar trends with respect to the threshold choice, although not all plots are included here.
- T5 predictions are generally slightly better than T10 with less outliers and unreasonable values, as expected. Extreme over-predictions at the lower thresholds were generally in the same locations as T10, with areas such as the Atlantic and Somalia showing precipitation rate differences larger than 60 mm hr^{-1}.

4.3.3 Summary

This report has worked through a process for predicting long-term return period precipitation events using extreme value theory methods. This was then applied to climate simulations, with and without parametrised convection. Although not complete, some conclusions were drawn regarding the effect of climate change on the return periods across east Africa and the effect parametrisation may have on these results. Although a future work plan is detailed in the following section, some immediate comments with respect to upcoming and ongoing work include:

- It may be worth looking at applying the GP distribution regionally with different thresholds as the model appears to behave well within certain regions of Africa using different values if other areas of Africa are of interest.
- Plots are in-progress work and therefore could be optimised e.g. some of the contour scales/colours used and the scatter plots orientation reversed. The $y = x$ line could be added to scatter plots.
- More comparison could be performed between T5, T10 for the various models.
- It is expected that both CP4-A simulations will have different outcomes to the threshold question than the P25 data that has currently been the focus in this report. There is a larger variation in the extreme precipitation events, therefore it is possible that the return period contour and scatter plots will show larger deviations than the P25 equivalents.
- Re-gridding the CP4-A data from the native 4 km grid to the 25 km will likely 'smooth' some of the more extreme values, however the data will nevertheless need testing for optimal threshold choice.

- The results for the individual locations in Fig. 20 discussed return periods of up to T100. For these values to be considered seriously, it would first be necessary to determine exactly how far ahead a ten-year data set can be reliably extrapolated using these methods. Caution should be exercised when quoting results predicted here, especially for above T10 and the error bars need to be considered. Nevertheless, the trends from the results certainly highlight differences between the parametrised and explicit models.

5 Project Plan

See Fig. 34 for chart detailing the timeline of the project over the coming year. A high level research plan for the last two years is also outlined in the below sub-sections. The work is split into approximately three distinct parts. The second chapter will aim to understand the physical mechanisms of how climate change affects storms and extreme precipitation at short time-scales. The third plans to look at the changing convective response to larger scale forcings affecting longer time-scales.

5.1 Current and Short-term Work

The next step within the first part of this project, following on from the results provided above, is to include the CP4-A data regridded to the P25 grid into the final results. Following the same methods, the T10 and T5 values across east Africa will be calculated for both current and future simulations. The ratios will be calculated, compared with the simulation values directly, as performed in Sec. 4.2 using P25.

Currently, the choice of threshold has a considerable impact on the return periods at some locations, as discussed in Sec. 4.3.2. In terms of appropriate threshold choice, other ad-hoc statistical methods exist, such as using L-moments (Ribatet, 2006), which may be more easily automated for larger data sets (numbers of locations) and be more accurate over large regions than choosing a fairly arbitrary percentile or set number of points. Other methods such as parameter stability plots (Coles et al., 2001) will also be investigated and sensitivity tests across the region of interest will be carried out where appropriate to determine the best option for this. Much of the other intended methods and progress for the near-future work are also detailed in (Sec. 4).

Another more sophisticated approach to using extreme value theory may be to spatially aggregate the data in particular ways to help avoid the potential of having any grid-point storm behaviours (very high hourly intensities, with a high large-scale fraction within an area of mostly convective rain) which effect the return period estimates (Chan et al., 2014). The regional frequency analysis method detailed in Hosking et al. (1993) demonstrates a statistical method of spatial pooling which could be applied to this data to avoid any unrealistic grid point extremes produced by the simulations. This uses measurements from the range of data that have similar averages of L-moments and aims to remove sites within a chosen region that are significantly discordant with the rest of the group, quantified by a discordancy measure D_i. An appropriate distribution is then applied to the extremal data as a whole without those discordant points. The difference between the predicted return periods using the initial method detailed in the previous sections versus this spatial pooling method will then be compared to determine if there is a significant, worthwhile difference between the processes. If it is apparent that large discrepancies exist between the results of the methods, it suggests that grid-point storm behaviours may be present in the data used here and may need further analysis.

Once a final method has been selected, this will then be applied to various spatial and temporal aggregates. For time averages such as 3, 6, 12, 24 and 48 hours, this will be relatively simple and will involve using simple convolutions as mentioned in the methods section. The spatial averages involve regridding both the P25 and CP4-A data to larger regions, such as 50x50 km and 125x125 km cell size. Although this will be more complex to do, it will involve fewer data points in total so the code should run faster. The return period data will then be analysed to see how explicit convection over different spatial and temporal averages behaves versus the parametrised model.

In terms of uncertainty analysis, the GP distribution can be tested for stability using 'moving-block' bootstrapping (Wilks, 1997). The error contribution can be obtained by applying the distribution procedure repeatedly to artificial samples made from the original data sets. This provides multiple values for a particular return period - the distribution of these values is a non-parametric estimate of the error contribution. This is common in studies using time-series such as this and would be a simple way to test the sensitivity of the model to the simulation data since each location is only a finite sample representing a population.

After this analysis, the plots and data will be prepared for writing a paper demonstrating how explicit

convection in simulations affects extreme precipitation return periods under climate change. Currently, either the Journal of Hydrometeorology or Journal of Climate is being considered for this publication. During this period, time will also be spent consolidating and tidying up the Python code written for this section to make it simple and functional for repeated use.

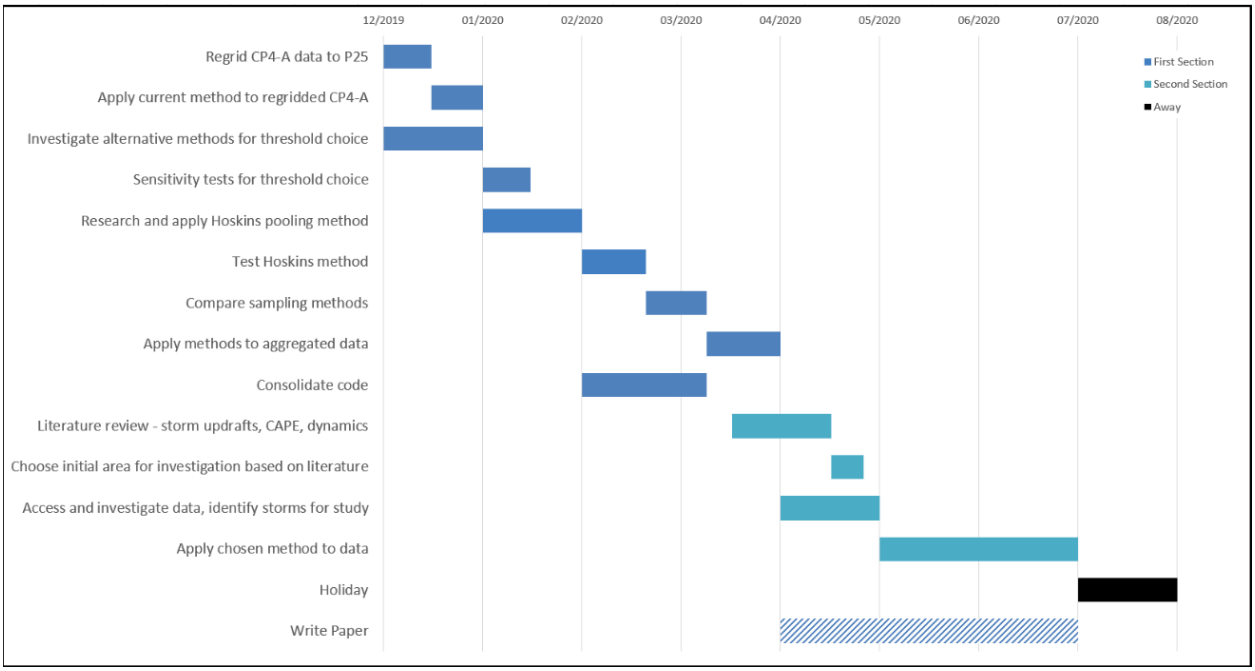

Figure 34: Short-term progress chart until August 2020, showing chapter one to be complete by April 2020. Future key dates include: chapter-two beginning April 2020 and chapter-three in April 2021.

5.2 Future Work - Years Two and Three

Currently, this report has only attempted to quantify how extreme precipitation changes under climate change between the two models. The following sections of this project will investigate the mechanisms behind these extreme precipitation events and aim to explain how and why these mechanisms vary under climate change, using the same present day and future climate simulation data. There are various physical reasons why a particular storm may produce substantially more precipitation than another, so for the second section of this project, the changing properties of individual storms will be investigated. Such properties include the updraft strength and width, CAPE, storm velocity and how the convection is organised.

Recent research on updrafts has looked aspects such as the asymmetry (or skewness) of storm updrafts and downdrafts worldwide and in the extra-tropics, determining that asymmetry intensifies as the climate warms, with updraft motion becoming faster than downdraft motion, causing an increase in precipitation (Tamarin-Brodsky et al., 2019). However, there are also open questions posed about how the vertical velocities behave at larger temperature increases (it is possible that the skewness may decrease depending on the model), over orography and specifically for storms in the tropics under a warming climate (O'Gorman et al., 2018). Climate change studies that employ storm-tracking as a method of studying the changing speed and direction of storm events often consider only extratropical cyclones, or storms in excess of several days in length that travel above a particular distance or in particular seasons, rather than storms that produce the most extreme precipitation (e.g. Pfahl et al., 2015). Relatively few appear to be focussed on regions in Africa and fewer still using convection-permitting models. CP studies for Africa are limited to research done using CP4-A, as the first convection-permitting climate change simulations for Africa. Some recent larger-scale rainfall studies using CP4-A have shown that precipitation frequency increases in east Africa under climate change (Finney et al., 2019) and that precipitation decreases in frequency in parts of west

Africa (Kendon et al., 2019). However, unlike these studies, it is intended that this section of the project be a more in-depth, focussed investigation into the changing individual storm dynamics at mesoscale and smaller, within the tropics region of Africa, that cause the rare precipitation events.

Other features that are known to have an effect on the internal dynamics of a storm are CAPE (convective available potential energy, the vertically integrated buoyant energy; J kg^{-1}) and wind shear (often measured as the vertical change in the horizontal wind vector measured as the difference between the horizontal wind velocity at 6km and ground level, S06; m s^{-1}). These features influence the storm intensity, organisation and longevity, all of which have an impact on the amount of precipitation (Lilly, 1979, Klemp, 1987). It is suggested that CAPE scales to maximum updraft velocity as $\sqrt{(2 \times \text{CAPE})}$, implying that strong updrafts come from large CAPE, leading to an increase in precipitation (Holton, 2004). The shear can also have an influence on the storm behaviour, as it can encourage storm organisation and helps sustain the occurrence of precipitation-driven downdrafts. Shear can also affect the dissipation of storm events, potentially reducing the precipitation. These factors all impact the amount of rain a storm will produce.

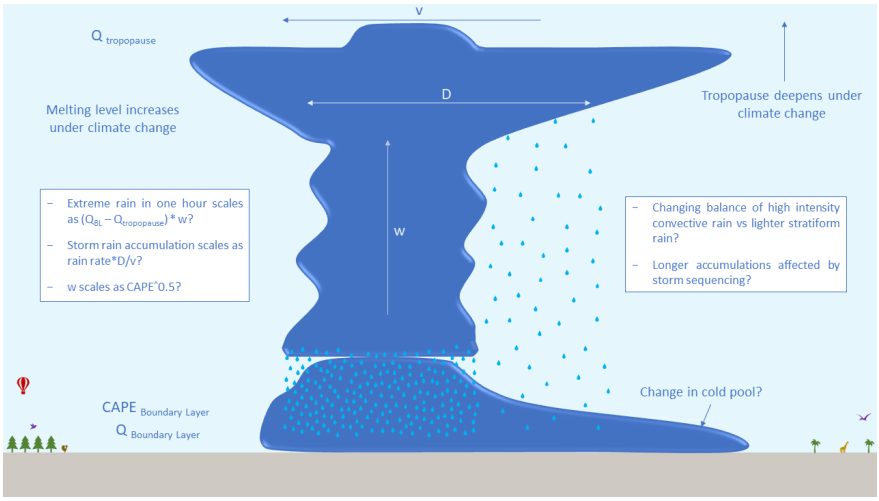

Figure 35: Simple schematic of the cross-section of a storm. Shown here is the updraft velocity, w; width of the rainfall, D; storm velocity, v; water vapour mixing ratio at the boundary layer and tropopause, Q_{BL} and Q_{trop}; and the convective available potential energy at the boundary layer, CAPE $_{\text{BL}}$. Several hypotheses for investigation are noted.

Using the first chapter of this project, relevant extremes will be identified at time-scales of hours or one day for the region of interest (at the moment is east Africa). Identifying the storm events that generate these extremes will be performed using storm tracks and composites from CP4-A, having already been produced by the FCFA project using the simulation data. Utilising this will provide an efficient method of studying the storm changes between present day and future climate. The changes in the storms that generate extreme events will then be compared to less intense storms. The aim of this is to produce physical composites of extreme and less extreme storms by averaging certain features such as wind vectors, temperatures and available water vapour to create $x - y$ and $x - z$ diagrams of the storm structure.

Some specific hypotheses are noted in the schematic in Fig. 35, showing a simple storm cross-section. Here, some features of interest are highlighted, including the width of the rain, (D); updraft velocity (w); the water vapour mixing ratio at the boundary layer and tropopause (Q); storm velocity (v) and cold pool. Various features that affect a convective storm event under a warming climate are also noted - the tropopause deepens, the melting level increases and wind shear will change, affecting storm organisation and updraft speeds.

Some specific hypotheses/questions to be tested include:

- does extreme hourly precipitation scale as $w \times (Q_{\text{BL}} - Q_{\text{trop}})$?
- does storm accumulation scale as rain-rate $\times \frac{D}{v}$?

- what is the effect of the changing balance of high-intensity convective rain versus lighter stratiform rain?
- are longer accumulations affected by storm sequencing?
- does w scale as $\sqrt{\text{CAPE}}$?

It is worth noting that this part of the project is a departure from the statistics based work that has been performed so far, but will build on this by using the statistical analysis to identify extreme events that can then be analysed mechanistically. The beginning of this section of the project will therefore involve a significant amount of literature research and reading on storm and weather dynamics, specifically aimed at extreme precipitation events, since it involves physics that is currently less familiar. Producing a literature review will aid progress and guide the direction of the project, with the available data in mind.

Time permitting, for the third section, after the effect of climate change on individual storm events has been addressed, the aim is to look at larger-scale synoptic features, such as African easterly waves (AEWs; for west Africa), the Madden-Julian Oscillation (MJO; for east Africa) and Kelvin waves (east Africa). These disturbances cause the formation of cumulonimbus and mesoscale convective systems (MCSs), which are the primary cause of extreme rainfall in tropical Africa. How the local convective response to such large-scale forcings changes with climate change will be the next focus, linking the changing rain accumulation with changes in the synoptic events that cause them. Alternatively, the coupling between the mesoscale forcings such as changing sea, mountain or soil-moisture induced breezes could provide a third focus. As land warms faster than the ocean, it affects the sea breezes and so under a warming climate, sea breezes are expected to increase.

The exact content of this section will depend on the methods and results found in the previous chapter. It may transpire that there is far more to investigate in the second section than currently predicted, dictating the quantity and direction of the third. Currently, the emphasis for the above is on east Africa, however there is scope to extend this to other regions (including pan-Africa).

References

[1] L. Alexander et al. "Global observed changes in daily climate extremes of temperature and precipitation". In: *Journal of Geophysical Research: Atmospheres* 111.D5 (2006).

[2] R. P. Allan et al. "Atmospheric warming and the amplification of precipitation extremes". In: *Science* 321.5895 (2008), pp. 1481–1484.

[3] R. P. Allan et al. "Current changes in tropical precipitation". In: *Environmental Research Letters* 5.2 (2010), p. 025205.

[4] C. J. Allen et al. "Dust emission and transport mechanisms in the central Sahara: Fennec ground-based observations from Bordj Badji Mokhtar, June 2011". In: *Journal of Geophysical Research: Atmospheres* 118.12 (2013), pp. 6212–6232.

[5] M. R. Allen et al. "Constraints on future changes in climate and the hydrologic cycle". In: *Nature* 419.6903 (2002), p. 228.

[6] A. Aubréville et al. "Climats, forêts et désertification de l'Afrique tropicale". In: (1949).

[7] C. for Basic Systems (CBS). "Progress/activity reports presented at CBS-XIV". In: *World Meteorological Organization* (2009).

[8] S. Berthou et al. "Improved climatological precipitation characteristics over West Africa at convection-permitting scales". In: *Climate Dynamics* (2019), pp. 1–21.

[9] A. K. Betts. "Climate-convection feedbacks: Some further issues". In: *Climatic Change* 39.1 (1998), p. 35.

[10] A. K. Betts et al. "Evaluation of the diurnal cycle of precipitation, surface thermodynamics, and surface fluxes in the ECMWF model using LBA data". In: *Journal of Geophysical Research: Atmospheres* 107.D20 (2002), LBA–12.

[11] C. E. Birch et al. "A seamless assessment of the role of convection in the water cycle of the West African Monsoon". In: *Journal of Geophysical Research: Atmospheres* 119.6 (2014), pp. 2890–2912.

[12] G. Boer. "Climate change and the regulation of the surface moisture and energy budgets". In: *Climate Dynamics* 8.5 (1993), pp. 225–239.

[13] B. G. Brown et al. "Exploratory analysis of precipitation events with implications for stochastic modeling". In: *Journal of climate and applied meteorology* 24.1 (1985), pp. 57–67.

[14] M. P. Byrne et al. "The response of precipitation minus evapotranspiration to climate warming: Why the "wet-get-wetter, dry-get-drier" scaling does not hold over land". In: *Journal of Climate* 28.20 (2015), pp. 8078–8092.

[15] J. Carreau et al. "A hybrid Pareto model for asymmetric fat-tailed data: the univariate case". In: *Extremes* 12.1 (2009), pp. 53–76.

[16] R. Chadwick et al. "Large rainfall changes consistently projected over substantial areas of tropical land". In: *Nature Climate Change* 6.2 (2016), p. 177.

[17] R. Chadwick et al. "Spatial Patterns of Precipitation Change in CMIP5: Why the Rich Do Not Get Richer in the Tropics". In: *Journal of Climate* 26.11 (2013), pp. 3803–3822. DOI: 10.1175/JCLI-D-12-00543.1.

[18] S. C. Chan et al. "The value of high-resolution Met Office regional climate models in the simulation of multihourly precipitation extremes". In: *Journal of Climate* 27.16 (2014), pp. 6155–6174.

[19] J. G. Charney. "Dynamics of deserts and drought in the Sahel". In: *Quarterly Journal of the Royal Meteorological Society* 101.428 (1975), pp. 193–202.

[20] C. Chou et al. "Evaluating the "rich-get-richer" mechanism in tropical precipitation change under global warming". In: *Journal of Climate* 22.8 (2009), pp. 1982–2005.

[21] C. Chou et al. "Increase in the range between wet and dry season precipitation". In: *Nature Geoscience* 6.4 (2013), p. 263.

[22] C. Chou et al. "Mechanisms of global warming impacts on regional tropical precipitation". In: *Journal of climate* 17.13 (2004), pp. 2688–2701.

[23] S. Coles et al. "A fully probabilistic approach to extreme rainfall modeling". In: *Journal of Hydrology* 273.1-4 (2003), pp. 35–50.

[24] S. Coles et al. *An introduction to statistical modeling of extreme values*. Vol. 208. Springer, 2001.

[25] J. Crook et al. "Assessment of the representation of West African storm lifecycles in convection-permitting simulations". In: *Earth and Space Science* (2019).

[26] C. Cunnane. "A note on the Poisson assumption in partial duration series models". In: *Water Resources Research* 15.2 (1979), pp. 489–494.

[27] W. Cunnington et al. "Simulations of the Saharan atmosphere—dependence on moisture and albedo". In: *Quarterly Journal of the Royal Meteorological Society* 112.474 (1986), pp. 971–999.

[28] A. Dai. "Precipitation characteristics in eighteen coupled climate models". In: *Journal of Climate* 19.18 (2006), pp. 4605–4630.

[29] A. Dai. "Recent changes in the diurnal cycle of precipitation over the United States". In: *Geophysical Research Letters* 26.3 (1999), pp. 341–344.

[30] C. A. Davis et al. "Coherence of warm-season continental rainfall in numerical weather prediction models". In: *Monthly Weather Review* 131.11 (2003), pp. 2667–2679.

[31] A. C. Davison et al. "Models for exceedances over high thresholds". In: *Journal of the Royal Statistical Society: Series B (Methodological)* 52.3 (1990), pp. 393–425.

[32] T. L. Delworth et al. "Simulation of early 20th century global warming". In: *Science* 287.5461 (2000), pp. 2246–2250.

[33] P. A. Dirmeyer et al. "Simulating the diurnal cycle of rainfall in global climate models: Resolution versus parameterization". In: *Climate dynamics* 39.1-2 (2012), pp. 399–418.

[34] M. G. Donat et al. "More extreme precipitation in the world's dry and wet regions". In: *Nature Climate Change* 6.5 (2016), p. 508.

[35] C. M. Dunning et al. "Later wet seasons with more intense rainfall over Africa under future climate change". In: *Journal of Climate* 31.23 (2018), pp. 9719–9738.

[36] D. Dupuis et al. "A hybrid estimator for generalized Pareto and extreme-value distributions". In: *Communications in Statistics-Theory and Methods* 27.4 (1998), pp. 925–941.

[37] S. Emori et al. "Dynamic and thermodynamic changes in mean and extreme precipitation under changed climate". In: *Geophysical Research Letters* 32.17 (2005).

[38] S. Engelstaedter et al. "North African dust emissions and transport". In: *Earth-Science Reviews* 79.1-2 (2006), pp. 73–100.

[39] C. A. Ferro et al. "Inference for clusters of extreme values". In: *Journal of the Royal Statistical Society: Series B (Statistical Methodology)* 65.2 (2003), pp. 545–556.

[40] D. L. Finney et al. "Implications of improved representation of convection for the East Africa water budget using a convection-permitting model". In: *Journal of Climate* 32.7 (2019), pp. 2109–2129.

[41] A. Fowler et al. "Potential impacts of global warming on the frequency and magnitude of heavy precipitation". In: *Natural Hazards* 11.3 (1995), pp. 283–303.

[42] H. Fowler et al. "Estimating change in extreme European precipitation using a multimodel ensemble". In: *Journal of Geophysical Research: Atmospheres* 112.D18 (2007).

[43] N. van de Giesen et al. "The Trans-African Hydro-Meteorological Observatory (TAHMO)". In: *Wiley Interdisciplinary Reviews: Water* 1.4 (2014), pp. 341–348.

[44] F. Giorgi et al. "Addressing climate information needs at the regional level: the CORDEX framework". In: *World Meteorological Organization (WMO) Bulletin* 58.3 (2009), p. 175.

[45] F. Giorgi et al. "Evaluating uncertainties in the prediction of regional climate change". In: *Geophysical Research Letters* 27.9 (2000), pp. 1295–1298.

[46] B. Gnedenko. “Sur la distribution limite du terme maximum d’une serie aleatoire”. In: *Annals of mathematics* (1943), pp. 423–453.

[47] J. A. Greenwood et al. “Probability weighted moments: definition and relation to parameters of several distributions expressable in inverse form”. In: *Water resources research* 15.5 (1979), pp. 1049–1054.

[48] P. Greve et al. “Global assessment of trends in wetting and drying over land”. In: *Nature geoscience* 7.10 (2014), p. 716.

[49] F. Guichard et al. “Modelling the diurnal cycle of deep precipitating convection over land with cloud-resolving models and single-column models”. In: *Quarterly Journal of the Royal Meteorological Society* 130.604 (2004), pp. 3139–3172.

[50] E. J. Gumbel. “Statistical theory of floods and droughts”. In: *Journal of the Institution of Water Enigneers and Scientists* 12 (1958), pp. 157–184.

[51] E. J. Gumbel. “The return period of flood flows”. In: *The annals of mathematical statistics* 12.2 (1941), pp. 163–190.

[52] T. Haktanir et al. “Evaluation of various distributions for flood frequency analysis”. In: *Hydrological Sciences Journal* 38.1 (1993), pp. 15–32.

[53] I. M. Held et al. “Robust responses of the hydrological cycle to global warming”. In: *Journal of climate* 19.21 (2006), pp. 5686–5699.

[54] K. Hennessy et al. “Changes in daily precipitation under enhanced greenhouse conditions”. In: *Climate Dynamics* 13.9 (1997), pp. 667–680.

[55] J. R. Holton. “An introduction to dynamic meteorology”. In: *American Journal of Physics* 41.5 (2004), pp. 752–754.

[56] J. R. M. Hosking. “L-moments: Analysis and estimation of distributions using linear combinations of order statistics”. In: *Journal of the Royal Statistical Society: Series B (Methodological)* 52.1 (1990), pp. 105–124.

[57] J. R. M. Hosking et al. “Estimation of the generalized extreme-value distribution by the method of probability-weighted moments”. In: *Technometrics* 27.3 (1985), pp. 251–261.

[58] J. R. M. Hosking et al. “Some statistics useful in regional frequency analysis”. In: *Water resources research* 29.2 (1993), pp. 271–281.

[59] P. Huang et al. “Patterns of the seasonal response of tropical rainfall to global warming”. In: *Nature Geoscience* 6.5 (2013), p. 357.

[60] G. J. Huffman et al. “Global precipitation at one-degree daily resolution from multisatellite observations”. In: *Journal of hydrometeorology* 2.1 (2001), pp. 36–50.

[61] M. Hulme et al. “African climate change: 1900-2100”. In: *Climate research* 17.2 (2001), pp. 145–168.

[62] W. Ingram. “On the robustness of the water vapor feedback: GCM vertical resolution and formulation”. In: *Journal of Climate* 15.9 (2002), pp. 917–921.

[63] B. Jackson et al. “Mesoscale convective systems over western equatorial Africa and their relationship to large-scale circulation”. In: *Monthly Weather Review* 137.4 (2009), pp. 1272–1294.

[64] R. James et al. “Evaluating climate models with an African lens”. In: *Bulletin of the American Meteorological Society* 99.2 (2018), pp. 313–336.

[65] A. F. Jenkinson. “The frequency distribution of the annual maximum (or minimum) values of meteorological elements”. In: *Quarterly Journal of the Royal Meteorological Society* 81.348 (1955), pp. 158–171.

[66] A. Joubert et al. “Droughts over southern Africa in a doubled-CO2 climate”. In: *International Journal of Climatology* 16.10 (1996), pp. 1149–1156.

[67] A. Joubert et al. “Simulating present and future climates of southern Africa using general circulation models”. In: *Progress in physical geography* 21.1 (1997), pp. 51–78.

[68] R. W. Katz et al. "Statistics of extremes in hydrology". In: *Advances in water resources* 25.8-12 (2002), pp. 1287–1304.

[69] E. J. Kendon et al. "Enhanced future changes in wet and dry extremes over Africa at convection-permitting scale". In: *Nature communications* 10.1 (2019), p. 1794.

[70] E. J. Kendon et al. "Heavier summer downpours with climate change revealed by weather forecast resolution model". In: *Nature Climate Change* 4.7 (2014), p. 570.

[71] V. V. Kharin et al. "Changes in temperature and precipitation extremes in the CMIP5 ensemble". In: *Climatic change* 119.2 (2013), pp. 345–357.

[72] V. V. Kharin et al. "Changes in temperature and precipitation extremes in the IPCC ensemble of global coupled model simulations". In: *Journal of Climate* 20.8 (2007), pp. 1419–1444.

[73] T. Kittel et al. "Intercomparsion of regional biases and doubled CO2-sensitivity of coupled atmosphere-ocean general circulation model experiments". In: *Climate Dynamics* 14.1 (1997), pp. 1–15.

[74] J. B. Klemp. "Dynamics of tornadic thunderstorms". In: *Annual review of fluid mechanics* 19.1 (1987), pp. 369–402.

[75] C. Knote et al. "Changes in weather extremes: Assessment of return values using high resolution climate simulations at convection-resolving scale". In: *Meteorologische Zeitschrift* 19.1 (2010), pp. 11–23.

[76] D. Koutsoyiannis et al. "Analysis of a long record of annual maximum rainfall in Athens, Greece, and design rainfall inferences". In: *Natural Hazards* 22.1 (2000), pp. 29–48.

[77] S. Kumar et al. "Revisiting trends in wetness and dryness in the presence of internal climate variability and water limitations over land". In: *Geophysical Research Letters* 42.24 (2015), pp. 10–867.

[78] M. Kumari et al. "Clustering data and incorporating topographical variables for improving spatial interpolation of rainfall in mountainous region". In: *Water resources management* 31.1 (2017), pp. 425–442.

[79] C. Kummerow et al. "The status of the Tropical Rainfall Measuring Mission (TRMM) after two years in orbit". In: *Journal of applied meteorology* 39.12 (2000), pp. 1965–1982.

[80] K. E. Kunkel et al. "Long-term trends in extreme precipitation events over the conterminous United States and Canada". In: *Journal of climate* 12.8 (1999), pp. 2515–2527.

[81] J. M. Landwehr et al. "Probability weighted moments compared with some traditional techniques in estimating Gumbel parameters and quantiles". In: *Water Resources Research* 15.5 (1979), pp. 1055–1064.

[82] R. Laprise et al. "Climate projections over CORDEX Africa domain using the fifth-generation Canadian Regional Climate Model (CRCM5)". In: *Climate Dynamics* 41.11-12 (2013), pp. 3219–3246.

[83] M. R. Leadbetter. "Extremes and local dependence in stationary sequences". In: *Probability Theory and Related Fields* 65.2 (1983), pp. 291–306.

[84] M. R. Leadbetter et al. *Extremes and related properties of random sequences and processes*. Springer Science & Business Media, 2012.

[85] H. W. Lean et al. "Characteristics of high-resolution versions of the Met Office Unified Model for forecasting convection over the United Kingdom". In: *Monthly Weather Review* 136.9 (2008), pp. 3408–3424.

[86] G. Lenderink et al. "Increase in hourly precipitation extremes beyond expectations from temperature changes". In: *Nature Geoscience* 1.8 (2008), p. 511.

[87] Y. Li et al. "Statistical modeling of extreme rainfall in southwest Western Australia". In: *Journal of climate* 18.6 (2005), pp. 852–863.

[88] D. K. Lilly. "The dynamical structure and evolution of thunderstorms and squall lines". In: *Annual Review of Earth and Planetary Sciences* 7.1 (1979), pp. 117–161.

[89] C. Liu et al. "Observed and simulated precipitation responses in wet and dry regions 1850–2100". In: *Environmental Research Letters* 8.3 (2013), p. 034002.

[90] V. Lucarini et al. “Comparison of mean climate trends in the Northern Hemisphere between National Centers for Environmental Prediction and two atmosphere-ocean model forced runs”. In: *Journal of Geophysical Research: Atmospheres* 107.D15 (2002).

[91] D. Lumbroso et al. “The challenges of developing rainfall intensity–duration–frequency curves and national flood hazard maps for the Caribbean”. In: *Journal of Flood Risk Management* 4.1 (2011), pp. 42–52.

[92] H. Madsen et al. “Comparison of annual maximum series and partial duration series methods for modeling extreme hydrologic events: 1. At-site modeling”. In: *Water resources research* 33.4 (1997), pp. 747–757.

[93] J. H. Marsham et al. “The role of moist convection in the West African monsoon system: Insights from continental-scale convection-permitting simulations”. In: *Geophysical Research Letters* 40.9 (2013), pp. 1843–1849.

[94] M. J. McPhaden et al. “Slowdown of the meridional overturning circulation in the upper Pacific Ocean”. In: *Nature* 415.6872 (2002), p. 603.

[95] G. A. Meehl et al. “Response of the NCAR Climate System Model to increased CO2 and the role of physical processes”. In: *Journal of Climate* 13.11 (2000), pp. 1879–1898.

[96] S.-K. Min et al. “Human contribution to more-intense precipitation extremes”. In: *Nature* 470.7334 (2011), p. 378.

[97] S. Minobe. “Spatio-temporal structure of the pentadecadal variability over the North Pacific”. In: *Progress in Oceanography* 47.2-4 (2000), pp. 381–408.

[98] J. Mitchell et al. “Equilibrium climate change and its implications for the future”. In: *Climate change: The IPCC scientific assessment* 131 (1990), p. 172.

[99] J. Mitchell et al. “The effect of stabilising atmospheric carbon dioxide concentrations on global and regional climate change”. In: *Geophysical Research Letters* 27.18 (2000), pp. 2977–2980.

[100] R. H. Moss et al. “The next generation of scenarios for climate change research and assessment”. In: *Nature* 463.7282 (2010), p. 747.

[101] C. J. Muller et al. “Intensification of precipitation extremes with warming in a cloud-resolving model”. In: *Journal of Climate* 24.11 (2011), pp. 2784–2800.

[102] G. Nikulin et al. “Precipitation climatology in an ensemble of CORDEX-Africa regional climate simulations”. In: *Journal of Climate* 25.18 (2012), pp. 6057–6078.

[103] J. Norris et al. “Thermodynamic versus dynamic controls on extreme precipitation in a warming climate from the Community Earth System Model Large Ensemble”. In: *Journal of Climate* 32.4 (2019), pp. 1025–1045.

[104] P. A. O’Gorman et al. “Increase in the skewness of extratropical vertical velocities with climate warming: fully nonlinear simulations versus moist baroclinic instability”. In: *Quarterly Journal of the Royal Meteorological Society* 144.710 (2018), pp. 208–217.

[105] P. A. O’Gorman et al. “The physical basis for increases in precipitation extremes in simulations of 21st-century climate change”. In: *Proceedings of the National Academy of Sciences* 106.35 (2009), pp. 14773–14777.

[106] B. Oueslati et al. “Revisiting the dynamic and thermodynamic processes driving the record-breaking January 2014 precipitation in the southern UK”. In: *Scientific reports* 9.1 (2019), p. 2859.

[107] R. K. Pachauri et al. *Climate change 2014: synthesis report. Contribution of Working Groups I, II and III to the fifth assessment report of the Intergovernmental Panel on Climate Change*. IPCC, 2014.

[108] P. Pall et al. “Testing the Clausius–Clapeyron constraint on changes in extreme precipitation under CO 2 warming”. In: *Climate Dynamics* 28.4 (2007), pp. 351–363.

[109] A. G. Pendergrass. “What precipitation is extreme?” In: *Science* 360.6393 (2018), pp. 1072–1073.

[110] A. G. Pendergrass et al. “Changes in the distribution of rain frequency and intensity in response to global warming”. In: *Journal of Climate* 27.22 (2014), pp. 8372–8383.

[111] A. G. Pendergrass et al. "The rain is askew: Two idealized models relating vertical velocity and precipitation distributions in a warming world". In: *Journal of Climate* 29.18 (2016), pp. 6445–6462.

[112] S. Pfahl et al. "Extratropical cyclones in idealized simulations of changed climates". In: *Journal of Climate* 28.23 (2015), pp. 9373–9392.

[113] S. Pfahl et al. "Understanding the regional pattern of projected future changes in extreme precipitation". In: *Nature Climate Change* 7.6 (2017), p. 423.

[114] N. A. Phillips. "The general circulation of the atmosphere: A numerical experiment". In: *Quarterly Journal of the Royal Meteorological Society* 82.352 (1956), pp. 123–164.

[115] J. Pickands III et al. "Statistical inference using extreme order statistics". In: *the Annals of Statistics* 3.1 (1975), pp. 119–131.

[116] J. J. Ploshay et al. "Simulation of the diurnal cycle in tropical rainfall and circulation during boreal summer with a high-resolution GCM". In: *Monthly Weather Review* 138.9 (2010), pp. 3434–3453.

[117] D. Polson et al. "Strengthening contrast between precipitation in tropical wet and dry regions". In: *Geophysical Research Letters* 44.1 (2017), pp. 365–373.

[118] A. F. Prein et al. "The future intensification of hourly precipitation extremes". In: *Nature Climate Change* 7.1 (2017), p. 48.

[119] A. F. Prein et al. "A review on regional convection-permitting climate modeling: Demonstrations, prospects, and challenges". In: *Reviews of Geophysics* 53.2 (2015), pp. 323–361.

[120] J. Räisänen et al. "Changes in average and extreme precipitation in two regional climate model experiments". In: *Tellus A* 53.5 (2001), pp. 547–566.

[121] P. J. Restrepo-Posada et al. "Identification of independent rainstorms". In: *Journal of Hydrology* 55.1-4 (1982), pp. 303–319.

[122] M. Ribatet. "A user's guide to the PoT package (version 1.4)". In: *University of Quebec* (2006).

[123] H. Riehl. "On the heat balance of the equatorial trough zone". In: *Geophysica* 6 (1958), pp. 503–538.

[124] M. D. Risser et al. "Attributable human-induced changes in the likelihood and magnitude of the observed extreme precipitation during hurricane Harvey". In: *Geophysical Research Letters* 44.24 (2017), pp. 12–457.

[125] A. J. Robson et al. *Statistical Procedures for Flood Frequency Estimation. Volume 3 of the Flood Estimation Handbook*. Centre for Ecology and Hydrology, 1999.

[126] M. Roderick et al. "A general framework for understanding the response of the water cycle to global warming over land and ocean". In: (2014).

[127] D. M. Romps. "Response of tropical precipitation to global warming". In: *Journal of the Atmospheric Sciences* 68.1 (2011), pp. 123–138.

[128] R. J. Ross et al. "Radiosonde-based Northern Hemisphere tropospheric water vapor trends". In: *Journal of Climate* 14.7 (2001), pp. 1602–1612.

[129] W. B. Rossow et al. "Tropical precipitation extremes". In: *Journal of Climate* 26.4 (2013), pp. 1457–1466.

[130] D. P. Rowell. "Sources of uncertainty in future changes in local precipitation". In: *Climate dynamics* 39.7-8 (2012), pp. 1929–1950.

[131] D. P. Rowell et al. "Causes of the Uncertainty in Projections of Tropical Terrestrial Rainfall Change: East Africa". In: *Journal of Climate* 31.15 (2018), pp. 5977–5995.

[132] C. Schär et al. "Percentile indices for assessing changes in heavy precipitation events". In: *Climatic Change* 137.1-2 (2016), pp. 201–216.

[133] J. Scheff et al. "Robust future precipitation declines in CMIP5 largely reflect the poleward expansion of model subtropical dry zones". In: *Geophysical Research Letters* 39.18 (2012).

[134] R. Seager et al. "Does global warming cause intensified interannual hydroclimate variability?" In: *Journal of Climate* 25.9 (2012), pp. 3355–3372.

[135] M. E. Shongwe et al. "Projected changes in mean and extreme precipitation in Africa under global warming. Part II: East Africa". In: *Journal of Climate* 24.14 (2011), pp. 3718–3733.

[136] B. J. Soden et al. "Global cooling after the eruption of Mount Pinatubo: A test of climate feedback by water vapor". In: *science* 296.5568 (2002), pp. 727–730.

[137] E. P. Stebbing. "The encroaching Sahara: the threat to the West African colonies". In: *The Geographical Journal* 85.6 (1935), pp. 506–519.

[138] G. L. Stephens et al. "Controls of global-mean precipitation increases in global warming GCM experiments". In: *Journal of Climate* 21.23 (2008), pp. 6141–6155.

[139] G. L. Stephens et al. "Dreary state of precipitation in global models". In: *Journal of Geophysical Research: Atmospheres* 115.D24 (2010).

[140] B. Stevens et al. "Untangling aerosol effects on clouds and precipitation in a buffered system". In: *Nature* 461.7264 (2009), p. 607.

[141] E. Stewart et al. "The FORGEX method of rainfall growth estimation I: Review of requirement". In: *Hydrology and Earth System Sciences Discussions* 3.2 (1999), pp. 187–195.

[142] R. A. Stratton et al. "A pan-African convection-permitting regional climate simulation with the Met Office Unified Model: CP4-Africa". In: *Journal of Climate* 31.9 (2018), pp. 3485–3508.

[143] R. A. Stratton et al. "Improving the diurnal cycle of convection in GCMs". In: *Quarterly Journal of the Royal Meteorological Society* 138.666 (2012), pp. 1121–1134.

[144] M. Sugiyama et al. "Precipitation extreme changes exceeding moisture content increases in MIROC and IPCC climate models". In: *Proceedings of the National Academy of Sciences* 107.2 (2010), pp. 571–575.

[145] Y. Sun et al. "How often does it rain?" In: *Journal of Climate* 19.6 (2006), pp. 916–934.

[146] T. Tamarin-Brodsky et al. "The asymmetry of vertical velocity in current and future climate". In: *Geophysical Research Letters* 46.1 (2019), pp. 374–382.

[147] N. F. Tandon et al. "Understanding the dynamics of future changes in extreme precipitation intensity". In: *Geophysical Research Letters* 45.6 (2018), pp. 2870–2878.

[148] K. E. Taylor et al. "An overview of CMIP5 and the experiment design". In: *Bulletin of the American Meteorological Society* 93.4 (2012), pp. 485–498.

[149] H. Tokinaga et al. "Regional patterns of tropical Indo-Pacific climate change: Evidence of the Walker circulation weakening". In: *Journal of Climate* 25.5 (2012), pp. 1689–1710.

[150] K. E. Trenberth. "Atmospheric moisture residence times and cycling: Implications for rainfall rates and climate change". In: *Climatic change* 39.4 (1998), pp. 667–694.

[151] K. E. Trenberth. "Conceptual framework for changes of extremes of the hydrological cycle with climate change". In: *Weather and Climate Extremes*. Springer, 1999, pp. 327–339.

[152] K. E. Trenberth et al. "Earth's global energy budget". In: *Bulletin of the American Meteorological Society* 90.3 (2009), pp. 311–324.

[153] K. E. Trenberth et al. "Effects of Mount Pinatubo volcanic eruption on the hydrological cycle as an analog of geoengineering". In: *Geophysical Research Letters* 34.15 (2007).

[154] K. E. Trenberth et al. "The changing character of precipitation". In: *Bulletin of the American Meteorological Society* 84.9 (2003), pp. 1205–1218.

[155] P. D. Tyson. "Climatic change in southern Africa: past and present conditions and possible future scenarios". In: *Climatic Change* 18.2-3 (1991), pp. 241–258.

[156] G. J. Van Oldenborgh et al. "Attribution of extreme rainfall from Hurricane Harvey, August 2017". In: *Environmental Research Letters* 12.12 (2017), p. 124009.

[157] G. A. Vecchi et al. "Weakening of tropical Pacific atmospheric circulation due to anthropogenic forcing". In: *Nature* 441.7089 (2006), p. 73.

[158] J. Wadsworth et al. “Likelihood-based procedures for threshold diagnostics and uncertainty in extreme value modelling”. In: *Journal of the Royal Statistical Society: Series B (Statistical Methodology)* 74.3 (2012), pp. 543–567.

[159] D. Walters et al. “The Met Office unified model global atmosphere 6.0/6.1 and JULES global land 6.0/6.1 configurations”. In: *Geoscientific Model Development* 10.4 (2017), pp. 1487–1520.

[160] S. S. Wang et al. “Quantitative attribution of climate effects on Hurricane Harvey’s extreme rainfall in Texas”. In: *Environmental Research Letters* 13.5 (2018), p. 054014.

[161] S. Westra et al. “Global increasing trends in annual maximum daily precipitation”. In: *Journal of Climate* 26.11 (2013), pp. 3904–3918.

[162] D. Wilks. “Resampling hypothesis tests for autocorrelated fields”. In: *Journal of Climate* 10.1 (1997), pp. 65–82.

[163] P. Willetts et al. “Moist convection and its upscale effects in simulations of the Indian monsoon with explicit and parametrized convection”. In: *Quarterly Journal of the Royal Meteorological Society* 143.703 (2017), pp. 1073–1085.

[164] H. T. J. Wu et al. “Detecting climate signals in precipitation extremes from TRMM (1998–2013)— Increasing contrast between wet and dry extremes during the “global warming hiatus””. In: *Geophysical Research Letters* 43.3 (2016), pp. 1340–1348.

[165] P. Wu et al. “Anthropogenic impact on Earth’s hydrological cycle”. In: *Nature Climate Change* 3.9 (2013), p. 807.

[166] S.-P. Xie et al. “Global warming pattern formation: Sea surface temperature and rainfall”. In: *Journal of Climate* 23.4 (2010), pp. 966–986.

[167] G. Zhang et al. “The diurnal cycle of warm season rainfall over West Africa. Part II: Convection-permitting simulations”. In: *Journal of Climate* 29.23 (2016), pp. 8439–8454.

[168] Y. Zhang et al. “ENSO-like interdecadal variability: 1900–93”. In: *Journal of climate* 10.5 (1997), pp. 1004–1020.

[169] X. Zheng et al. “The response to deforestation and desertification in a model of West African monsoons”. In: *Geophysical Research Letters* 24.2 (1997), pp. 155–158.

[170] O. Zolina et al. “Improving estimates of heavy and extreme precipitation using daily records from European rain gauges”. In: *Journal of Hydrometeorology* 10.3 (2009), pp. 701–716.

[171] F. W. Zwiers et al. “Changes in the extremes of the climate simulated by CCC GCM2 under CO2 doubling”. In: *Journal of Climate* 11.9 (1998), pp. 2200–2222.

A Physics Literature

This section includes a short discussion about some of the physical mechanisms behind these changes in extreme precipitation events. This is often addressed by decomposing the thermodynamic and dynamic contributions to the changes; the former relating to the enhancement of the atmospheric moisture content due to temperature increases (the Clausius-Clapeyron relation) and the latter associated with variation in atmospheric circulations. It is widely expected that the hydrological cycle will intensify under climate change (e.g. M. R. Allen et al., 2002; P. Wu et al., 2013; Donat et al., 2016). Despite some uncertainty in the magnitude of future global temperatures, it is generally recognised that particular climatic responses such as precipitation are strongly coupled with these increases (Held et al., 2006). With a warming climate, the current IPCC report predicts a 1-2% K^{-1} total moisture increase in the atmosphere (Pachauri et al., 2014). If it is expected that the global mean precipitation will increase by a maximum of around 2% K^{-1} (Held et al., 2006; Pachauri et al., 2014) and the intensity of rare events is expected to increase by a minimum of 5.5% K^{-1} (O'Gorman et al., 2009), this difference suggests an increase in heavy rain events along with a reduction in the frequency of lighter rain (Trenberth, 1999).

A.1 The Clausius-Clapeyron Relation

The simplest explanation of intensifying extreme precipitation under warmer temperatures is that atmospheric water-holding capacity increases. An increase in saturation water vapour content has been observed since 1973 when reliable records began (Ross et al., 2001). This can be understood by considering the Clausius-Clapeyron (C-C) relation (Fig. 36):

$$\frac{\partial e_s}{\partial T} = \frac{L_v e_s}{RT^2} \tag{7}$$

where e_s is the saturation vapour pressure, T is the temperature, R is the gas constant and L_v the latent heat of vaporisation. This relation between moisture holding capacity, pressure and temperature for water vapour at standard temperature and pressure (273.15 K and 10^5 Pa respectively), indicates that the atmosphere can hold approximately 7% K^{-1} more water in the absence of other factors and will raise exponentially with temperature (Trenberth et al., 2003):

$$\frac{\Delta e_s}{e_s} \approx \frac{L_v}{RT^2}\Delta T = \alpha \Delta T \approx 0.07\ K^{-1} \tag{8}$$

Under warming, it is expected that relative humidity will remain approximately constant (Fig. 37a; Ingram, 2002; Soden et al., 2002), so the actual atmospheric precipitable water will also increase by a comparable rate of around 7% K^{-1}. It is therefore a straightforward argument that during extreme events, nearly all vapour in the atmosphere is precipitated out so event intensity scales with vapour availability.
The warmer the atmosphere, the more available moisture and consequently heavier potential rainfall implying that theoretically C-C puts an upper limit on the changes in extremes. However, this is an overly simplistic statement and the reality is more complex, with no definitive consensus. It is well known that global mean precipitation does not scale with C-C (Fig. 37b), closer to 1-3% K^{-1} (Betts, 1998; Boer, 1993; Trenberth, 1998), however, for extreme precipitation events it is less clear.

Trenberth (1999) claimed that extreme events increase in intensity and frequency predominantly due to thermodynamic factors such as the atmospheric water content. Models have produced results in agreement with this theory of C-C scaling, but only in a regional sense. Romps (2011) found that local precipitation

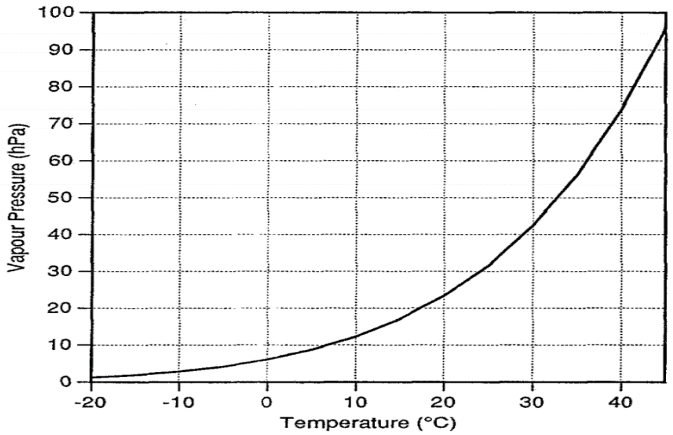

Figure 36: Exponential relation between the air temperature (C) and saturation vapour pressure (hPa). From A. Fowler et al. (1995).

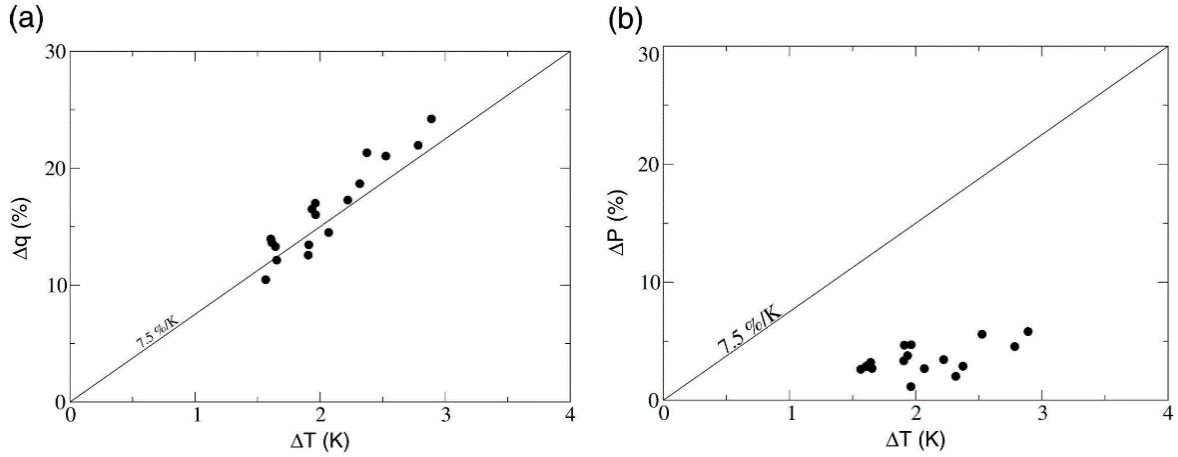

Figure 37: Plot of (a) the change in global column integrated water vapour per temperature increase and (b) change in global mean precipitation with temperature increase. Solid line is the C-C scaling, in the pictured study taken as 7.5% K^{-1}. From Held et al. (2006).

fluxes for heavy rain events obeyed the C-C relation when using a very fine cloud-resolving model, however globally the precipitation flux only increased by 3% K^{-1}, so in general agreement with Fig. 37b. Muller et al. (2011) also used an explicit convection model with a coarser grid and obtained results agreeing with Romps (2011) that precipitation extremes locally follow the C-C scale. This suggests that for a specific region during an extreme event, the C-C relation may be a valid indicator for the amount of precipitation to anticipate. Pall et al. (2007) agreed that the thermodynamic constraint provided by C-C was a valid predictor of future changes in precipitation extremes, but only over the mid-latitudes. They noted that although the tropics do not follow the scaling, C-C is still a better estimation than the mean increase. It is suggested that dynamical features of the atmosphere are the cause of deviations from the scaling.

M. R. Allen et al. (2002) collated 19 coupled global climate models (CGCMs) and found that they predicted a global mean precipitation increase of 3.4% K^{-1} which is, as expected, far lower than the C-C relation but in line with the global value of Romps (2011), Held et al. (2006) and the IPCC (2013) report (Pachauri et al., 2014). It is reasoned that changes in the hydrological cycle are due to the amount of available energy, so the mean global precipitation is energetically constrained. The study suggests that a large proportion of the net radiative cooling is not dependent on the temperature, so changes to the atmospheric

moisture content is not necessarily the deciding factor in precipitation increase. The study also showed that for models with doubled CO_2, rain intensities below the 85th percentile decreased in frequency while more intense events increase around the rate predicted by C-C.

O'Gorman et al. (2009) considered 11 different coupled models, comparing the 99.9th percentile extremes of precipitation in a future climate scenario. It was found that at all latitudes water vapour in the atmosphere increased with temperature as expected, however precipitation extremes did not increase at the same rate (Fig. 38), over the average for the models or individually. Particularly for the tropics, models were widely different in their predictions: between 1.3% - 30% K^{-1}. The variation in this region is likely associated with the parametrisation of vertical processes such as convection (see Sec. 2.3.1).

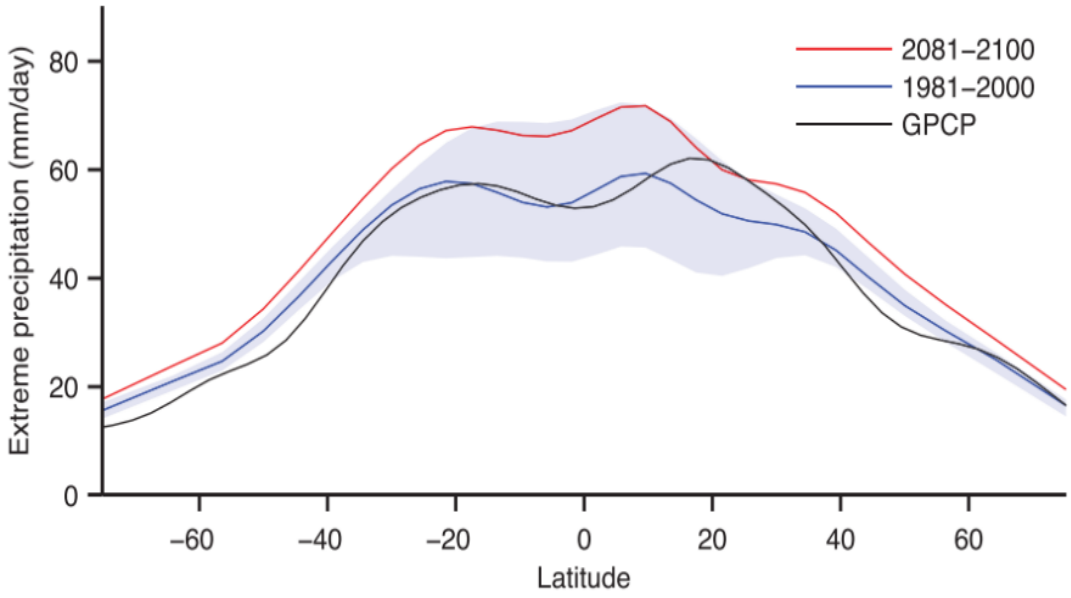

Figure 38: Plot of the 99.9th percentile of daily precipitation for two different time intervals. The black line is observational data from the Global Precipitation Climatology Project (GPCP), red and blue are multi-model median values from 11 different GCMs. Shading is the inter-quartile range, showing a larger interval over tropical latitudes. From O'Gorman et al. (2009).

Other studies do not agree with the scaling argument (Pendergrass et al., 2014; Pendergrass et al., 2016; Pfahl et al., 2017). Values far lower are reported, around 3% K^{-1} increase for extreme events. Multiple other studies have looked at individual real-life extreme events, such as Hurricane Harvey, a 2017 storm over the gulf of Mexico. Using models and rain gauge data, it was determined that the intensity of the event was exacerbated by climate change far above (between 13-30%) the expected 7% increase rate in atmospheric moisture as dictated by C-C (Risser et al., 2017; Wang et al., 2018; Van Oldenborgh et al., 2017), in disagreement with Romps (2011) and Muller et al. (2011).

This is echoed in other studies, some of which address more specific questions such as how the C-C scale is adhered to at different timescales. It has been suggested that daily precipitation extremes increase less rapidly than sub-daily extremes, the latter being above the C-C rate in some cases (Lenderink et al., 2008). It is argued that this could be due to the release of latent heat during convective precipitation which energises storms vertically, allowing for more intensive upward motion, causing stronger precipitation events (more detail in Sec. A.5).

A.2 The Wet-Gets-Wetter Paradigm

As previously mentioned, the intensification of the hydrological cycle is expected to continue, however it is less apparent how the temporal and spatial distribution of rainfall will shift under climate change. A popular proposal is the amplification of existing wet and dry precipitation patterns - the wet-gets-wetter and dry-gets-drier (WWDD) theory (sometimes called the 'rich-get-richer' mechanism (Chadwick et al., 2013)). This is a simplified description of observed precipitation patterns (Allan et al., 2010; Liu et al., 2013; Chou et al., 2013) and suggests that the response is due to the increase in water vapour in the atmosphere as discussed in Sec. A.1.

Surface evaporation moderates the surface temperature increase. However during heavy rainfall events the precipitation significantly exceeds evaporation rates, therefore must depend on low-level advected moisture convergence. A simple thermodynamic approach to this is to consider the net water flux, or the difference between precipitation and evaporation ($P-E$) at the planet surface which is balanced by moisture convergence in the atmosphere:

$$P - E = -\nabla \cdot \mathbf{F} \tag{9}$$

and scales as per C-C (Byrne et al., 2015):

$$\delta(P - E) \approx \alpha \delta T (P - E) \tag{10}$$

where $\mathbf{F}$ is the horizontal moisture flux integrated vertically, δ is the change in the climates, T is the temperature change and α is the same as in Eqn. 2. The atmospheric water vapour increases leading to increased transport of water. Held et al. (2006) showed that $\Delta(P-E) \propto (P-E)$ and that $P-E$ becomes more positive when already positive and vice-versa (assuming lower-tropospheric relative humidity remains constant and the values are zonally averaged) supporting the amplification theory mentioned above.

At larger scales a significant number of studies have shown the WWDD theory to be a valid description of patterns of extreme precipitation (e.g. Seager et al., 2012; Liu et al., 2013; Chou et al., 2013; H. T. J. Wu et al., 2016). However, other studies contest this result, claiming there is a discrepancy between land and ocean $P - E$ values and precipitation. Over the ocean it broadly follows the simple thermodynamic scaling from CC (Chou et al., 2004; Allan et al., 2010; Chou et al., 2013). Over land however, it has been shown that below 11% of land area globally follows the WWDD paradigm (Greve et al., 2014). This study determined that although the WWDD theory is likely valid over the ocean due to moisture availability, it is an oversimplification in land areas and did not appear to be present in observations. Roderick et al. (2014) looked at local scales (small enough to be relevant for agricultural and hydrological purposes) in terms of P–E. They found that $\Delta(P - E) \propto (P - E)$ is valid over zonal averages and over the ocean. However, at local (grid-box level), the WWDD theory does not hold over ocean or land. Byrne et al. (2015) showed only minimal increases in $P - E$ over land, far less that the 7% K^{-1} from the CC scaling. A more complex scaling was introduced that provided improved results for $P - E$ over land.

Contrary to this, more recent studies have shown the WWDD theory to hold for land regions. Using observations and simulations, a tendency for already wet regions in the tropics to become wetter (an increase of 3% K^{-1} over oceans) and dry areas becoming drier (a decrease of 2% K^{-1} over dry land regions) was shown using data from 1850-2100 (Liu et al., 2013). Polson et al. (2017) considered the WWDD paradigm by tracking changes in tropical wet and dry regions over time (using methods that track seasonal and inter-annual precipitation shifts). The study considered natural variability and circulation changes using satellites and simulations and found that the WWDD theory does hold robustly over land as well as oceans.

Discrepancies in these studies imply a lack of consensus, but it is clear that water availability over land (especially very dry regions) put a limit on the change in $P - E$ and therefore changes in precipitation. It appears that if there is enough available moisture the WWDD paradigm does, in general, hold. Along with unforced climate variability, the contradictory conclusions can be explained by the differing approaches of studies which produce a wide range of results (Kumar et al., 2015).

A.3 Dynamical Changes in the Atmosphere

One of the possible explanations for the WWDD theory not being consistently and correctly predicted is due to the dynamical component of the precipitation change. Regional features such as the location of well-known atmospheric instabilities, areas of convergence and subsidence and varying surface temperatures at differing latitudes means the changes in extreme precipitation are unlikely to be uniform as suggested by the CC relation (Trenberth et al., 2003). These dynamics imply that there are favoured regions of convergence and divergence, so locally, the dynamic contribution to precipitation increase is important (Xie et al., 2010, Huang et al., 2013). Unlike the thermodynamic contribution to changes in precipitation events which are fairly robust and cause spatially homogeneous rainfall increases, the dynamic processes are still relatively uncertain at a regional scale. Although the global mean rainfall is reasonably well predicted in GCMs by balancing the changes in radiative cooling and latent heat release (Lambert and Webb 2008), the spatial changes are far less predictable. This applies particularly in the tropics, where there is only a 0.2 spatial correlation between the change in precipitation under climate change when looking at CMIP5 (the fifth Coupled Model Inter-comparison Project; Taylor et al., 2012) models between current day and end of century under RCP8.5 scenario (Chadwick et al., 2013). This suggests that dynamical changes are influencing the otherwise relatively robust thermodynamic ones.

Large-scale variations in atmospheric dynamics will contribute to changes in precipitation in a warming climate. The thermodynamically driven increase, especially in tropical precipitation (discussed in Sec. A.5) will be moderated by circulations such as the Walker cell weakening and Hadley cell expansion. These cells dictate favourable regions for convergence and subsidence. Within these zones in particular, the dynamic feedback can significantly change the expected thermodynamic mechanism (Chou et al., 2009). The Walker circulation is a large, steady, zonal overturning flow in the tropics. Studies have found it to be weakening over the past century (Vecchi et al., 2006; Tokinaga et al., 2012; McPhaden et al., 2002) whilst others have found it to oscillate in intensity over decadal scales (Minobe, 2000). Others attribute the variations in the circulation to be directly related to the El-Niño Southern Oscillation (ENSO) (Y. Zhang et al., 1997; Trenberth, 1998; Dai, 1999). Many of these studies attribute the observed variations to climate change and simulations of the circulation response to warming (Chadwick et al., 2013). The resulting decrease in convective mass flux from weakening circulations has been observed to be at least partially 'cancelling out' the effects of thermodynamic mechanisms (Held et al., 2006; Chadwick et al., 2013). In an idealised sense, this can be explained by the relation $P = Mq$ where P is precipitation, M is the convective mass flux and q is the boundary layer specific humidity (Held et al., 2006). This suggests that as q increases as per the C-C relation, P increases globally at 1-3% (Stephens et al., 2008) then M must be constrained to decrease, suggesting a weakening atmospheric circulation. Hadley cell (a meridional low-latitude large-scale circulation) variation is not as strong as with Walker circulations (Vecchi et al., 2006) however pole-ward expansion has been noted (Scheff et al., 2012).

Separating the contributions to changing precipitation patterns is often used to provide a breakdown of the impact of significant components. More recent studies include Chadwick et al. (2013), who compared 13 models and determined that the dominant balance against the thermodynamic component was the divergence feedback of the convective mass flux. This is a direct dynamic amplification due to the weakening circulation. Westra et al. (2013) found that the median rate of increase for annual maximum daily rain is 7% K^{-1} globally but noted important meridional variations which suggest that atmospheric circulations contribute to precipitation increases. Dynamical components of precipitation extremes, particularly in the tropics and sub-tropics, significantly modify the precipitation intensity and can even modify the sign of

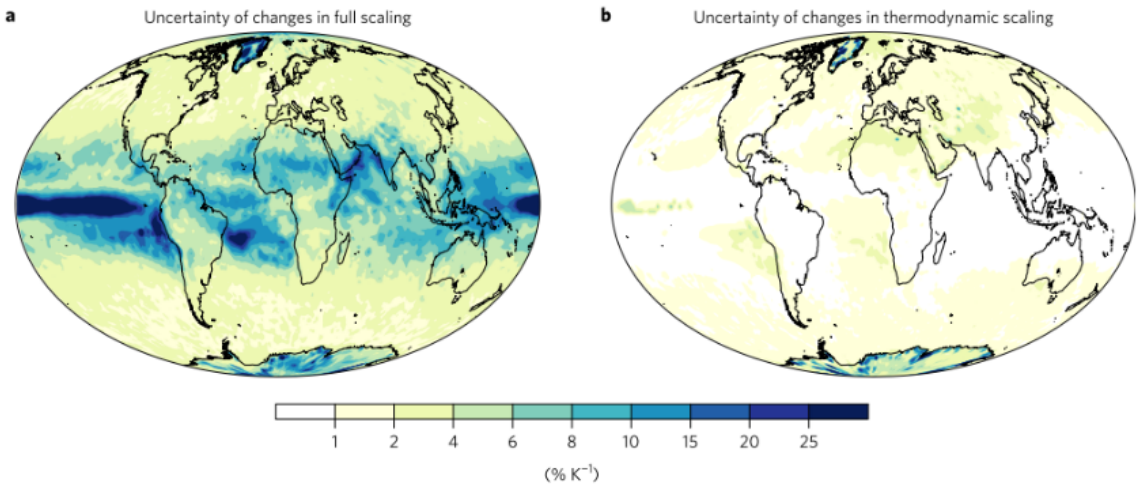

Figure 39: Uncertainty of changes in dynamic and thermodynamic components of precipitation extremes with warming. a) Uncertainty in all changes. b) Uncertainty in the thermodynamical scaling. From Pfahl et al. (2017).

the change, the opposite of the WWDD theory (Pfahl et al., 2017). Tandon et al. (2018) also had results agreeing with Pfahl (2017), where regional patterns of extreme precipitation events were strongly influenced by ascent. A study looking at an extreme event in the United Kingdom determined that based on statistical decompositions of the atmospheric fields (splitting the vertical moisture advection into a component that relates to vertical velocity change and a thermodynamic one that relates to changes in water vapour), the atmospheric circulation, specifically the vertical motion, is the dominant component over the thermodynamic contribution that caused precipitation extremes (Oueslati et al., 2019).

These studies are limited as they rely only on model data and not observations, as atmospheric vertical motion is difficult to observe therefore few exist (Tandon et al., 2018). From 12 climate model simulations taken from the Fourth IPCC Assessment Report, half were noted to model precipitation extremes in the tropics increasing at up to double the rate that C-C would dictate. Thus suggesting that vertical atmospheric motion has a significant impact (Sugiyama et al., 2010).

Contrary to these studies, Emori et al. (2005) questioned how much atmospheric moisture content can be attributed to changes compared with dynamical in both mean and extreme (99th percentile) daily precipitation. They determined that thermodynamic changes are the primary source of increasing extremes, with dynamic components being only a minor factor.

A.4 Physical Mechanisms Summary

The thermodynamical behaviour of the atmosphere under climate change allows confidence in predicting certain behaviours relating to changing precipitation averages and extremes. The relatively simple exponential relation between water-holding capacity of the atmosphere and temperature is demonstrated to hold in many observational and simulated extreme precipitation studies. This is particularly evident when considering the atmosphere over oceans where there is an unlimited amount of moisture. The effect from the large scale circulations on precipitation changes is more complex and isolating their impact is problematic.

The continuing discrepancy between results from computational studies suggest that there are shortfalls relating to accuracy of the models, particularly in the tropics. The complex physics and dynamics involved in the vertical modelling and the related parametrisations is likely to play a major role. This review also does not consider other factors such as aerosols (Stevens et al., 2009) which can reduce the intensity of the hydrological cycle (Trenberth et al., 2007) and may add to discrepancies between studies. A further

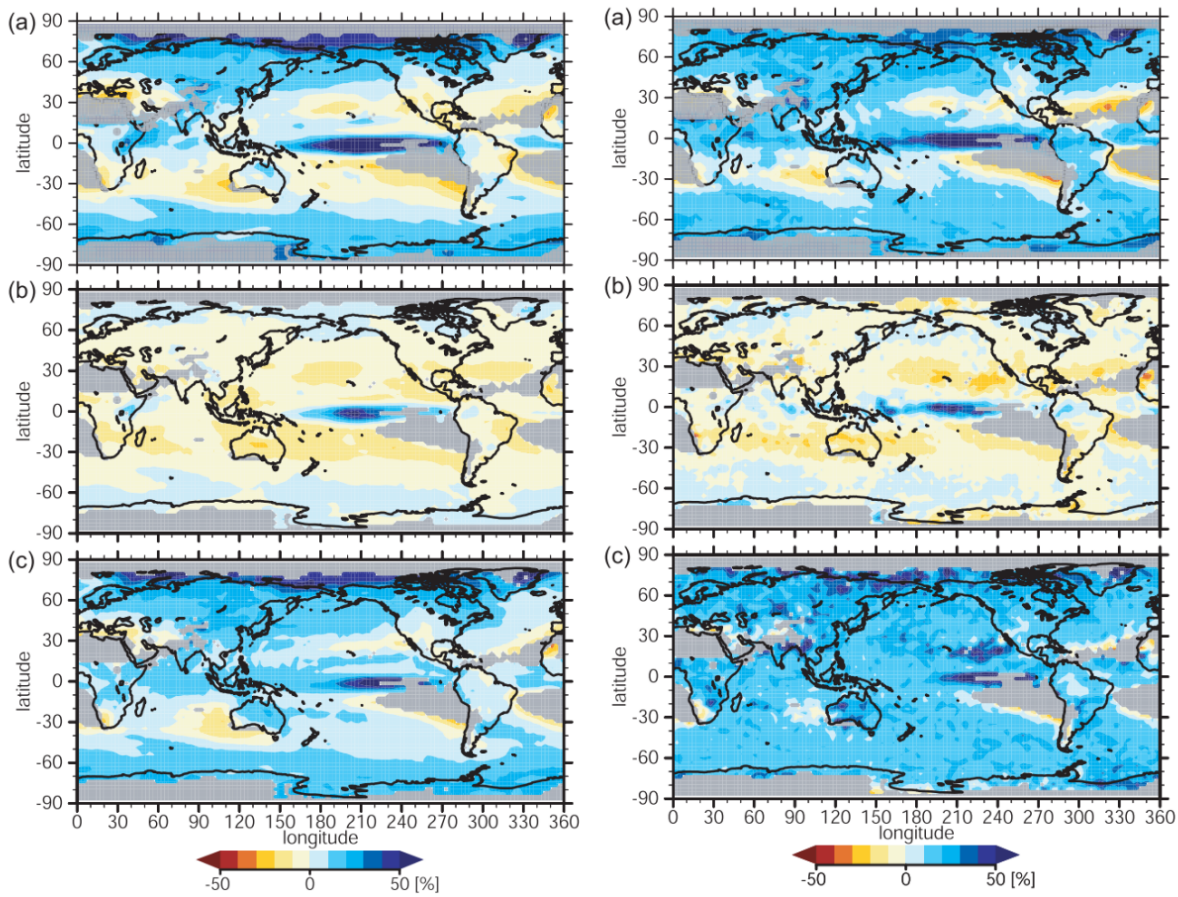

Figure 40: Left column: ensemble mean change in the annual mean precipitation under climate change where (a) total change, (b) change in dynamic component, (c) change in thermodynamic component. Right column: change in 99th percentile of daily precipitation under climate change where (a) total change, (b) change in dynamic component, (c) change in thermodynamic component. From Emori et al. (2005).

issue when examining studies of extremes is the varying definitions used, for example the difference between high-impact and really rare events. Another issue comes from the length of the data sets used and if they are appropriate for very rare event analysis.

A.5 What makes the Tropics Unique?

The tropics see much of the precipitation and evaporation across the planet; around two-thirds fall in equatorial regions. Deep convection driven by latent heat release is the primary source for rainfall and as such the tropics do not follow the same chief physical processes as the mid-latitudes and poles. In reaction to a warming climate, it is expected that tropical (30°N-30°S) precipitation will see major changes both in location, pattern and intensity (Pachauri et al., 2014; Chadwick et al., 2016). The tropics are also at significant risk of impact from the wet-become-wetter, dry-become-dryer scenario (Held et al., 2006; Chou et al., 2009) as discussed in Sec. A.2. Several important factors affect the hydrological cycle in the tropics – the atmospheric circulations, significant deep convection, the associated latent heat release with precipitation and large organised mesoscale convective systems (MCSs). Much of this is not resolved in global models (Rossow et al., 2013). The strong diurnal cycle observed in the tropics is also another feature of this region, which is notoriously difficult to model (Nikulin et al., 2012). These features make the observed atmospheric behaviour differ from higher latitudes. There are also few observational records of these features to help validate long-term projections from simulations, making tropical regions a challenge to study.

A.6 Energy, Convection and Latent Heat Release

From a thermodynamic perspective, the hydrological cycle behaves like a heat engine – moisture evaporating at the surface, condensing at colder temperatures further up in the atmosphere, followed by precipitation. Just like in a traditional heat engine, the importance of available energy in the atmosphere cannot be ignored, for example, most of the incoming solar radiation at the surface is used for evaporation, around 80% (Trenberth et al., 2009), which is then released when the moisture in the atmosphere condenses. This means that globally, there are energetic constraints on the increase in mean precipitation (mentioned in Sec. A.1). However, at individual event level, precipitation can be far higher, especially in the tropics where the release of latent heat due to deep convection condensation plays a major role in tropical heavy rainfall (Riehl, 1958).

Deep convection in the equatorial region is critical to the circulations observed in the atmosphere. During moist convection, a control volume of air containing water vapour rises in the troposphere. When the parcel reaches the level of condensation, the vapour will condense, releasing energy as latent heat. The energy works against the cooling of the parcel as it rises, so will be positively buoyant, meaning latent heat drives vertical circulations, often on km scales. A result of this latent heat is further enhancement of the convergence of moisture in the parent storm (Trenberth et al., 2009). In the tropics, latent heat is the primary energy source in the circulation cycles with the heat moving poleward, stopping the tropics from getting continually warmer. Latent heat is a significant factor in the tropics - it is thought that around three quarters of the atmospheric circulation happens due to latent heat released by precipitation (Kummerow et al., 2000).